The Thesis Committee for Kristopher James Voorhees
Certifies that this is the approved version of the following thesis:

Anatomy, Dimensions, and Significance of the Penultimate Yates Tepee-Shelf Crest Complex, G25 Hairpin HFS, Guadalupe Mountains, New Mexico and Texas

APPROVED BY
SUPERVISING COMMITTEE:

Supervisor:

Charles Kerans

William L. Fisher

Xavier Janson

Anatomy, Dimensions, and Significance of the Penultimate Yates Tepee-Shelf Crest Complex, G25 Hairpin HFS, Guadalupe Mountains, New Mexico and Texas

by

Kristopher James Voorhees, B.S.

Thesis

Presented to the Faculty of the Graduate School of

The University of Texas at Austin

in Partial Fulfillment

of the Requirements

for the Degree of

Master of Science in Geological Sciences

The University of Texas at Austin

May, 2016

Dedication

To my family for their tremendous love and support. They have taught me the meaning of hard work and complete dedication to my pursuits in life.

Acknowledgements

First, I would like to thank Dr. Charlie Kerans for giving me the opportunity to conduct impactful research that has contributed to the carbonate research community. I am grateful that you saw my potential beyond what was documented on a piece of paper and granted me the privilege of being a member of the RCRL team. There is no doubt that you were the best mentor I could have asked for. My most fond memories of graduate school will be the field trips and experiences we had as a group. Thank you for challenging me to be a better scientist and for reminding me to enjoy the ride along the way.

This thesis benefited from the guidance of committee members, Dr. William Fisher and Dr. Xavier Janson, whose valuable feedback and comments helped significantly improve the manuscript. I gratefully acknowledge the research scientists and staff of the Reservoir Characterization Research Laboratory (RCRL) and the Bureau of Economic Geology (BEG) that helped fund this research and offered assistance throughout the process: Dr. Zahm, Josh Lambert, and Stephaine Lane. I would also like to thank my fellow graduate students in the RCRL as well as in the Jackson School for their friendship and memories made together throughout my graduate career. Special thanks to Ben Smith, Jeff Sitgreaves, and Kyle McKenzie for providing assistance in the field and for the sleepless nights spent discussing tepees, geology, and plans for the future.

Finally, I would like to thank my family and friends outside of geology who have supported my pursuit for higher education and reminded me to work hard and play hard.

Abstract

Anatomy, Dimensions, and Significance of the Penultimate Yates Tepee-Shelf Crest Complex, G25 Hairpin HFS, Guadalupe Mountains, New Mexico and Texas

Kristopher James Voorhees, M.S. Geo. Sci.

The University of Texas at Austin, 2016

Supervisor: Charles Kerans

The steep-rimmed Permian Capitan platform in the Guadalupe Mountains has been studied in extensive detail to understand the effect of eustacy on platform architecture as seen in continuously exposed 700 m relief shelf-to-basin depositional profile. The Guadalupian Hairpin member (G25 High-Frequency Sequence) of the Yates Formation represents a major regional shelf marker and displays continuous 2.5 km dip-width exposures of the Capitan platform in McKittrick, Big, Double, Gunsight, Slaughter, Rattlesnake, and Walnut Canyons. Compared to the sequences above and below it, the G25 HFS is unique in that it reveals pronounced expansion of the shelf crest tepee-pisolite complex from an average of 1 km width to greater than 2 km. Tepee structures are 2-20 m diameter expansion megapolygons with compressional ridges formed by syndepositional expansive crystallization of micritic cement in arid to evaporitic supratidal settings. Increased dip-width of the shelf crest tepee-belt reflects a prolonged

period where repeated cycles of wetting, evaporation, precipitation, and buckling of storm-ridge washover facies (grainy tidal flats/beaches) dominated the shelf. This study seeks to examine the role that eustacy/accommodation play in expansion of the shelf crest tepee complex by quantifying the dimensions of Capitan-equivalent shelf facies in McKittrick and Rattlesnake Canyons.

Dip-oriented regional cross sections in Rattlesnake and McKittrick Canyons were created from 21 measured sections from 50-500 m spacing covering 30 to 70 m in thickness calibrated to 3 high-resolution gigapan photomosaics that are in turn constrained spatially using airborne lidar data. Cross sections in both canyons constrain facies tract dimensions as well as depositional topography and spatial distribution of the tepee complexes, allowing construction of a new tightly controlled depositional profile. 29 thin sections aid in grain identification, cement composition, and facies classification.

Two main results of this study are (1) a new tightly constrained model for the Capitan shelf unequivocally showing that the tepee-belt is the topographic high-point of the profile, and (2) the Hairpin G25 highstand marks a period of prolonged supratidal exposure of the shelf and rapid volumetrically significant marine cementation from a supersaturated fluid, marking the first phase of silling of the Delaware Basin and onset of basinal restriction prior to end-Capitan Castile evaporite deposition.

Table of Contents

List of Tables

List of Figures

INTRODUCTION

The constant sea-level hypothesis for the Capitan Reef was most persuasively presented by Lloyd Pray over many papers, presentations, and field trips. Subsequent detailed studies have questioned this hypothesis, but little if any clear evidence has been presented to demonstrate major eustatic drops during Capitan margin progradation. An important challenge to this stable sea-level model has come from the work of Kosa and Hunt who documented important karstification at the top of a major regional shelf marker known as the Hairpin dolomite, or Guadalupian 25 HFS of Kerans et al. (2013). In addition to top-Hairpin karst development, high-frequency cycle field mapping by Tinker (1998) and Harman (2011) has shown that the tepee-pisolite shelf crest facies tract of the Hairpin expands to more than double the average dip-width of the underlying high-frequency sequences belonging to the stratigraphic framework constructed by the work of Kerans et al. (1992), Kerans (1995), Kerans and Kempter (2002), and most recently modified by Kerans et al. (2013).

Previous studies have improved our understanding of the G25 HFS by placing it into a sequence stratigraphic framework, but mainly focus on antecedent topography and progradation:aggradation (P/A) ratios as being the primary drivers of platform architecture (Tinker 1998; Harman 2011). This study documents the dramatic facies tract dip-width expansion of the shelf crest by acquiring 21 measured sections through the Hairpin sequence in dip profiles in McKittrick and Rattlesnake Canyon. I present a new, tightly-constrained model for G25 HFS deposition and propose geochemistry as a critical control influencing expansion of the shelf crest during Hairpin time. High-resolution

quantification of depositional parameters such as facies tract dimensions and spacing and heights of tepees within the shelf crest facies tract should improve our understanding of the intrinsic and extrinsic stratigraphic variables (Kerans and Tinker 1999) affecting the development of the G25 HFS tepee belt.

Measured sections in McKittrick and Rattlesnake Canyons document deposition characterized by coupled high-frequency siliciclastic-carbonate reciprocal sedimentation patterns. These observations corroborate with the work done by Kerans (1995) that proposed a well-developed reef-rimmed margin that grew in relatively shallower depths than the underlying sequences such as the Seven Rivers. Dip-oriented cross sections produced in both canyons unequivocally confirm the topographically higher position of the shelf crest tepee-pisolite complex within the Capitan Platform. The comparison of these dip-oriented profiles of the G25 HFS from McKittrick and Rattlesnake Canyons, located approximately 30 km apart, documents the along-strike variability of the shelf crest. Analogs are drawn from modern settings in the Bahamas and the British West Indies to support the interpretation developed from high-frequency cycle mapping. Supplementary data such as facies tract dimensions from Slaughter Canyon is adopted from the work of Harman (2011). Finally, the link between tepee development and supersaturated basinal waters is proposed as recording the first signal of an evolving Delaware Basin prior to Castile deposition.

BACKGROUND

GEOLOGIC SETTING

The Guadalupe Mountains of New Mexico and Texas, U.S.A. display an exhumed mid-upper Permian mixed carbonate-silicilcastic system deposited from 273 Ma (latest Leonardian) to 262 Ma (end Capitanian, Guadalupian) along the northwestern margin of the Delaware Basin (Kerans et al. 2013) (Figure 1). The Central Basin Platform separates the Delaware Basin from the Midland Basin to the east, and together they compose a majority of the greater Permian Basin. Paleogeographic reconstructions suggest that the Permian Basin was approximately 5° north of the equator during the late Guadalupian providing an arid to subtropical climate ideal for carbonate precipitation in shallow marine waters and evaporite precipitation in restricted (Ross 1978; Irving 1979; Bambach et al. 1980; Blakey et al. 1988; Scotese and McKerrow 1990; Walker et al. 1995). By this time, tectonism coeval with the Ouachita-Marathon orogeny that previously elevated the Central Basin Platform had stabilized and the flat, filled topography of the Midland Basin joined the Central Basin Platform making the Delaware Basin the locus of the Capitan system deposition comprised of shelf equivalent Artesia Group and the basinal equivalent Bell Canyon Formation (King 1948; Tyrell 1962; Hill 1996; Ye et al. 1996; Kerans and Kempter 2002) (Figure 2). The Capitan Platform was eventually uplifted and tilted 1-2° to the east generating superb exposures of shelf-to-basin strata. (Kosa and Hunt 2005).

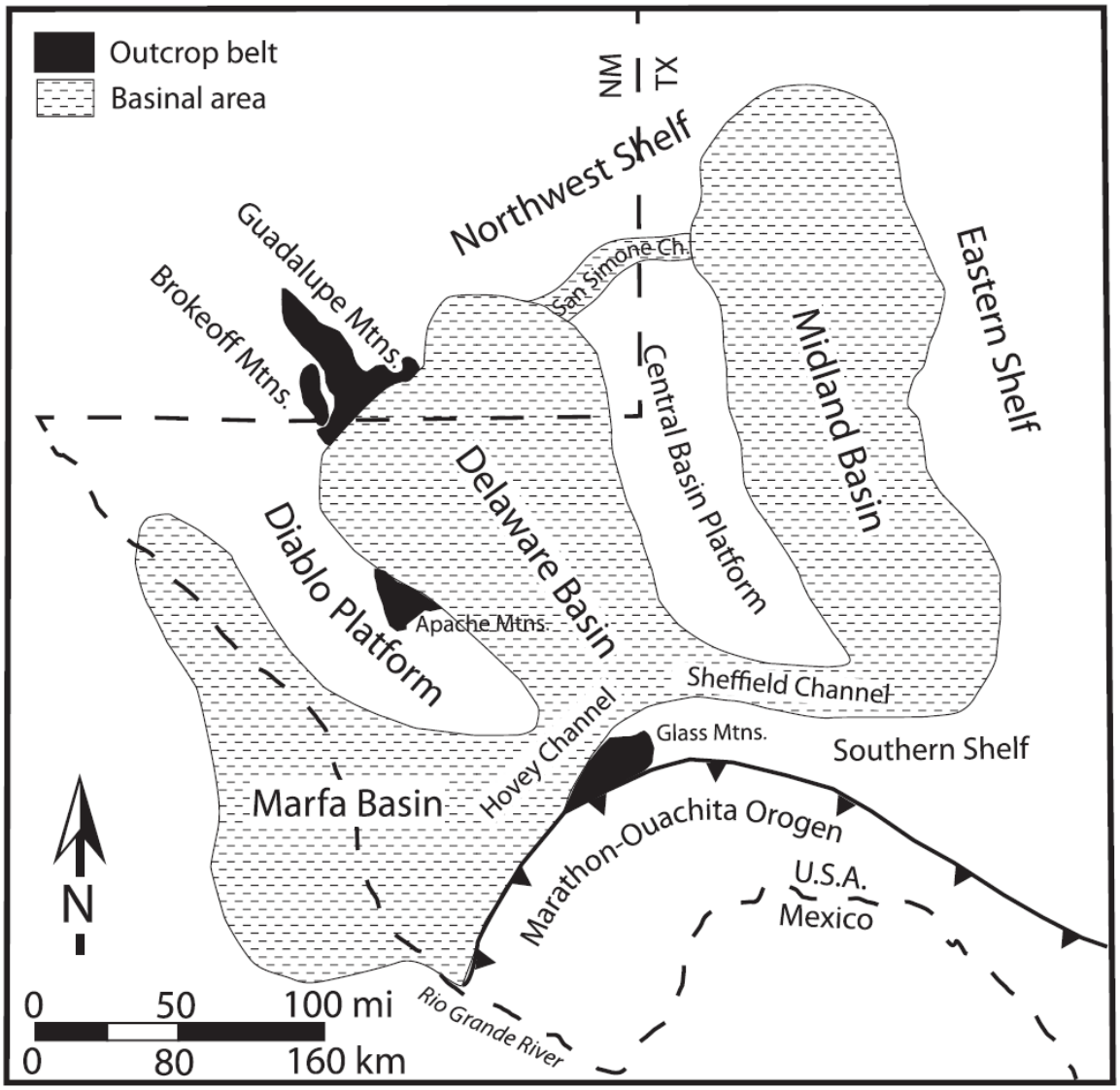

Figure 1. — Overview map of the Permian Basin highlighting its constituent platform tops and basins. The outline of the Guadalupe Mountains is filled in black. The outline of the state of Texas and the U.S.A. and Mexico border are annotated for reference. After Kerans et al. (2013).

Exposures of the Capitan system profile can be viewed in a series of WNW-ESE trending, dip-oriented canyons extending 45 km from the Western Escarpment and Pine Canyon in the south to Rattlesnake Canyon in the north (Kerans et al. 2013) (Figure 3). The north walls of both McKittrick and Rattlesnake Canyons are of particular interest for this study because of their continuous 2.5-3 km exposures from shelf-top strata to toe-of-slope deposits of the Yates Formation. The G25 Hairpin HFS of the Yates Formation allows documentation of a near-complete clinothem and is unique in that it reveals pronounced expansion to more than double that of underlying sequences of the shelf crest facies tract (Kerans et al. 2013). McKittrick and Rattlesnake Canyons were also selected as a result of reconnaissance mapping suggesting that these canyons reveal the most landward extent of the G25 HFS shelf crest facies tract, which is the setting for the primary focus of this study.

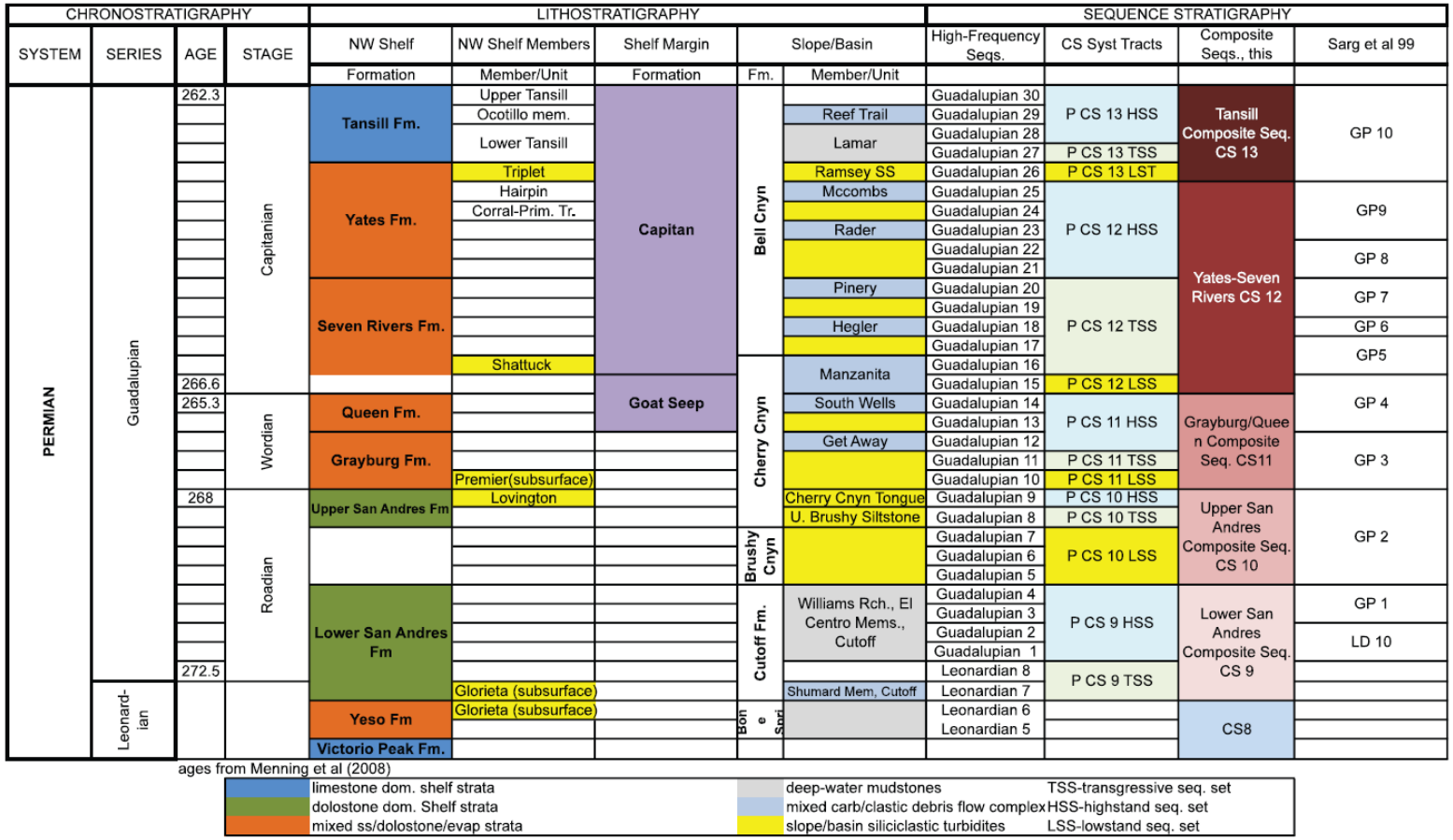

Figure 2. — Chronostratigraphic, lithostratigraphic, and high-frequency and composite-sequence-scale of latest Leonardian-Guadalupian section of the Guadalupe Mountains from Kerans et al. (2013).

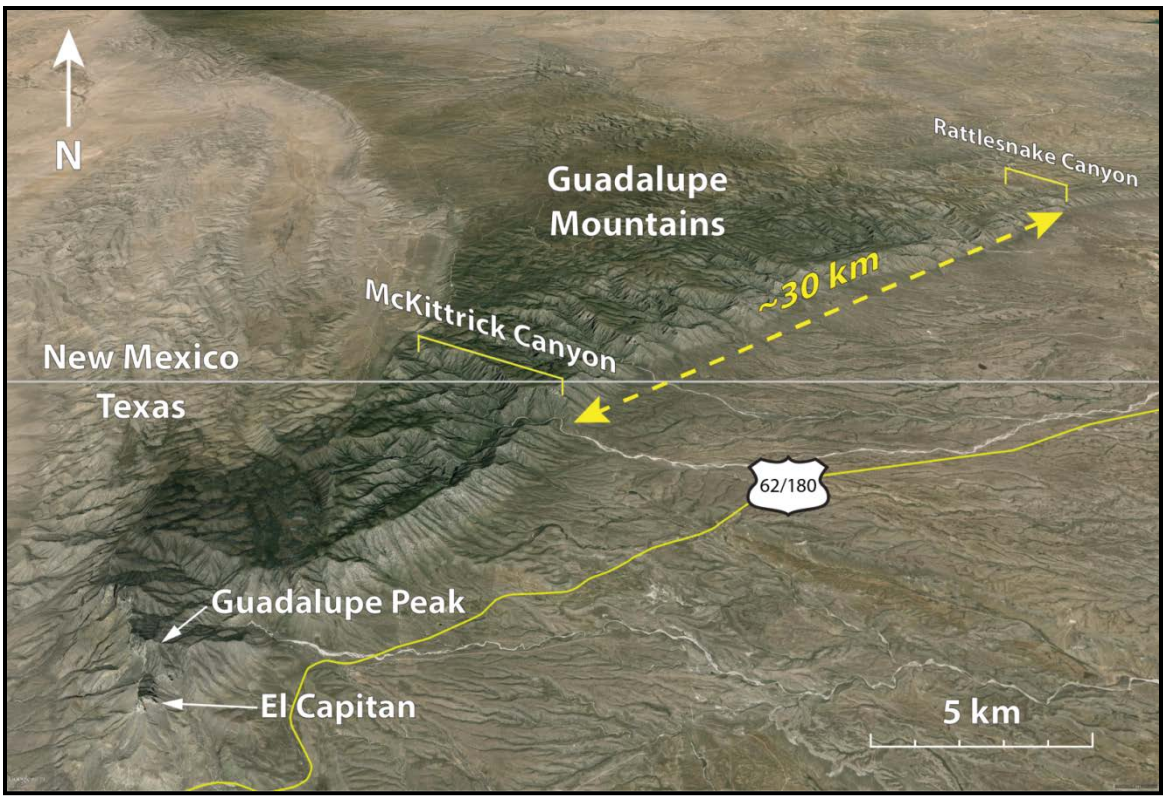

Figure 3. — Satellite image taken in Google Earth Pro showing locations of McKittrick and Rattlesnake Canyons as well as important landmarks for reference such as El Capitan. McKittrick and Rattlesnake Canyons are separated by approximately 30 km along-strike.

PREVIOUS STUDIES AND HISTORICAL SIGNIFICANCE

The Guadalupe Mountains is a type locale for researchers in both academia and industry focused on sequence stratigraphy, sedimentology, and depositional patterns of an ancient mixed carbonate-siliciclastic systems with one of the world's classic carbonate field trip stops, The Permian Reef Geology Trail, located at the mouth of McKittrick Canyon (Bebout and Kerans 1993). Shelf-to-basin outcrops of the Guadalupe Mountains oriented perpendicular to paleogeographic shelf margins serve as analogs to some of the most prolific hydrocarbon-producing reservoirs in the United States found within correlative strata in the Delaware and Midland basins (Ward et al. 1986).

Regional studies of the general geology of the Guadalupe Mountains began with work done by King (1948), Newell et al. (1953), Hayes (1964), and Dunham (1972). With an increase in understanding of the Guadalupe Mountains over time, critical questions pertaining to sedimentology, deposition, structure, and stratigraphy that remained unanswered became apparent and eventually triggered more detailed studies. Kendall (1969), Meissner (1972), Fischer and Sarnthein (1988), Mazzullo et al. (1985), Borer and Harris (1991) interpreted depositional patterns and cyclicity. Controls on sequence stratigraphic architecture were investigated by (Hurley 1989; Hunt and Fitchen 1999; Kerans and Tinker (1999), Hunt et al. 2002), Kosa and Hunt (2005), and Kerans et al. (2013). Detailed studies by Sarg and Lehmann (1986), Kerans et al. (1992), Kerans (1995), Kerans and Fitchen (1995), Tinker (1998), and Kerans and Kempter (2002) placed Permian strata into a sequence stratigraphic framework. Some of the most notable depositional models, based on both outcrop and subsurface data specific to the Yates

Formation, created by Tinker (1998), Osleger (1998), Rush and Kerans (2010), and Harman (2011) provide facies tract dimensions at the sequence-scale.

SEQUENCE STRATIGRAPHY

Meter-scale, high-frequency cycles are the foundation for the sequence stratigraphic interpretation used in this study. Measured sections were resolved on the order of decimeters and record a 1-D vertical succession of facies that are grouped into shoaling-upward high-frequency cycles. These high-frequency cycles are akin to upward-shallowing cycles (e.g., James 1979), punctuated aggradational cycles (PACs) (Goodwin and Anderson 1985), parasequences (Van Wagoner et al. 1988), and fifth-order cycles (Goldhammer et al. 1990), and have been placed into the pre-existing sequence stratigraphic framework established by the work of Kerans et al. (1992), Kerans (1995), Kerans and Kempter (2002), and Kerans et al. (2013) (Figure 4); though other studies have helped to place Permian strata of the Guadalupe Mountains into a sequence stratigraphic framework (e.g., Sarg and Lehmann 1986; Sarg 1988; Kerans and Nance 1991; Sonnenfeld and Cross 1993; Kerans et al. 1994; Kerans and Fitchen 1995; Gardner and Sonnenfeld 1996). High-frequency sequences, which are relatively conformable sets of strata bounded by subaerial unconformities or their correlative conformities, are composed of high-frequency cycles and have utility in sequence stratigraphic interpretation at the 1-D core-scale to the 3-D seismic-scale (Fisher and McGowen 1969; Vail 1987; Van Wagoner et al. 1988; Mitchum and Van Wagoner 1991; Kerans 1995).

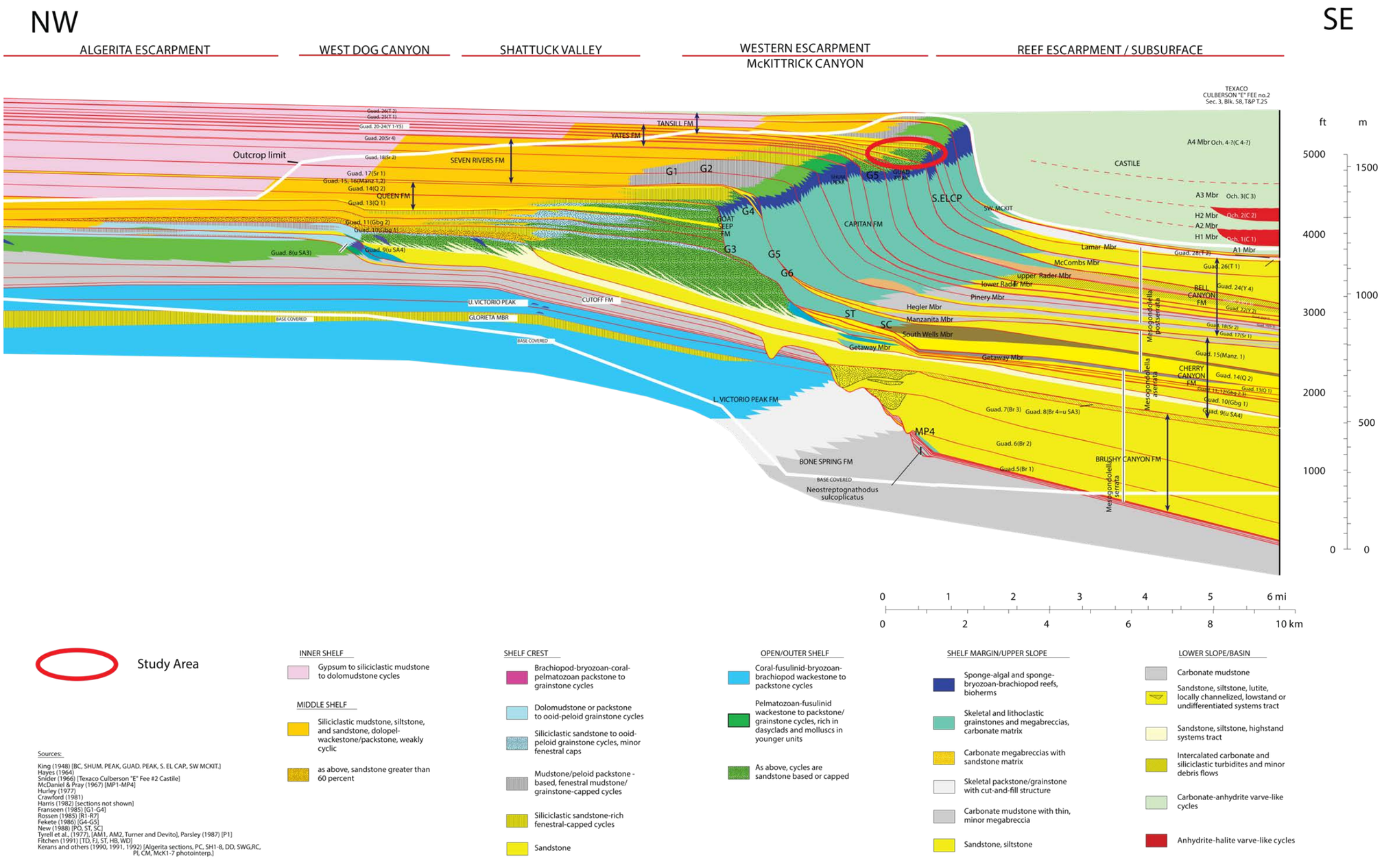

Figure 4. — Sequence stratigraphic framework of Leonardian to Guadalupian aged strata showing the transition from ramp to rim platform morphology. Established from the work of Kerans et al. (1992), Kerans (1995), and Kerans and Kempter (2002). Additional work from other authors incorporated into construction of the framework noted in the legend.

High-frequency cycle mapping within McKittrick and Rattlesnake Canyons allows for the development of an outcrop-based, high-resolution, quantified sequence stratigraphic model for the G25 Hairpin HFS. This model offers the ability to test the relative importance of processes controlling platform architecture through analysis of facies distribution, geometry, and the resulting depositional profile (Harman 2011). Quantified dimensional data from the G25 HFS provides a reproducible means to evaluate possible intrinsic and extrinsic stratigraphic controls on platform architecture. The G24, G26, and G27-28 high-frequency sequences serve as comparison to the G25 HFS to document the overall evolution of the Capitan Platform as well as the changing dip-widths of each respective sequences' facies tracts.

Variation of depositional patterns within the aforementioned sequences has been attributed to (1) orbitally forced, low-amplitude, eustatic variation (Borer and Harris 1991), (2) antecedent topography of underlying sequences, (3) sediment supply, (4) oceanographic effects, (5) salinity (Kerans and Tinker 1999), and (6) differential compaction and early structural deformation (Hurley, 1989; Hunt and Fitchen 1999; Hunt et al. 2002). When present, sandstones and siltstones in the Yates Formation are interpreted as cycle bases of high-frequency cycles. These sands were transported across the shelf via aeolian processes and were deposited during periods of sea level lowstand and subsequent exposure of the platform (Kendall 1969; Meissner 1972; Fischer and Sarnthein 1988; Mazzullo et al. 1985). During later periods of sea level rise and sea level highstand, the sands were marine reworked and thus occur as basal, deeper water deposits (Smith 1974; Candelaria 1989; Borer and Harris 1991). Shelf-carbonate accumulation

occurred during highstand systems tracts when phases of high accommodation coincided with an active carbonate factory (Osleger and Tinker 1999).

TEPEE DEVELOPMENT AND SIGNIFICANCE

The term tepee was coined by Adams and Frenzel (1950) for their resemblance to dwellings of early American Indians during a study of the Capitan Reef (Warren 1983). Tepees have been documented by multiple authors and are described as antiform structures that develop at buckled margins of saucer-like megapolygons (Smith 1974; Assereto and Kendall 1977; Warren 1983; Kendall and Warren 1987). Individual tepees typically have fairly symmetrical, chevron-like cross sections with crests that are truncated by overlying beds that thin laterally as they onlap the flanks of tepee crests suggesting syndepositional origin (Assereto and Kendall 1977; Esteban and Pray 1977) (Figure 5). Tepees form through multiple cycles of exposure, dessication, flooding, sediment infill, and/or marine cementation (Kerans and Tinker 1999). Modern examples exhibit crusts, formed from early cementation of surface sediments, that have expanded and crumpled into tepee structures as a result of thermal expansion and contraction of cement fill of cracks (Type II. Tepees) (Kendall and Warren 1987). Expansion of surface sediments can be as much as 15% and the most likely cause of expansion is due to crystal growth (Smith 1974; Assereto and Kendall 1977). Tepee formation is favored by high-frequency, low-amplitude sea level oscillations and predominately occur in an intertidal to supratidal coastal-flat environment with a semi-arid climate (Smith 1974; Peterhänsel and Egenhoff 2008). The work of Kerans and Fowler (1995), Tinker (1998), and Kerans and Tinker (1999) found that well-developed tepee complexes only form on shelf

Figure 5. — Field photograph of an asymmetric tepee with overlying strata onlapping onto the crest of the tepee. Photograph courtesy of Dr. Charles Kerans from the type locality for tepees in the parking lot of the Carlsbad Caverns visitor center. Host rock consists of fenestral and pisoid rudstones and are lighter in color than the interbedded dark grey sheet cracks. The curb at the bottom of the frame is estimated at 10-20 centimeters for scale.

margins with progradation to aggradation ratios of <20 where an approximately stable shoreline undergoes repeated cycles of desiccation and flooding (Figure 6).

Tepee structures can develop in three major paleogeographic positions: (1) at the margin of bedded lagoonal sequences, (2) capping carbonate buildups, and (3) capping glacial diamictites (Assereto and Kendall 1977; Gammon et al. 2005). The majority of tepees documented in the rock record form at seaward margins of middle shelf lagoons and are most famously displayed in regions such as the Guadalupe Mountains, U.S.A. and in the classical Middle Triassic platforms of the southern Alps, Italy (Assereto and Kendall 1977). Tepees capping carbonate buildups are meager in the geologic record, but can be found in the Triassic Presolana Group and the Val Seriana Formation in Lombardy, Northern Italy (Gnaccolini and Jadoul 1990; Berra and Jadoul 2002). Even more rare are the cap carbonates of late Neoproterozoic age found in areas such as south China and at Parachilna Gorge in the Adelaide Fold-Thrust Belt, Australia (Gammon et al. 2005; Jiang et al. 2006). Modern tepee structures have also been recorded along coastal salinas of South Australia and in the intertidal zone in the Arabian Gulf near Abu Dhabi (Warren 1983; Lokier and Steuber 2009).

Apart from being a key shoreline indicator, which is critical to paleogeographic reconstruction of carbonate platforms, tepees are postulated by Kerans and Tinker (1999) as being intrinsically linked to reef development. The authors believed that topographically-high tepee complexes acted as a barrier to evaporitic inner shelf waters that could hinder development of the Capitan Reef (Figure 7). Comparison throughout the composite sequence 12 (CS 12) of Kerans et al. (2013) reveals reef growth in the

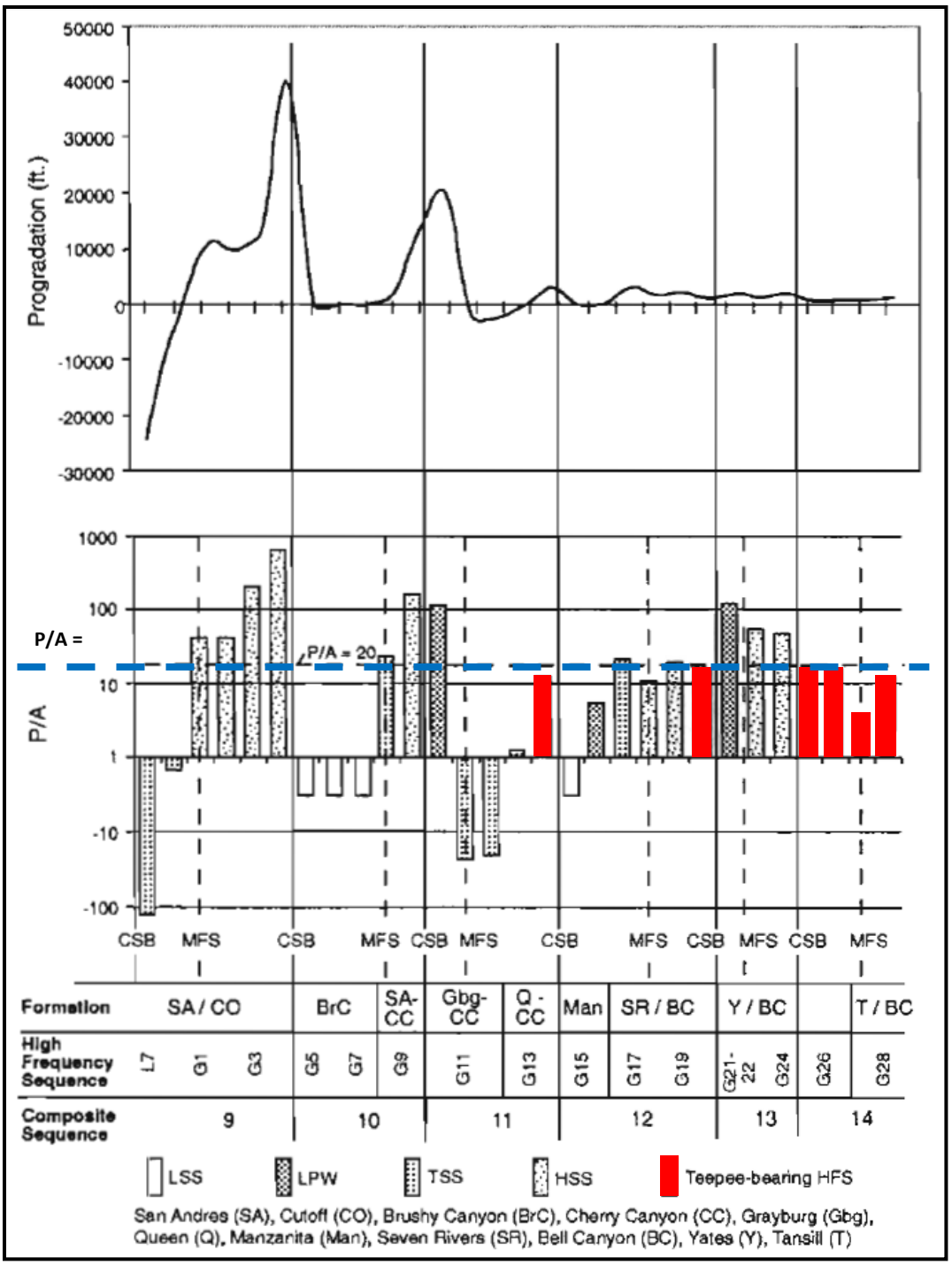

Figure 6. — Progradation-aggradation ratios for the Leonardian-Guadalupian sequences of the Guadalupe Mountains. Tepees within high-frequency sequences are highlighted as red bars. The blue dashed line indicates a P/A ratio of 20. Modified after Kerans and Tinker 1999.

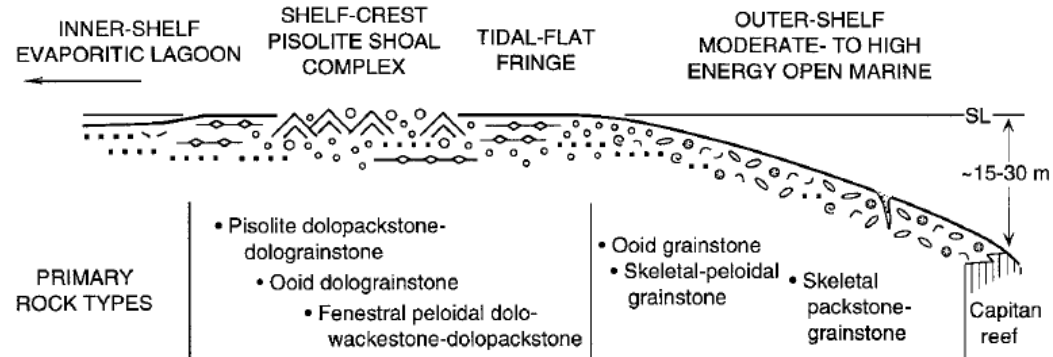

PRIMARY ROCK TYPES	• Pisolite dolopackstone-dolograinstone • Ooid dolograinstone • Fenestral peloidal dolo-wackestone-dolopackstone	• Ooid grainstone • Skeletal-peloidal grainstone • Skeletal packstone-grainstone
OUTCROP CHARACTERISTICS	• ledge- & cliff-forming, thin to massive beds • interbedded lithofacies commonly lensoid and laterally discontinuous • common teepees, vadose caliche crusts, horizontal sheet cracks, & intraclast lenses • common reverse grading from ooids upward into increasingly larger pisolites • primarily laminar fenestrae within white peloidal dolowackestone-dolopackstone • sandstone-filled neptunian dikes • uncommon cryptalgal laminites	• variable from resistant cliff-formers to stairstep topography • massive to thick bedding that increases in thickness downdip • typically structureless with less common low- to high-angle planar crossbedding • dolomitic limestones and limy dolostones • sandstone-filled neptunian dikes • degree of sorting increases updip • medium- to very coarse-grained textures • common fusulinid coquinas
INTERNAL COMPOSITION	• complex, polygenetic pisolites exhibiting multiple episodes of growth, leaching, & fracturing • abundant internal sediment and multiple generations of cement within fitted polygonal fabric • fenestral facies composed of dolomitized peloids and lime mud • common subrounded to subangular, micritic intraclasts • rare to common evaporite molds in laminar fenestral facies • rare to abundant subangular quartz silt	• abundant whole fusulinids and fragmental dascyclad algae • common bivalve, bryozoa, & echinoderm fragments and miliolid forams • large gastropod molds and steinkerns • common intraclasts and peloids • common superficially coated grains & micrite envelopes • common well-sorted, medium- to fine-grained ooid grainstones updip • widely disseminated subangular quartz silt
DIAGENETIC & PETROPHYSICAL CHARACTERISTICS	Pisolite Grainstones -- • cements: dolomicrite of pisolite laminae, isopachous bladed-to-fibrous dolomite after calcite, minor calcite spar, anhydrite • pore types: intraparticle and interparticle • pisolite grainstone avg. porosity = 6.6% avg. permeability = 0.36 md Fenestral Dolomites -- • cements: isopachous bladed, fibrous botryoidal, minor calcite spar, anhydrite • pore types: fenestral, moldic, & vuggy • fenestral dolomite avg. porosity = 6.6% avg. permeability = 1.43 md	• cements: isopachous bladed-to-fibrous calcite, blocky calcite spar, kaolinite • dolomite: partial to complete fabric-retentive replacement and void-lining cements • pore types: intraparticle, interparticle, moldic, shelter, and vuggy • common peloidal geopetal fill within gastropod shells • outer-shelf facies avg. porosity = 5.7% avg. permeability = 10.8 md

Figure 7. — Outcrop and petrographic characteristics of associated facies tracts along a schematic shelf crest to outer shelf profile showing the elevated profile of the shelf crest relative to the reef margin based on data from Slaughter Canyon from Osleger (1998).

lower sequences to water depths of >30m with poorly established tepee complexes, whereas reef fauna in the younger high-frequency sequences of the CS 12 grew to much shallower depths while well-developed tepee complexes thrived Kerans and Tinker (1999). Modern examples from the Great Bahama Bank and Florida show older Pleistocene elevated topography acting as a barrier to harmful platform interior fluids that can inhibit reef development further justifying the tepee-reef link hypothesis (Kerans and Tinker 1999).

Tepees also can have economic significance. Immature tepees that lack abundant cementation and are covered by an impermeable seal have the potential to be a reservoir rock for hydrocarbons due to their high structural position and topographic position, their proximity to a basin margin, and the high early porosity of unfilled fenestrae and tepee fractures (Assereto and Kendall 1977). Tepees can have economic importance in other industries besides the oil industry. For example, tepee facies are mined for metallic minerals in areas such as the Paglio Pignolino and Presolana mines in Italy (Assereto and Kendall 1977).

METHODOLOGY

This outcrop-based study integrates lidar data, high-resolution gigapan photomosaics, field observations and interpretations, and petrography in order to constrain facies tract dimensions as well as depositional topography and spatial distribution of the tepee complexes within the G25 Hairpin HFS. High-frequency sequences, including the G24 Corral, G26 Triplet, and G27-28 Lower Tansill, above and below the G25 were analyzed at a coarser scale using the lidar data and photomosaics. Comparing the G25 HFS to under- and over-lying sequences emphasized the dramatic expansion, unique to the G25, of the shelf crest facies tract at the expense of the outer shelf. Measured sections were placed into the sequence stratigraphic framework developed by Kerans et al. (2013).

Lidar point clouds cropped from a larger regional Guadalupe Mountains data set allowed for tracing of resistant benches and stratigraphic datums in three-dimensions. High-resolution photomosaics offered a complete shelf-to-basin perspective of high-frequency sequences that is otherwise overlooked while measuring individual sections. Conventional field methods and petrographic analysis recorded detailed observations of constituent facies that were later placed into representative facies tracts for correlation and interpretation of depositional environments. Standard sequence stratigraphic principles adopted from the work of Fisher and McGowen (1969), Vail (1987), Van Wagoner et al. (1988), Mitchum and Van Wagoner (1991), and Kerans (1995) were applied for sequence stratigraphic interpretation. This integrated approach yields a high-resolution dataset that reveals spatial and temporal variations in the G25 HFS at the high-

frequency cycle-scale as well as a new dip-oriented profile displayed at the high-frequency sequence-scale.

LIDAR DATA

Light detection and ranging (lidar) data, in the case of the Guadalupe Mountains dataset, provides a sub-meter DEM that offers the ability to track stratigraphic horizons in 3-D and extract more precise three-dimensional shape information from an outcrop (Bellian et al. 2005). The lidar dataset used in this study, originally collected by the UT-BEG Reservoir Characterization Research Laboratory in 2009, covers a regionally extensive area of the Guadalupe Mountains. Digital outcrop models (DOM) in McKittrick and Rattlesnake Canyons created from the lidar dataset afford perspectives of the outcrop in three dimensions that complement data collected during field work. These DOMs were manipulated using QT Modeler, which was essential for observations made in outcrops that were inaccessible and for quantifying facies tract dimensions as well as supplementary measurements.

Measured section thicknesses were calibrated using the profile analysis feature in the software. Distinct bedding planes and stratigraphic horizons were traced in three-dimensions revealing both strike- and dip-oriented stratal geometries as well as depositional topography of the platform (Figure 8). Offset along laterally continuous beds suggested candidates for faults that were later either confirmed from field work or remain inferred. Measurements were obtained of crest-to-crest spacing between tepees, and individual dimensions were acquired for tepees recognizable at the resolution of the lidar.

FIELD METHODS

A total of 21 measured sections ranging from 30 to nearly 80 m in height recorded at the decimeter-scale were collected in McKittrick and Rattlesnake Canyons. These canyons were selected for their continuous 2.5-3 km exposures of shelf strata. In McKittrick Canyon, 11 measured sections were collected along approximately 2.5 km of outcrop roughly oriented perpendicular to the Hairpin HFS terminal margin, while 10 measured sections covered nearly 2.6 km of exposed strata in Rattlesnake Canyon. The spacing between measured sections in both canyons depended predominately on outcrop

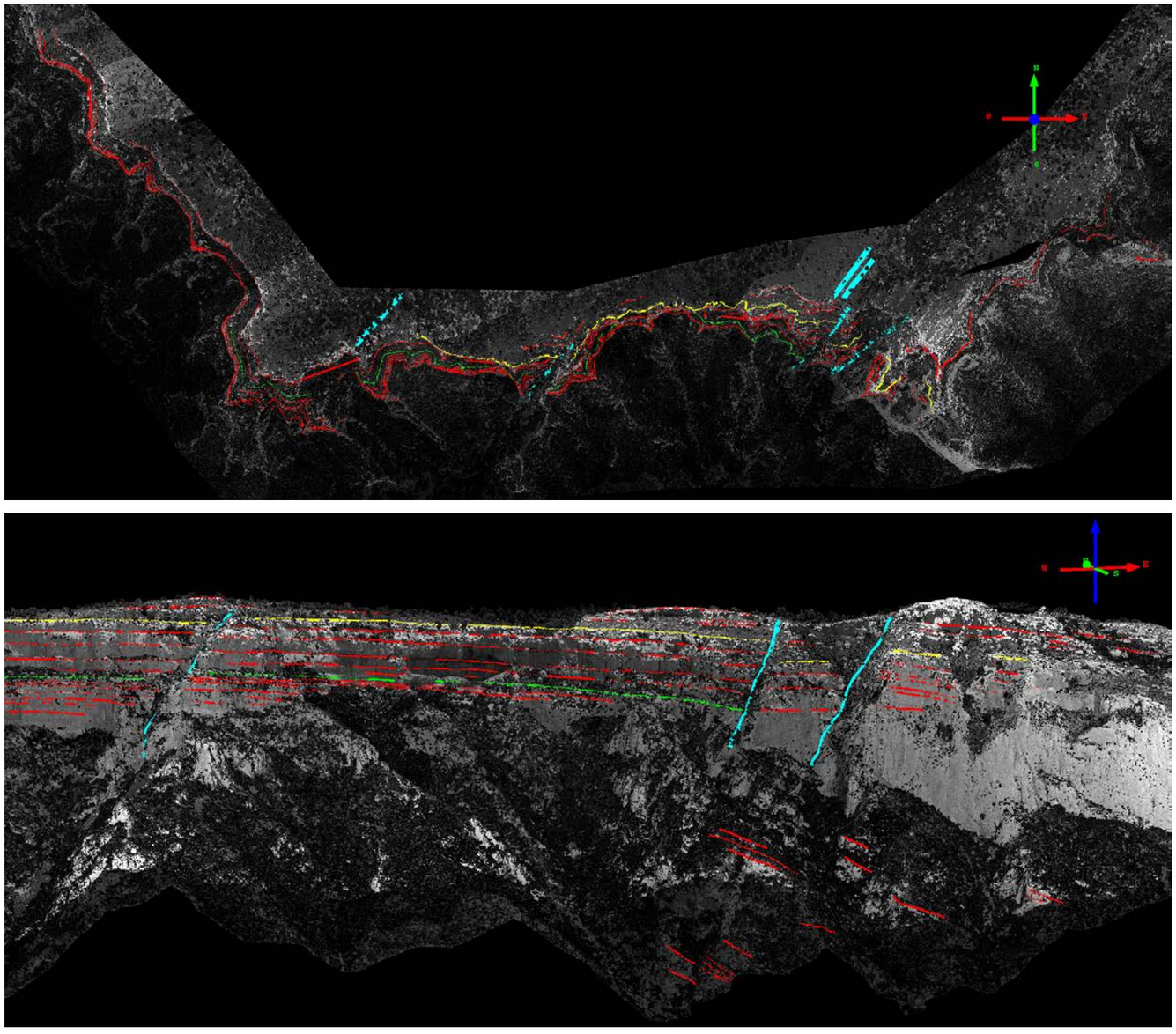

Figure 8. — Screenshot from QT Modeler of the 3D point cloud generated from the lidar data as described in the methodology. A.) Map view of the extent of the study area. B.) Cross sectional view of the above transect from A to A'. Distinct bedding planes are traced in red lines revealing the stratal geometry and depositional topography of the platform. Red lines in the lower vegetated area reveal

accessibility and quality and varied from 30 to 650 meters apart. Resistant bench tops within measured sections served as control points that were mapped onto photomosaics used for later correlation. Cross sections in both canyons were generated by projecting the locations of each measured section onto a dip line in Google Earth oriented perpendicular to the G25 shelf margin (Figure 9). Key observations documented include relative abundance of dominant grains, pore types, fabrics and textures, sedimentary structures, bedding geometries and thicknesses. Of the 42 hand samples procured, 29 thin sections were taken to understand diagenetic history within tepees and aid in grain identification, cement composition, and facies classification.

HIGH-RESOLUTION GIGAPAN PHOTOMOSAICS

Photomosaics were created using a Canon 5D Mark II camera coupled with a GigaPan EPIC robotic camera mount fixed to a tripod in order to create clear, high-resolution images that could be seamlessly stitched together. Several photopans were necessary to display the complete extent of the G25 HFS and to compensate for the three-dimensionality of the canyon walls. Photos were acquired and stitched using GigaPan Stitch software. Five photomosaics with approximately 10 cm resolution were created. Images were obtained of the North walls in both Rattlesnake and McKittrick Canyons and were acquired from the South walls on the opposite side of the canyons. Prime vantage points were selected using Google Earth with an attempt to minimize distortion related to acquisition position and the three-dimensionality of the canyon.

Similar to the lidar data, these photomosaics were critical for observing stratal geometries and depositional topography of the platform. Weathering profiles of the Yates

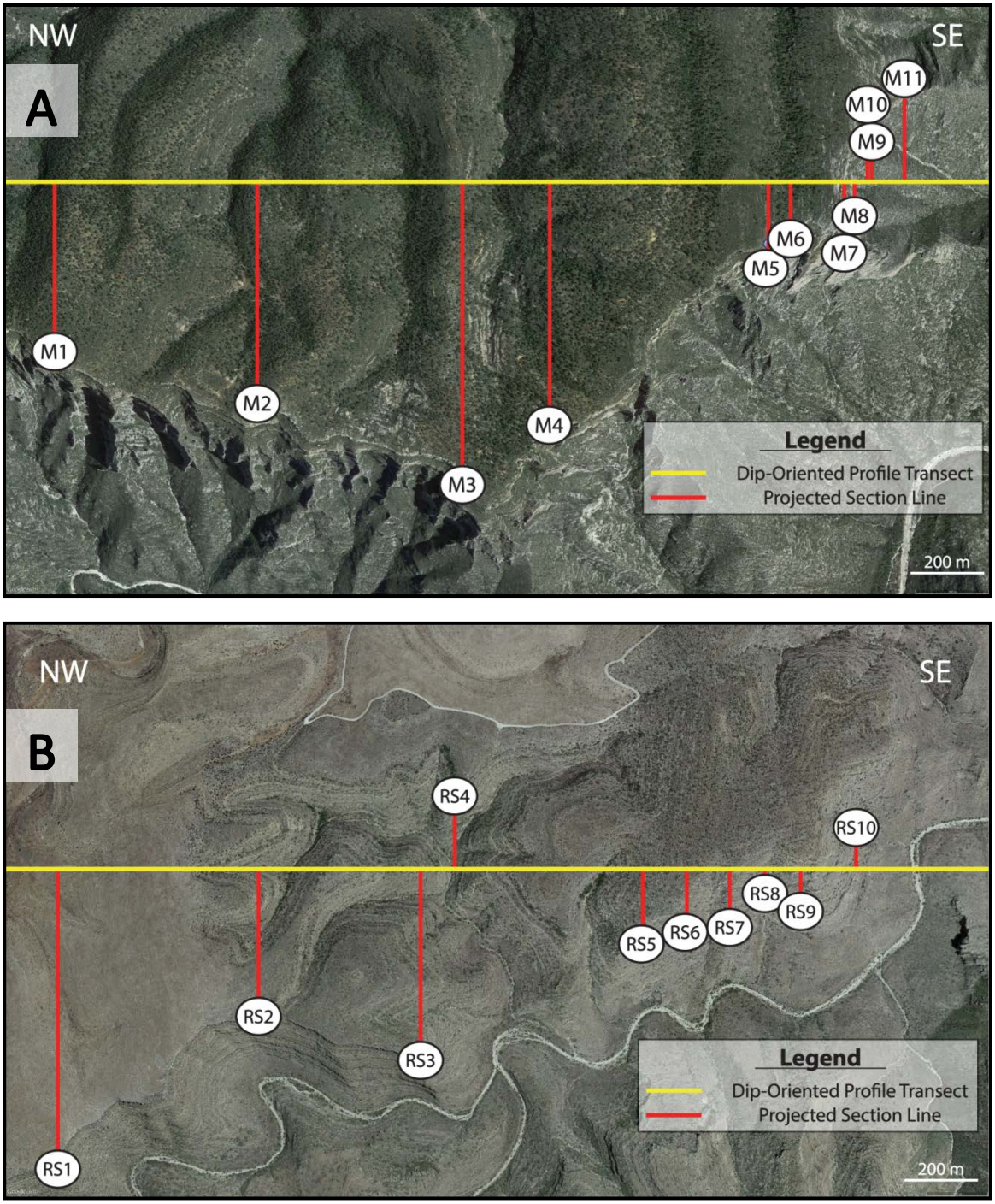

Figure 9. — Satellite image taken in Google Earth A.) Dip-line with projected measured sections from McKittrick Canyon. B.) Dip-line with projected measured sections from Rattlesnake Canyon.

Formation, and of generally all strata in the Guadalupe Mountains, tend to indicate lithology which aided in mapping along the photomosaics. The sandstones typically form recessive, vegetated/scree-dominated slopes, while the carbonates generate bedded-to-massive cliffs. This distinct, stair-step outcrop morphology allowed for interpretation of lithology on the photomosaic in inaccessible areas. Distinct bedding planes that were laterally continuous and interpreted to be cycle tops were traced and represent timelines used for correlating between measured sections. A previously acquired photomosaic with superimposed measured sections obtained from this study displays facies tract boundaries of the G25; boundaries are generalized with variable degrees of confidence dependent on areas with measured section control. A similar workflow was followed with all other photopans (Figure 10-14).

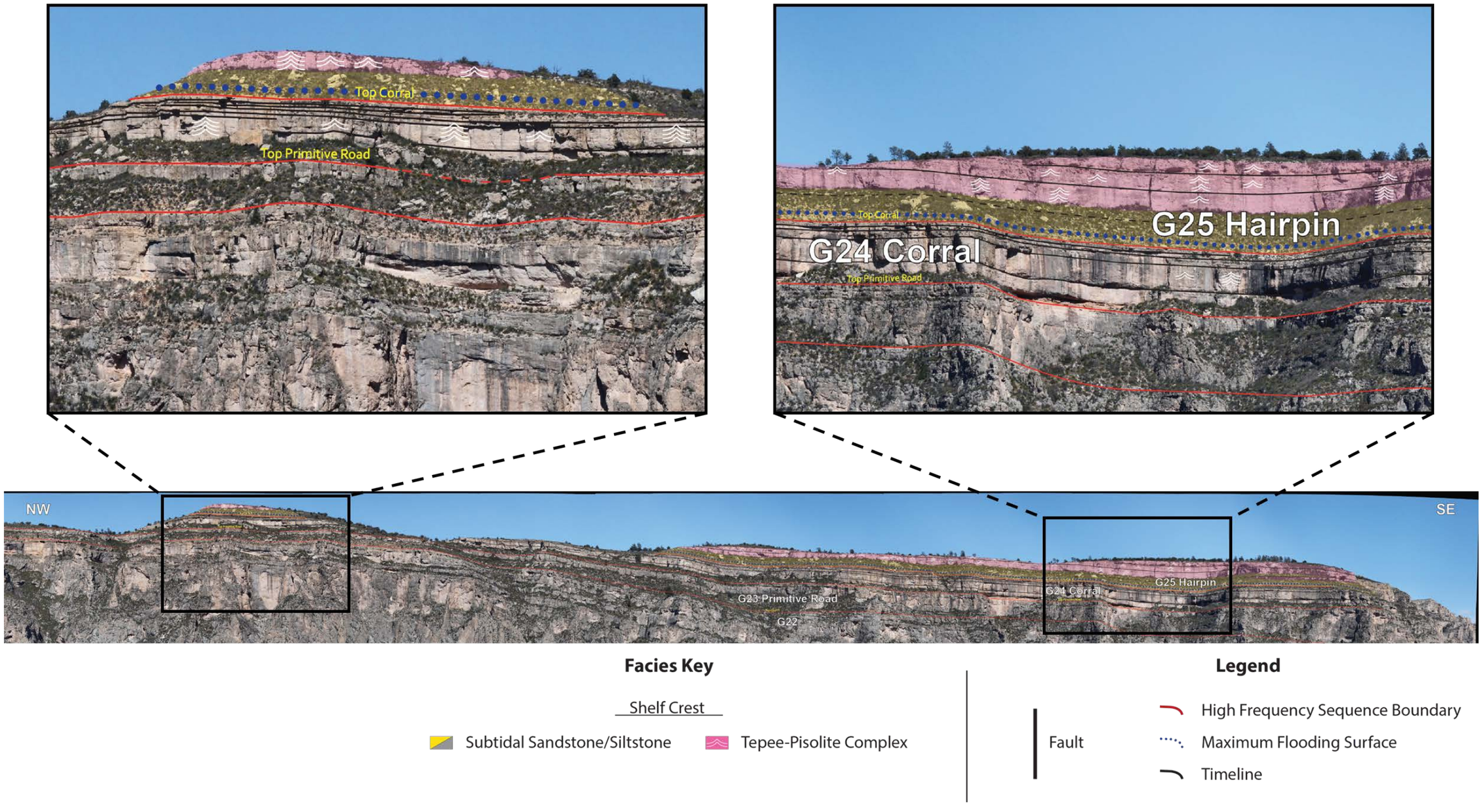

Figure 10. — Photomosaic of the most landward extent of the G25 HFS along the North wall in McKittrick Canyon. G22-G25 sequences are highlighted. The upper 3 packages within the G25 are progressively lost landward due to the erosional limit of the outcrop. The predominate facies recognized this far landward are the basal marine re-worked sandstones and facies associated with the shelf crest tepee-pisolite complex.

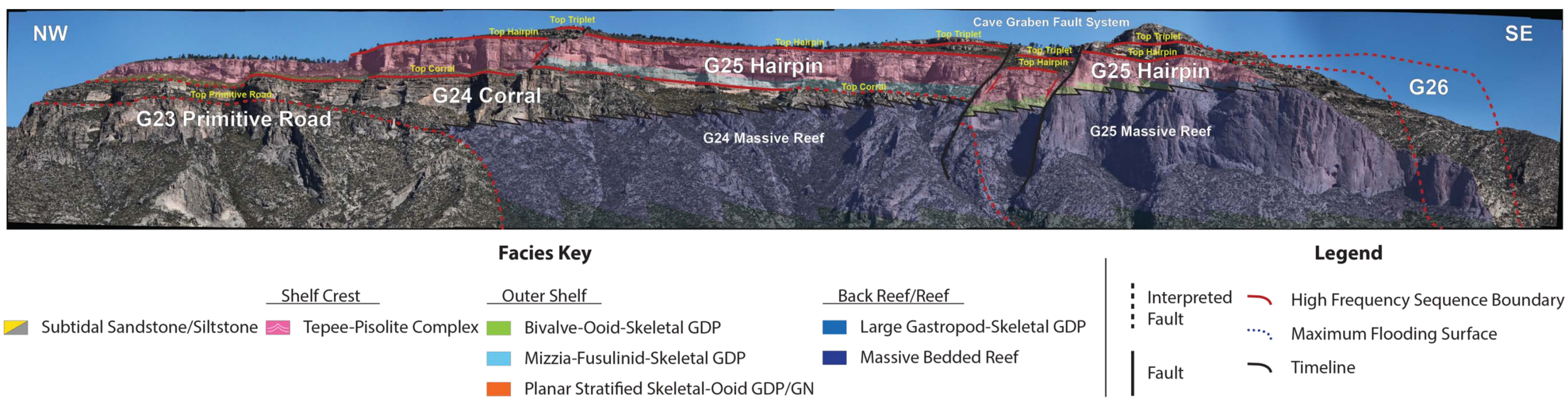

Figure 11. — Photomosaic of the North wall at the mouth of McKittrick Canyon near the visitor center. G23-G27 sequence boundaries are delineated with the G25 and G26 rollovers being projected into space showing their interpreted extent. Depositional environments ranging from the shelf crest to the foreslope are revealed in this overview perspective of the North wall. Note the extent of the CGFS is interpreted based on high-frequency cycle mapping along the graben.

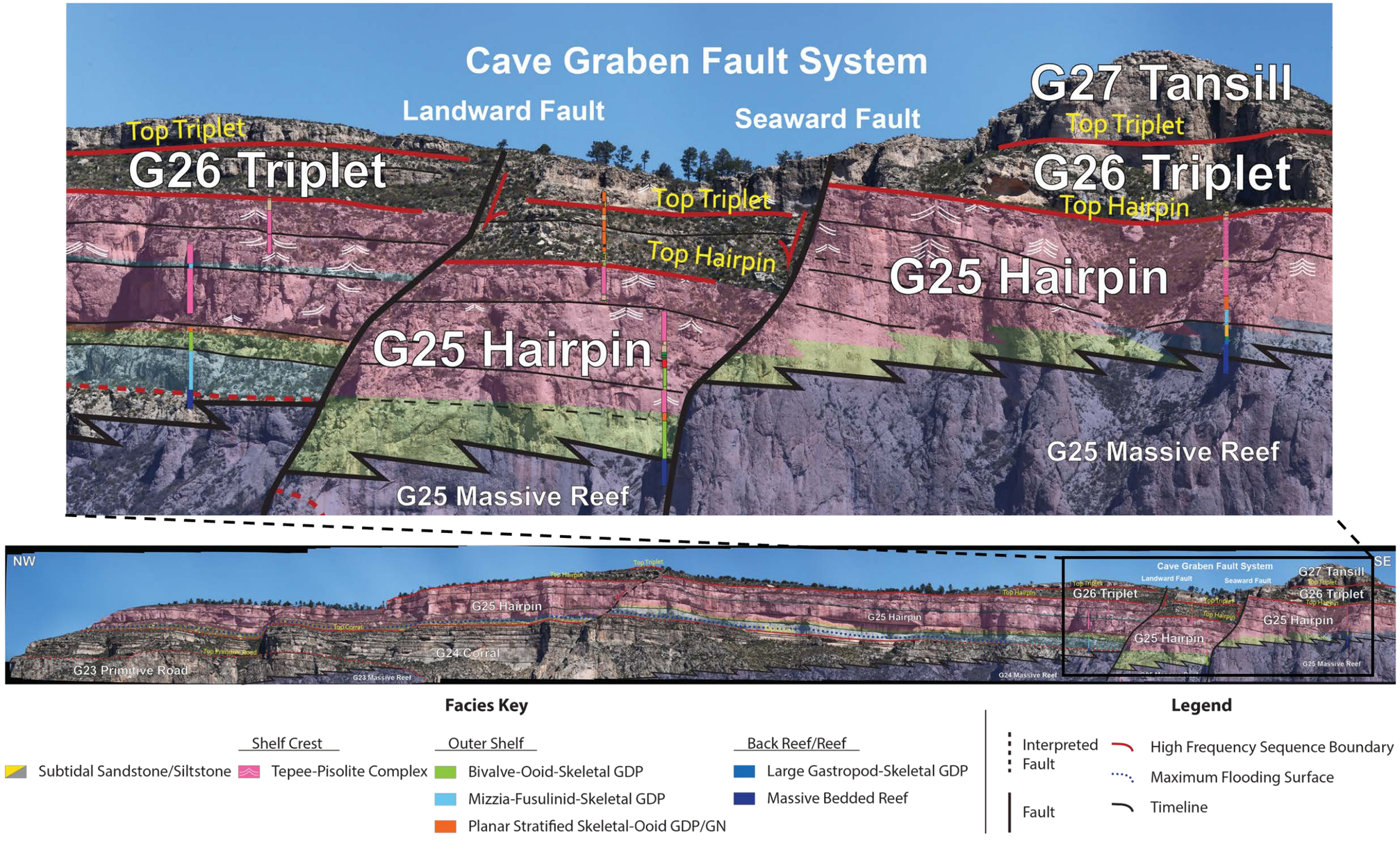

Figure 12. — Photomosaic of the North wall at the mouth of McKittrick Canyon near the visitor center. This perspective highlights the superimposed sections onto the outcrop and the packages identified within the G25 HFS. The outcrop is highly three-dimensional which is reflected by stratal tracings that abruptly change in various areas.

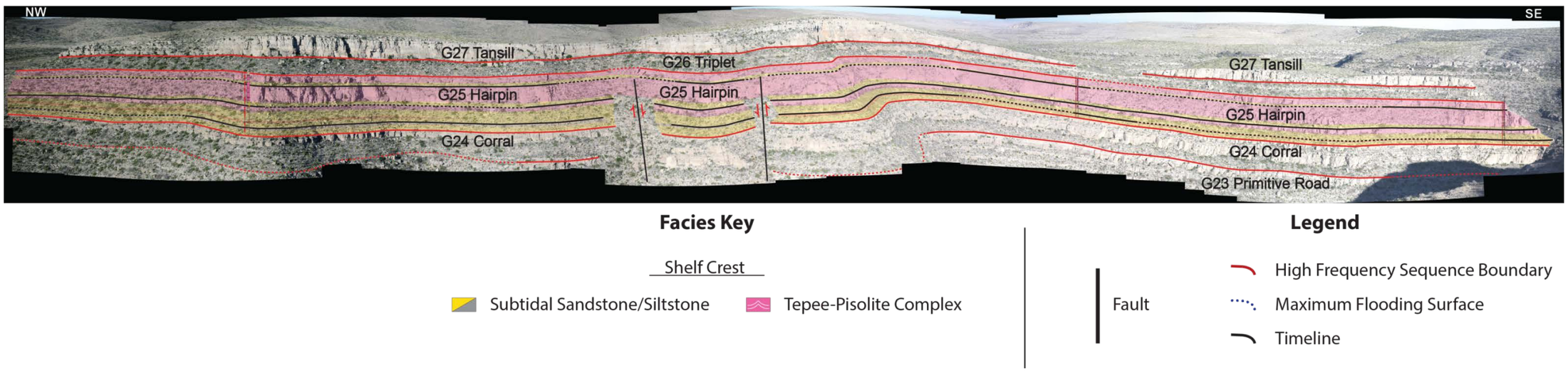

Figure 13. — Photomosaic of the North wall landward of the Walnut Syncline. Complete sections from G24-G26 are exposed while the G23 and G27 are incompletely exposed stratigraphic sections. Measured sections RS1-RS3 are superimposed from the NW to the SE along their respective locations along the wall. The only facies represented this far landward are the basal marine re-worked sands and facies associated with the shelf crest facies tract.

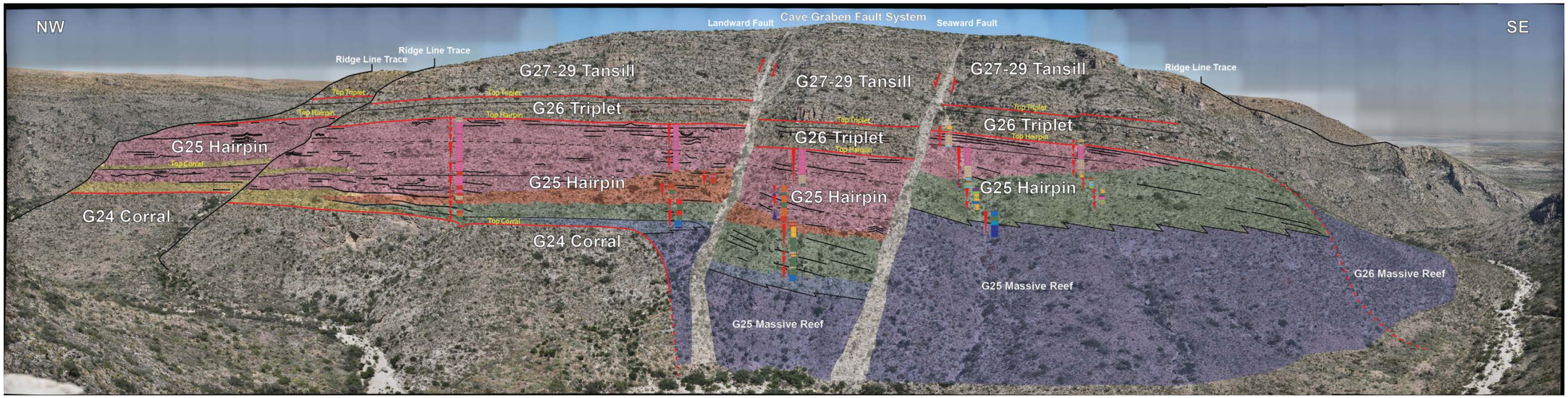

Facies Key

Shelf Crest
- Subtidal Sandstone/Siltstone
- Tepee-Pisolite Complex

Foreshore/Outer Shelf
- Cross-Bedded Ooid Grainstone
- Oncoid-Fusulinid Rudstone

Back Reef/Reef
- Large Gastropod-Skeletal GDP
- Massive Bedded Reef

Legend
- Fault
- High Frequency Sequence Boundary
- Maximum Flooding Surface
- Timeline

Figure 14. — Photomosaic of Rattlesnake Canyon along the Cave Graben Fault System. The intense three-dimensionality distorts perspective and thicknesses moving progressively younger through the sequence hierarchy. Black lines labeled as ridge line trace attempt to minimize confusion due to three-dimensionality of the canyon. Note loaction of the Cave Graben Fault System and increase of the outer shelf facies within the graben.

RESULTS AND DISCUSSION

FACIES TRACTS AND CONSTITUENT FACIES

A total of 14 distinct lithofacies were selected to encompass the depositional patterns observed in both McKittrick and Rattlesnake Canyons. The lithofacies are defined by incorporating field-observations made from lithology, texture, grain composition, and sedimentary structures, and are classified using the Dunham classification scheme (Tinker 1998; Dunham 1962) (Figure 15). A majority of these facies have been described previously by other geologists examining the upper Guadalupian strata in the Guadalupe Mountains (e.g., Dunham 1972; Babcock 1977; Yurewicz 1976; Hurley 1978; Bebout and Kerans 1993; Kerans 1995; Tinker 1998). The identified facies can be grouped into facies tracts that represent paleogeographic-bathymetric regions associated with distinct sediment supply, dominant grain types, sedimentary structures, and energy regimes. Facies tracts represent a genetically linked association of facies and are useful for sequence stratigraphic interpretation for the reason that individual facies are not always laterally continuous due to autocyclic processes, depositional topography, and position in the long-term relative sea level hierarchy (Tinker 1998). This study focuses on three main facies tracts: (1) shelf crest, (2) outer shelf, and (3) shelf margin. These facies tracts are analogous to the facies belts of Wilson (1975) and are adopted from the work of Pray (1977). Other workers have built upon and improved these facies tracts to include additional detail and depositional environments along an idealized dip profile of the Guadalupe Mountains (e. g., Kerans 1995).

Facies Tract	*Facies Name*	*Fabric*	*Dominant Grain Types*	*Sedimentary Structures*	*Diagenesis*	*Bedding Geometry*	*Interpretation*
Middle Shelf	Silty Fenestral Peloid Wackestone-Packstone	Wackestone-Packstone	Peloids, silt-sized quartz and feldspar, rare skeletal fragments	Sheet cracks, irregular microbial lamination, fenestrae	Extensively dolomitized, evaporite psuedomorphs after gypsum	Flat, sub-meter scale bedding, recessive	Intertidal flats and washover from the Shelf Crest
Shelf Crest - Low to Moderate Energy	Tepee-Pisoid Rudstone	Rudstone	Pisoids, composite grains, superficial ooids, ooids, peloids	Meter-scale TP-buckle structures, aragonite botryoids, fenestrae, irregular laminations	Displacive syn-depositional cement growth, dolomitization	Concave-upward buckled TP's, cliff-forming	Intertidal-supratidal island complex
Shelf Crest - Low to Moderate Energy	Fenestral Coated Grain-Peloid Laminite	Mud-dominated Packstone to Rudstone	Peloids, coated grains, pisoids, ooids, skeletal fragments, rare sand	Fenestrae, irregular microbial laminations	Dolomitization, blocky isopachus cement rimming pores	Planar sub-meter scale bedding	Intertidal Flats
Shelf Crest - High Energy	Ooid-Fusulinid Grainstone/Rudstone	Grainstone/Rudstone	Polydiexodina fusulinids, ooids	Seaward-aligned (imbricate) tests, vertical rosettes of tests, seaward-dipping cross beds, beachrock intraclasts, fenestrae	Meniscus cements, isopachus radiaxial cement	Planar meter-scale bedding	Very high energy foreshore
Shelf Crest - High Energy	Ooid Grainstone	Grainstone	Ooids after peloids, skeletal fragments; peloids, pisoids, fusulinids	Shingled seaward-dipping cross beds	Extensively dolomitized, oomoldic porosity, isopachus to pore-filling blocky cement	Planar meter-scale bedding	Foreshore
Middle-Outer Shelf	Dolomitic Siltstone to UVFSS	Lower very fine to upper very fine sandstone/siltstone	Quartz, feldspars, peloids, rare skeletal fragments, fusulinids	HCS, planar thin bedded, ripple laminated, bioturbated to massive, fenestrae, LLH stromatolites	Dolomitization of peloids, dolomite and clay cements	Recessive, slope-forming	Aeolian transport, transgressive subtidal to intertidal reworking
Outer Shelf - High Energy	Skeletal-ooid Grainstone	Grainstone	Ooids, forams, fusulinids, peloids, gastropods, crinoid fragments	multidirectionally cross stratified, planar, massive	Dolomitization, micritized grain rims	Planar to seaward dipping meter-scale bedding	High energy subtidal shoal
Outer Shelf - High Energy	Skeletal-Mizzia-fusulinid Grainstone/Rudstone	Grainstone/Rudstone	Polydiexodina fusulinids, Mizzia, forams, crinoids, oncoids, peloids	Low angle cross stratification to massive	Minor Dolomitization, micritized grains, isopachus bladed and radiaxial cements	Planar to seaward dipping meter-scale bedding	High energy subtidal intershoal
Outer Shelf - Low to Moderate Energy	Skeletal-Peloid-Oncoid Grain-dominated Packstone/Rudstone	Grain-dominated Packstone/Rudstone	Oncoids, peloids, bivalves, crinoids, forams	Massive, bioturbated	Minor Dolomitization, blocky rim cement	Seaward dipping meter-scale bedding	Moderate energy subtidal
Outer Shelf - Low to Moderate Energy	Oncoid-foram-peloid Mud-dominated Packstone	Mud-dominated Packstone	Peloids, forams, small oncoids, crinoids, bivalves	Massive, likely bioturbated	Minor Dolomitization	Seaward dipping meter-scale bedding	Moderate energy subtidal
Outer Shelf - Low to Moderate Energy	Foram-peloid Wackestone	Wackestone	Peloids, forams, crinoids	Massive	Minor Dolomitization	Seaward dipping meter-scale bedding	Low energy subtidal
Outer Shelf/Margin	Crinoid-Collenella Grain-dominated packstone	Grain-dominated Packstone	Collenella sponges, crinoids, bivalves, gastropods, peloids, bryozoan fragments	Massive	Minor Dolomitization, patchy brecciated dolomite at exposure surfaces	Seaward dipping, poorly bedded	Moderate energy backreef to reef crest
Shelf Margin	Sponge-algal Boundstone	Boundstone	Sponges, Tubiphytes, internal sediment, brachiopods	Massive with internal cavities filled with aragonite botryoid cement, internal sediment (geopedals)	Aragonite Botryoids, radiaxial fibrous cement	Massive, cliff forming, 10's of meters thick	Moderate energy shelf margin reef
Upper Slope	Interclast-skeletal Grain-dominated Packstone-to-Rudstone	Grain-dominated Packstone, Grainstone, Rudstone	Sponge fragments, brachiopod fragements, crinoid fragments, reef-derived clasts, fusulinids, forams, peloids, oncoids	Graded bedding, internal sediment in shells, slumping around large clasts	Minor Dolominitzation, blocky isopachus cement	Meter-scale bedding, steep basinward dip (>20 degrees)	Upper Slope with rock fall, grain flows, debris flows

Figure 15. — Facies plate from Harman (2011) showing facies tracts and constituent facies as well as associated fabrics, dominant grains, sedimentary structures, and interpretations of depositional environments. Though facies names are slightly different than facies provided from this study, this plate serves as a good summary chart of all grain types, fabrics, and sedimentary structures observed in McKittrick and Rattlesnake Canyons.

SHELF CREST FACIES TRACT

This facies tract is characterized by carbonate island complexes composed of tepee structures that form a topographic high-point with positive relief of up to 3 m and dip extents of 1-2.4 km throughout the Yates depositional profiles, and up to 2.5 km for the Hairpin specifically (Kerans et al. 2013). Deposition in this region ranges from supratidal to foreshore environments with the majority of deposition occurring in the former. This facies tract contains the highest energy deposits of the depositional profile (Kerans 1995). Pisoids are the dominant grain type found throughout this region, but outer shelf subtidal grains such as dasycladacean green algae and fusulinid foraminifera, in particular *Mizzia* and *Polydiexodina* respectively, are also incorporated. Key sedimentary structures indicative of position on the shelf crest are the ubiquitous tepees and sheet cracks as well as cross-bedding that occurs on the seaward flanks of the shelf crest. Cyclicity is difficult to interpret in this facies tract as most of the high frequency cycles are amalgamated especially within the tepee-belt. However, other workers have documented several “small-scale” centimeter to decimeter cycles preserved in tepee-belts of the Latemar Platform that would otherwise go unnoticed as they merge lagoon-wards into individual, meter-scale beds (Egenhoff et al. 1999; Peterhansel and Egenhoff 2008; Christ et al. 2012).

I. Tepee-Pisolite Complex

Characteristic grain types in this facies are pisoids but can also include carbonate grains from the outer shelf facies tract such as dasyclads, oncoids, fusulinids, and various skeletal grains which can be preserved as both fragmented and whole grains (Figure 16).

Figure 16. — Field photograph from McKittrick Canyon between M7 and M8 of vertically stacked tepees characteristic of the tepee-pisolite complex. Kyle McKenzie lays at the axis of the vertically stacked tepees for scale and reference of the outcrop. Tepee limbs are traced in white to show their anatomy.

Pisoids range in size from 2 mm to 5 cm. Diagnostic sedimentary structures include centimeter- to meter-scale tepees interbedded with sheet cracks. In the most landward portion of this facies tract, siliciclastic sediments are incorporated within sheet cracks and fractures along tepee cores. Sheet cracks filled with botryoidal marine cements near the center of the shelf crest can be preserved by dolomitization and displayed as fan-like needle-shaped molds of former aragonite (Melim and Scholle 2002). The most seaward tepees contain abundant marine sediments that fill any void present during formation.

This facies typically creates meter- to decimeter-scale resistant cliffs in areas where the tepees are the best developed, but can also be covered by scree in the most landward and seaward portions of this facies tract creating a sloping weathering profile. This facies represents deposition in the supratidal environment making it a cycle cap for upward-shallowing cycles.

II. Pisoid Rudstone

Pisoids range in size from 2 mm to 5 cm in this facies and can display normal and inverse grading (Figure 17). Grains can also be poorly sorted and fragmented. Bedding ranges from 10 to 60 cm and these pisoid beds are interbedded with fenestral boundstones and tepees within the tepee-pisolite complex. The lack of other grain types usually found in the shelf crest facies tract differentiates this facies from other units within the amalgamated cycles of the shelf crest.

This facies is interpreted to be deposited in depressions within individual tepees where precipitation from hypersaline ponds is prominent. Pisoid rudstones can also

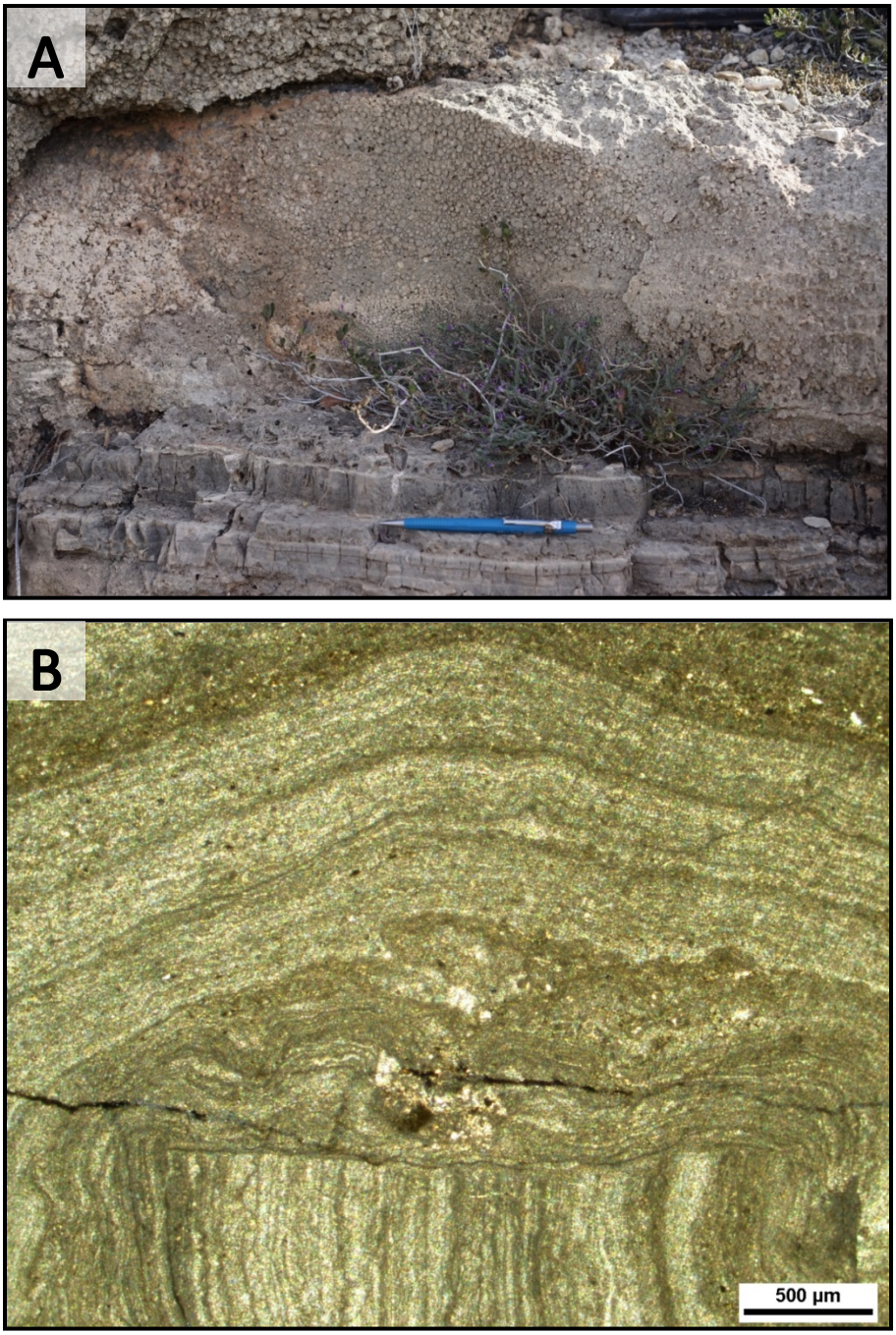

Figure 17. — A.) Field photograph from Rattlesnake Canyon of a pisoid rudstone between R2 and R3. The pencil sits on interbedded sheet cracks filled with botryoidal cements. Note the inverse grading of the pisoids. B.) Photomicrograph of a younger pisoid at the upper half of the frame nucleating on an older, fragmented pisoid on the bottom half of the frame.

represent cycle caps of higher order cycles similar to those defined by Christ et al. (2008) in the Latemar Platform.

III. Fenestral Boundstone

Peloids, pisoids, ooids, coated grains, and skeletal fragments are the most common grain types in this facies. Fenestrae that are commonly filled with blocky calcite cements are the diagnostic sedimentary structure throughout this lithofacies (Figure 18). Sheet cracks can also be found. Fenestral beds are tabular sub-meter to meter-scale units. The absence of irregular microbial to cryptalgal laminations distinguishes this from the algal laminated boundstone facies described below. Depending on position within the dip profile, this facies can contain up to 30% siliciclastic sediments (Figure 19).

Fenestral units represent cycle tops for cyclic accumulation on the flanks of the shelf crest where deposition in the intertidal environment is dominant.

IV. Algal Laminated Boundstone

Smooth to crinkly, irregular microbial to cryptalgal laminations are the dominant sedimentary structure of this facies. Grain types are similar to those in fenestral boundstones. Beds are typically recessive and on the order of centimeters in thickness. Mixing with siliciclastics is common where the most proximal sections are measured.

Deposition is interpreted to be in the intertidal environment where energy regimes are low to moderate.

Figure 18. — Field photograph from McKittrick Canyon between M8 and M9 of a fenestral boundstone with a pencil marking the base. Thickness is approximately 10-20 cm and elongate fenestrae are filled with cement.

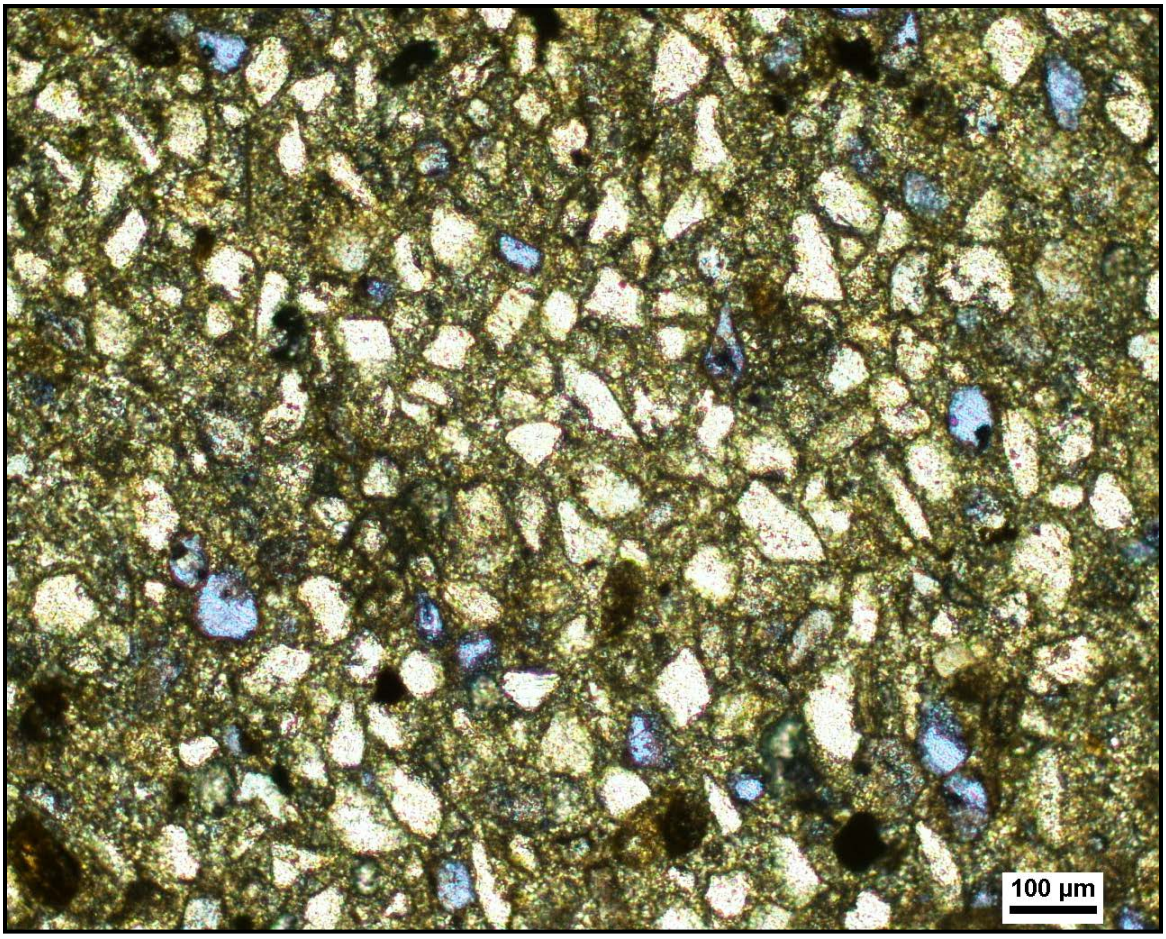

Figure 19. — Photomicrograph of sheet crack filled with 30% siliciclastic sediments within a fenestral boundstone. Sample taken from landward sections between M1 and M2 in McKittrick Canyon.

V. Fenestral Laminite Rudstone/Conglomerate

Units within this facies are displayed as fragmented blocks that have undergone some degree of deformation as evidenced by irregular folding within individual sheet cracks (Figure 20). Similar to other facies, botryoidal marine cements fill individual sheet cracks. Blocks appear to be floating in the matrix of the host rock.

This facies is key to the refined interpretation of the G25 HFS dip profile, specifically the foreshore beach environment. Individual fenestral blocks are believed to be deposited as intraclasts analogous to the modern, rocky beaches of Turks and Caicos and San Salvador in areas such as Donna Cut and Grouper's Gully respectively. This facies is best exposed in the Hairpin in McKittrick Canyon and in the G27 Lower Tansill in Walnut Canyon; whereas in Rattlesnake Canyon it is rare to absent.

VI. Cross-Bedded Ooid Grainstone

Ooids are the dominant grain type, but not exclusively, as similar sized grains such as *Mizzia* can be mixed with peloids, skeletal grains, and even fusulinids. Pores can occur as interparticle or oomoldic and are typically filled with isopachous to blocky cements. Swash laminations are very common in this facies (Figure 21). Bedding geometries are planar and are on the order of meter-scale in thickness.

Subtidal grains can be transported to shore by storm or other high energy events. Deposition is exclusive to the foreshore environment where some of the highest energy from incoming waves is concentrated. This facies is better displayed in Rattlesnake Canyon than in McKittrick Canyon and typically weathers to resistant benches.

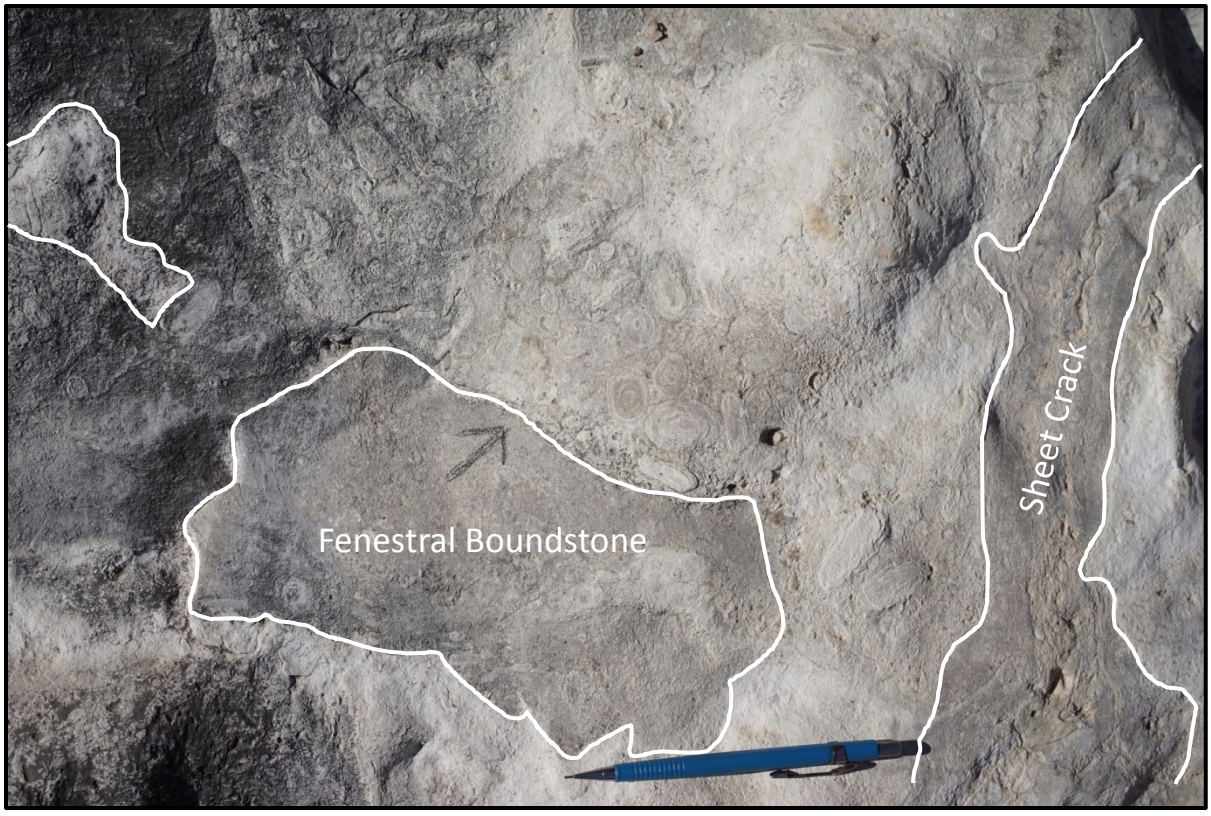

Figure 20. — Field photograph from McKittrick Canyon between M8 and M9 of a fenestral laminite Rudstone/Conglomerate. Note the white to tan fenestral blocks and sheet cracks that have been deformed and fragmented floating in the gray matrix of the host rock.

Figure 21. — Field photograph of a cross-bedded ooid grainstone in Rattlesnake Canyon. Cross beds are swash laminated. Jake for scale at the lower right side.

OUTER SHELF FACIES TRACT

This region is bounded updip by the tidal-flats and grainstone shoals of the shelf crest and down dip by shelf edge reefal deposits (Kerans 1995). Within the Yates Formation, outer shelf dip-widths range from less than 100 m to nearly 1.5 km (Tinker 1998). The G25 HFS contains the narrowest outer shelf of the Yates Formation measured to be less than 90 m. General deposits in this region represent open-marine environments ranging in depth from near sea level to approximately 60 m (Osleger and Tinker 1999). It is important to note, however, that outer shelf existed in depths of <30 specifically in the Hairpin. Because the deepest shelfal sediments were deposited across the outer shelf, the most landward position of this facies tract is used to define the maximum flooding at the high frequency sequence and composite sequence scale (Rush and Kerans 2010). This facies tract is comprised of oncoid-dasyclad-skeletal-fusulinid mud-dominated to grain-dominated packstones that are medium- to thick-bedded. The most seaward deposits in this region can be massive bedded making interpretation of the boundary between the outer shelf and the shelf margin reef difficult. Bedding planes in this facies tract display a distinctive 2 to 10° basinward inclination that has resulted from both differential compaction and primary depositional dip (Tinker 1998; Hunt et al. 2002; Kerans et al. 2013).

I. Planar Stratified Skeletal-Ooid Grain-Dominated Packstone to Grainstone

This facies consists of fragmented and whole skeletal grains, ooids, and peloids (Figure 22). Pores are filled with isopachus to blocky cements. Planar stratification ranges

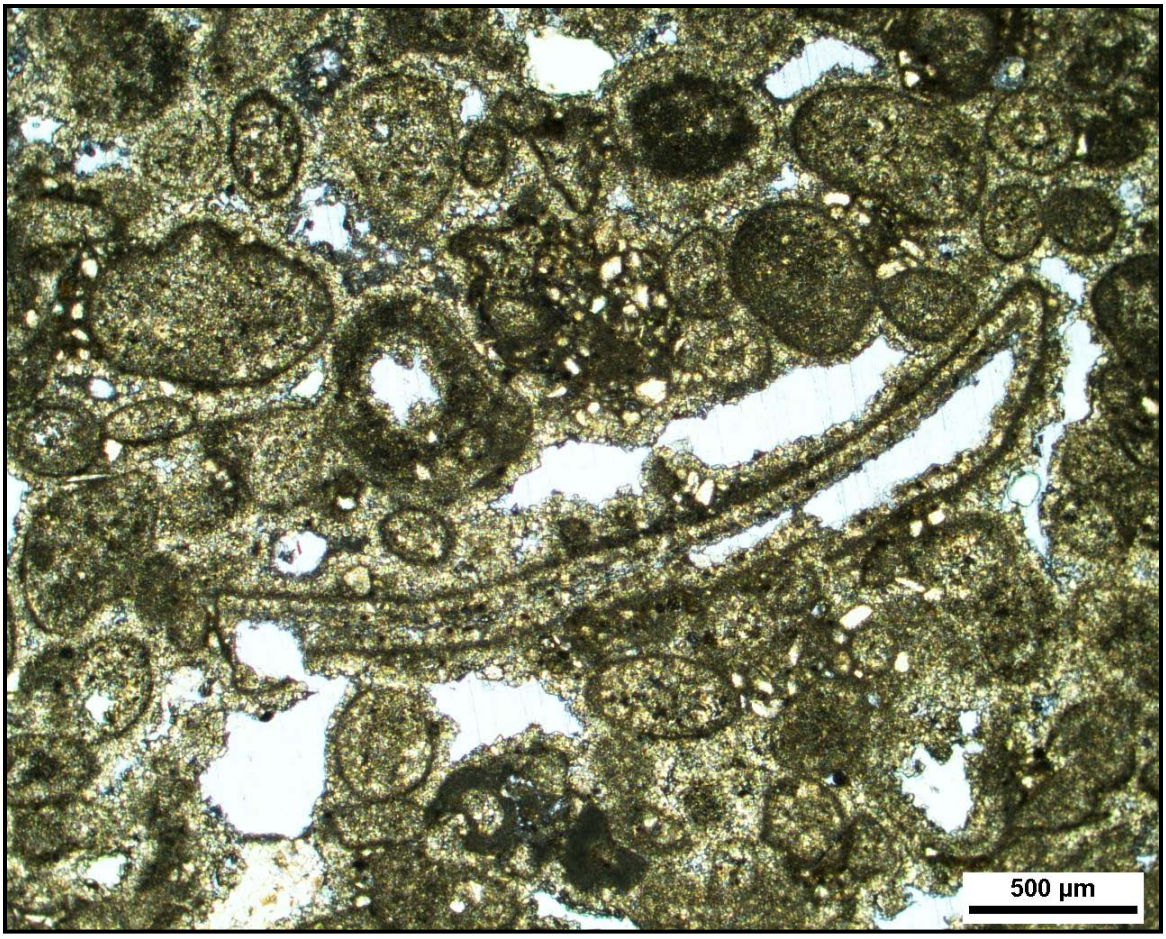

Figure 22. — Photomicrograph of a planar stratified skeletal-ooid grain-dominated packstone/grainstone taken from the overlying G26 HFS. Note the micritic

in appearance from faint to obvious and can be multidirectional. Beds range in thickness from 0.5 m to sub-decimeter-scale.

Deposition ranges from the shallow subtidal to intertidal regions associated with moderate to high energy regimes within the most proximal outer shelf. Landward of this facies are cross-bedded ooid grainstones while bivalve-ooid-skeletal grain-dominated packstones are found seaward. This facies typically forms resistant benches similar to the cross-bedded grainstones.

II. Bivalve-Ooid-Skeletal Grain-Dominated Packstone

Ooids, bivalves, skeletal grains, and coated grains characterize this facies (Figure 23). The absence of planar stratification distinguishes this facies from the lithofacies described above (Planar Stratified Skeletal-Ooid Grain-Dominated Packstone to Grainstone); though they are texturally similar. Bedding geometries are planar and are meter-scale in thickness

This facies is deposited throughout the outer shelf ranging from shallow subtidal to deeper (10 to 60 m) water depths (Tinker 1998). The presence of ooids implies proximity to shallow subtidal to intertidal settings where ooids are most prevalent.

III. Skeletal-Peloidal Grain-Dominated Packstone

This facies is grain supported with fragmented and whole skeletal grains and peloids. The lack of ooids differentiates this lithofacies from the facies above (Bivalve-Ooid-Skeletal Grain-Dominated Packstone). Beds are medium- to thick-bedded and display tabular geometries.

Figure 23. — Field photograph from McKittrick Canyon of a bivalve-ooid-skeletal grain-dominated packstone.

Sparse amounts of ooids suggests deposition in a more subtidal setting than the aforementioned facies. This facies is not indicative of a certain environment within the outer shelf as it can be deposited throughout the entire facies tract.

IV. Mizzia-Fusulinid-Skeletal Grain-Dominated Packstone

Mizzia and *Polydiexodina* are the most dominant grain type; though these grains can be mixed with other skeletal grains, peloids, and oncoids. Micritized grains and isopachus cements compose the matrix. Imbricated tests of *Polydiexodina* fusulinids are common but also can occur as chaotic in random orientation (Figure 24). Bedding ranges from centimeter- to meter-scale.

Grains within these facies can be incorporated into intertidal and supratidal facies as a result of high energy events such as storms, but origins of them are interpreted to be in the shallow subtidal outer shelf associated with moderate energy.

V. Oncoid-Fusulinid Rudstone

Oncoids and fusulinids characterize this facies, but not exclusively, as other skeletal grains and peloids are documented (Figure 25). Planar geometries of thin- to thick-bedded units commonly occur. Fusulinid tests can occur aligned in a specific orientation or as random.

This facies is commonly interpreted to be a marine flooding surface which aids as a cycle base when cycle-stacking patterns are analyzed and basal sandstones are absent. Grains from this lithofacies can also be incorporated into shallow subtidal to supratidal facies.

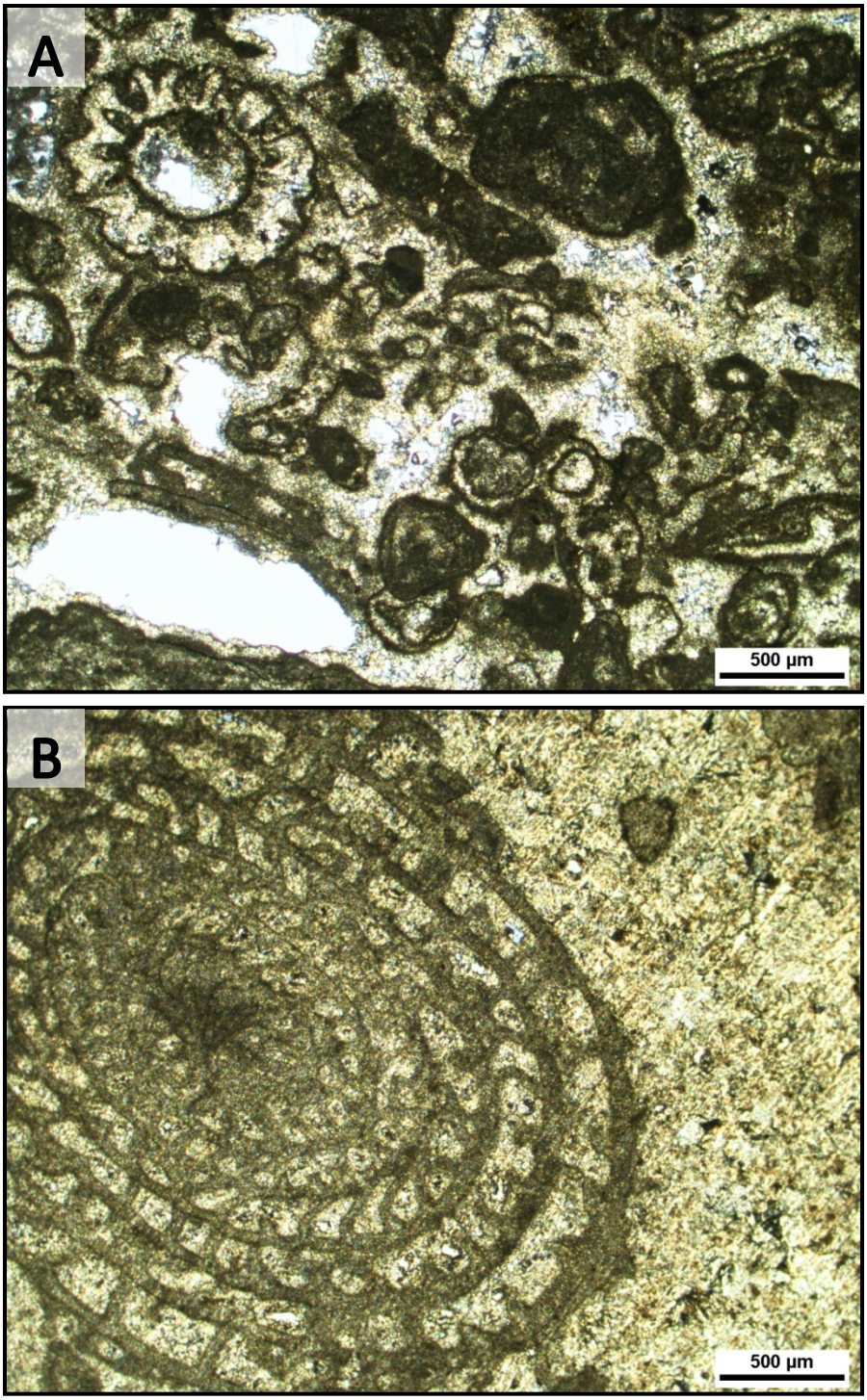

Figure 24. — A.) Photomicrograph of *Mizzia*-fusulinid-skeletal grain-dominated packstone with large *Mizzia* in upper left corner. B.) Photomicrograaph of fusulinid within the same facies as above. Note many of the grains have been micritized.

Figure 25. — Field photograph from McKittrick Canyon within M7 of an oncoid-fusulinid rudstone.

VI. Large Gastropod-Skeletal Grain-Dominated Packstone

Bellerophontid gastropods make up the dominant grain type of this facies and average in size from 2-5 cm (Figure 26). Additional, grains include crinoids, bivalves, and bryozoans and occur as both fragmented and whole. Bedding ranges from thick to massive and molds of large gastropods are common. The best exposure of this facies is on the Permian Reef Trail near Stop 24 of Bebout and Kerans (1993).

Deposition of this facies represents the most subtidal part of the outer shelf where a sharp boundary with the reef margin is gradational.

SHELF MARGIN FACIES TRACT

Most of the data and characteristics for this facies tract are adopted from previous work; though the reef and key frame-builders were documented while measuring sections in the field. This region begins at the interfingering outer shelf and ends at a transitional zone where in situ reef-margin deposits interfinger with detrital foreslope deposits (Kerans et al. 2013). Four distinct elements in the shelf margin facies tract are (1) *in situ* baffling and frame-building organisms; (2) encrusting and binding organisms; (3) internal sediment; and (4) extensive submarine cements (Babcock and Yurewicz 1989). The dominant morphologic feature of this facies tract is the massive Capitan reef characterized by a steep subvertical wall. The growth angle of the reef reaches its greatest value during G25 time recording significant aggradation of the reef margin (Osleger and Tinker 1999). Key frame-building fauna and early lithification due to marine cementation yield the opportunity for the Capitan reef to build up to its shallowest depths ranging from 10-60 m (Tinker 1998; Saller 1999).

Figure 26. — Field photograph from McKittrick Canyon near the base of M11 of large gastropod-skeletal grain-dominated packstone. Note the moldic porosity produced by the *Bellerophontid* gastropods.

I. Massive Bedded Reef

This facies is characterized by key framework-constructive fauna such as calcareous sponges, *Archaeolithoporella*, *Collonnella*, *Tubiphytes*, and bryozoans as well as botryoidal marine cements (Figure 27). Common sedimentary structures include geopetal sediment infills of varying composition. Coloring in outcrop ranges from light to dark grey and bedding is nonexistent.

This facies can be delineated in gigapan photomosaics and in lidar due to its massive bedding. Marine cementation and construction by framework building fauna aid in development of this facies. Cements found in the reef are similar to the botryoidal cements within the supratidal facies tract.

MCKITTRICK CANYON

I. Tepee Characteristics

Some of the best developed tepee complexes are apparent in the largest shelfal cliff faces along McKittrick Canyon. Crest to crest lateral dimensions for the tepees are on average 15-20 m but can vary depending on position along the dip-oriented profile (Figure 28) (Table 1). Height of individual tepees ranges from decimeters up to 2 m with the larger of these structures occurring at the center of the shelf crest. Tepees documented in McKittrick Canyon can be filled with siliciclastics, botryoidal marine cements, and marine sediments reflecting position along the shelf crest ranging from proximal to distal depositional environments respectively. Beds 30-50 cm thick filled with 2-5 cm pisoids alternate with sheet cracks and tepees in the center of the shelf crest facies tract where the

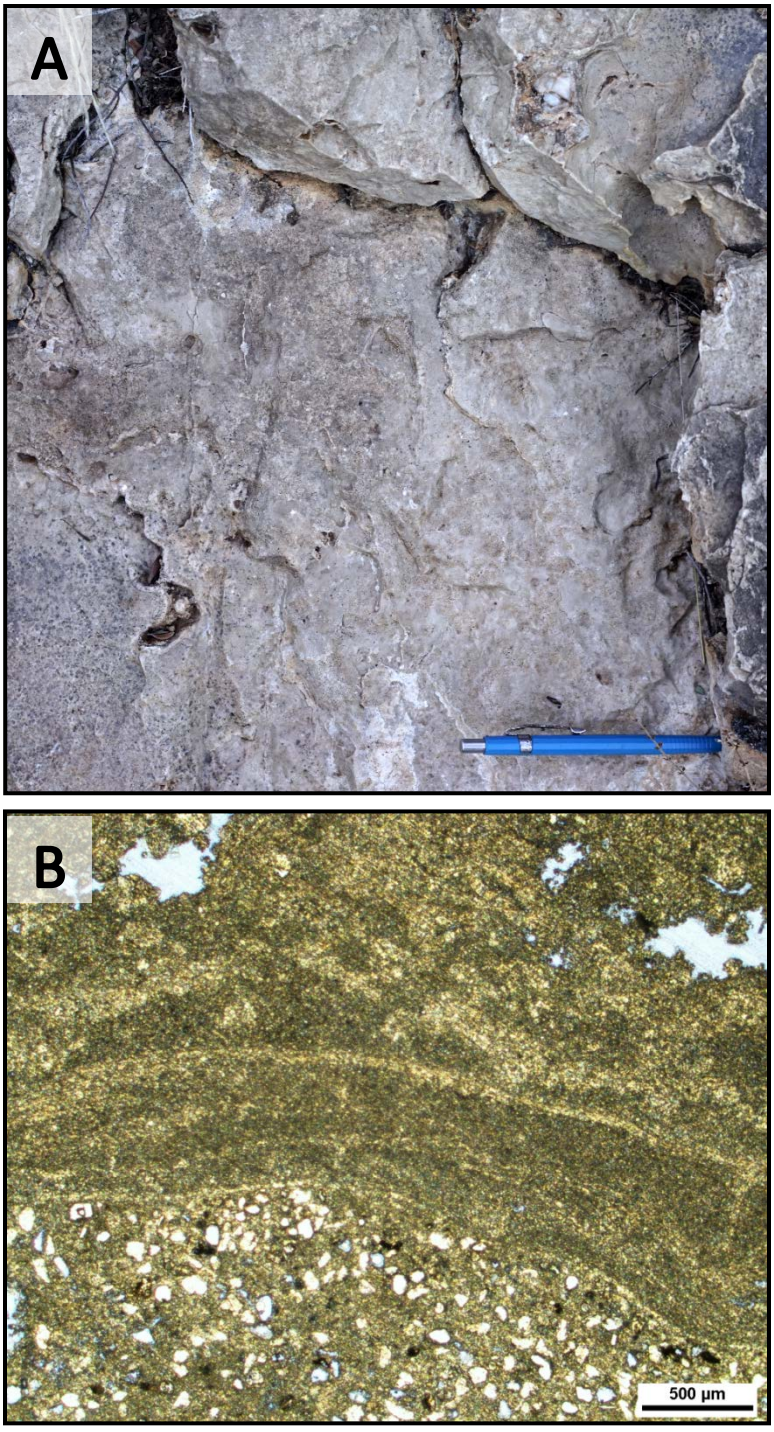

Figure 27. — A.) Field photograph of massive reef. Fauna include encrusting algae and byozoans. B.) Photomicrograph of reef showing encrusting organisms and infilled quartz sediments.

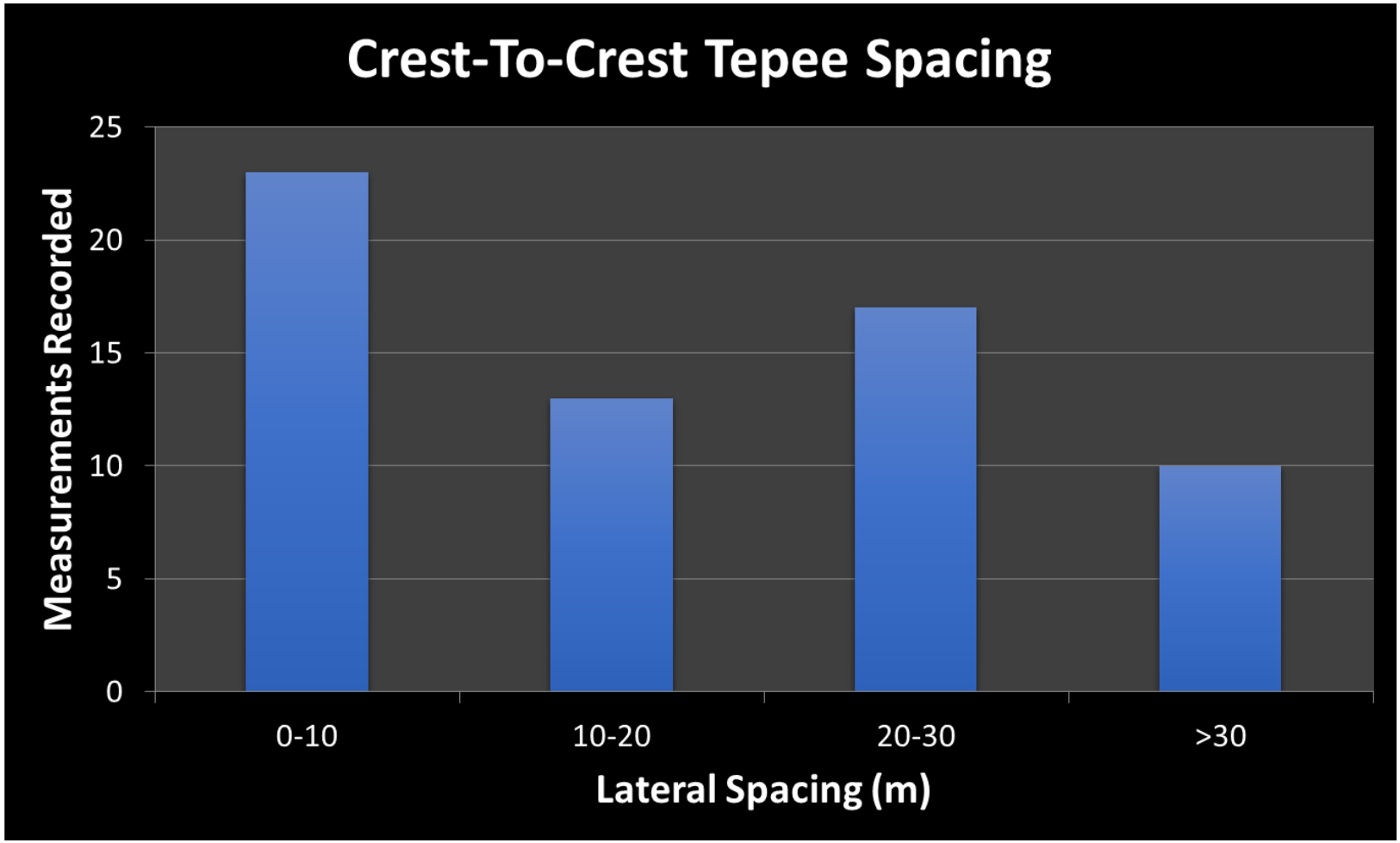

Figure 28. — Bar graph showing crest-to-crest spacing between tepees. Measurements were binned with respect to lateral spacing recorded in meters along the x-axis. Measurements were acquired from gigapans measured in the lidar as well as measured using a jake in the field.

Measurement (#)	Spacing (m)
1	1.3
2	1.4
3	1.7
4	1.8
5	1.9
6	2.5
7	3.5
8	3.6
9	3.7
10	3.7
11	3.7
12	4
13	4.7
14	5.2
15	5.3
16	5.7
17	5.8
18	6
19	6
20	6.3
21	6.5
22	9.4
23	10
24	10.9
25	11
26	11
27	11.1
28	11.5
29	12.5
30	12.5
31	12.6
32	17.3
33	17.8
34	19
35	19.4
36	19.7
37	20.2
38	20.6
39	21.4
40	22.7
41	23
42	23.4
43	24
44	24
45	24.2
46	25.3
47	25.9
48	26.3
49	27
50	28
51	28
52	28
53	28.9
54	31
55	31
56	32
57	33
58	34
59	34.7
60	35
61	36
62	38
63	40.5
Average	16.76
Std. Dev.	11.44

Table 1. — Measurements from McKittrick Canyon recording the lateral spacing between tepee crests. Measurements are sorted from smallest to largest values.

tepee-pisolite complex is best developed. Individual pisoids decrease in size (<2 cm) with interbedded pisoid rudstones thinning (5-20 cm) and occurring less frequently on the flanks of either side of the shelf crest. The degree of siliciclastic mixing within the tepee belt decreases moving basinward. The two most landward measured sections contain tan to light-orange siliciclastics of predominately quartz composition incorporated within fractures and in sheet cracks (Figure 29). Measured sections from the Cave Graben Fault System (CGFS) to the rollover of the G25 HFS (M5-M10) document grains from the subtidal outer shelf incorporated into the flanks of the tepee complex. These subtidal grains are predominately skeletal grains, fusulinids, oncoids, and bryozoans with relative abundance of each, as ordered, increasing towards the shelf margin. Subtidal sediments are interpreted to be transported to supratidal environments via high-energy events such as storms. The capacity for high-energy required for transportation of subtidal grains should be readily available considering the proximity of the shelf crest to the shelf margin at the expense of the narrow outer shelf.

II. Measured Sections and Correlation

A total of 11 measured sections focus on the G25 HFS, and various sections record strata from the underlying G24 Corral HFS as well as the overlying G26 HFS (Lower Triplet). Correlation across photomosaics combined with high-frequency cycle mapping from measuring sections confirm the presence of the CGFS extending into McKittrick Canyon. Measured section 1 (M1) represents the most landward extent of the G25 HFS but does not display the entire G25 HFS as it is limited to the erosional boundaries of the outcrop. The most distal extent is documented within measured section

Figure 29. — Field photograph taken by Jeff Sitgreaves showing a tepee complex where M1 was obtained in McKittrick Canyon. Light orange to tan siliciclastics fill in voids created by fracture networks and sheet cracks represented by the opaque yellow paint group. My hand is placed near the apex of a tepee.

11 (M11) represented by massive outer shelf and reef facies. Measured section 4 (M4) is interpreted to be the nearest to the center of the shelf crest facies tract as it displays the thickest (35 m) portion of the tepee-pisolite complex. Vertically stacked tepee complexes are most prominent in this region and can form resistant cliff faces of up to 40 m (Figure 30). Correlation between digitized measured sections produces a dip-oriented cross section of the McKittrick Canyon strata revealing G25 platform morphology, facies tract dimensions, and facies proportions placed into a sequence stratigraphic context (Figure 31). This cross section was hung on multiple datums to compensate the increasingly erosional boundaries of outcrops progressively landward as a result of the gentle dip of the of the Guadalupe Mountains to the east. The top Hairpin sequence boundary served as the most obvious datum but begins to roll downward transitioning to the outer shelf.

III. Stratigraphy and Cyclicity

An analysis of the McKittrick Canyon cross section utilizing stratal geometries, cycle stacking patterns, cycle symmetry, and facies proportions both at the high-frequency cycle- and sequence-scale provides a unique solution for characterization of the Hairpin HFS. While a near-complete clinothem of the G25 HFS exists, the actual location of the G25 shelf margin/reef wall had to be projected based on existing outcrop and lidar data as well as published information (Bebout and Kerans 1993). The cross section reveals an asymmetric high-frequency sequence comprising a thin (5 to no more than 10 m) transgressive systems tract (TST) and a thick (40-45 m) highstand systems tract (HST). The majority of the TST consists of massive marine reworked siliciclastic sands, as well as thin- to medium-bedded fenestral boundstones and peloid-skeletal grain-

Figure 30. — Field photograph taken by Charles Kerans displaying the massive vertically stacked tepee walls within McKittick Canyon near measured section M4. I stand on the first resistant bench for scale.

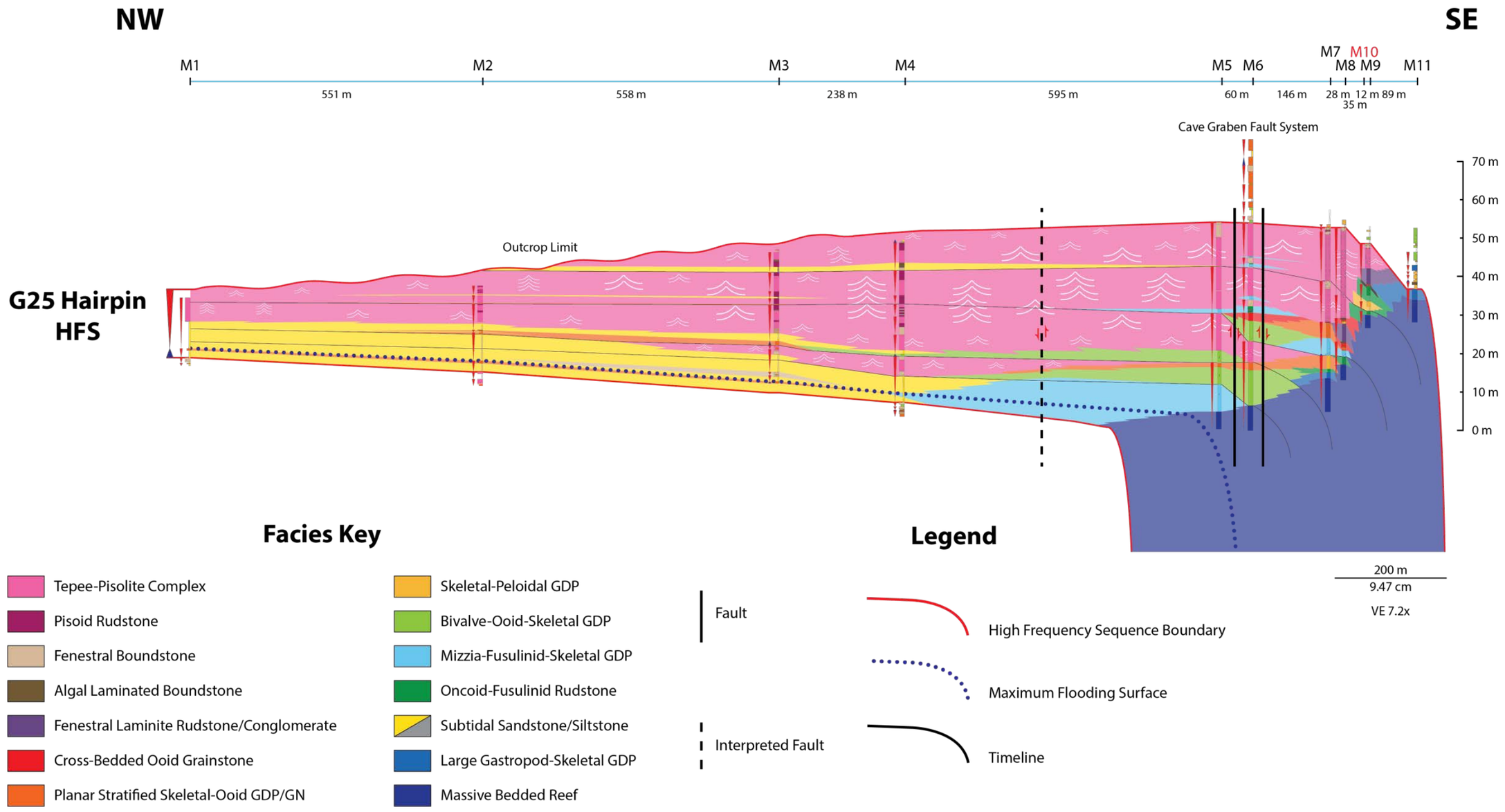

Figure 31. — Correlated cross section incorporating measured sections acquired in McKittrick Canyon. The G25 Hairpin is an asymmetric high-frequency sequence made up of 5 cycle sets. Tepee location and sizes are displayed schematically and represented by white inverted “V” –shaped lines. Note that the largest tepees are concentrated within the HST of the G25 and decrease in size approaching the sequence boundary indicating a decrease in accommodation.

dominated packstone. The HST is dominated by carbonate deposition, specifically the shelf crest tepee-pisolite complex. Cycle sets interpreted from the high-frequency cyclicity in the cross section make up 5 distinct units traced on the photomosaics that thin landward and expand seaward.

IV. Facies Tracts Dimensions

Based on data within McKittrick Canyon, this study proposes a new depositional profile that begins at the landward flank of the shelf crest because of the absence of data from the middle shelf environment. The shelf crest facies tract expands to 2.2 km based on measurements from the dip-oriented cross section. The seaward side of the shelf crest is characterized by the fenestral laminite rudstone/conglomerate and ooid grainstone facies. This type of shoreline differs from the classic foreshore-upper shoreface profile documented in areas such as the island of West Caicos, BWI (Kerans 2015; Danger in progress). Considering the proximity to the high-energy wave action at the shelf margin, a high-energy rocky shoreline is inferred. Other modern analogs can be drawn from Grouper Gully in San Salvador, Bahamas where the shoreline consists of early lithified strata and a thin (approximately 250 m) outer shelf (Figure 32). The outer shelf facies tract from the McKittrick Canyon cross section is measured to be 80-90 m in dip-width and transitions to the massive Capitan reef.

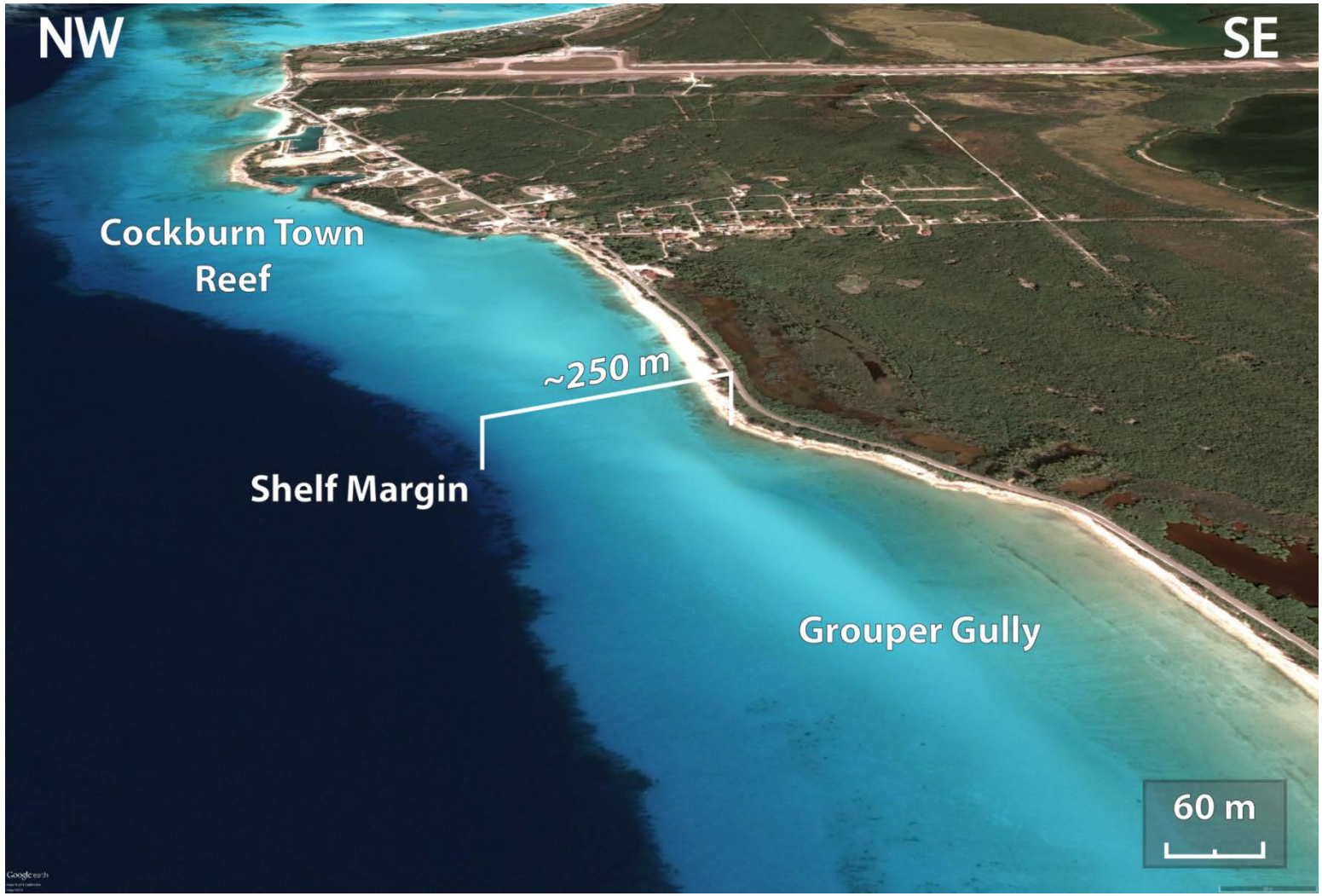

Figure 32. — Google Earth image of San Salvador, Bahamas dislpaying the width of the outer shelf near Grouper Gully.

RATTLESNAKE CANYON

I. Tepee Characteristics

The nature of tepees and the tepee complex in Rattlesnake Canyon resembles tepees documented in McKittrick Canyon. Crest to crest lateral spacing between tepees ranges between 10-20 m with anomalous measurements both above and below this range due to variability in the orientation displayed in outcrop along the tepee belt. The most landward tepees are mixed with siliciclastics; though siliciclastics in this area are dark red to purple in color. Moving seaward, the siliciclastics interbedded within the tepee complex change to the more common tan to light orange color. Interbedded units of 20-60 cm pisoid rudstones decrease in frequency with increased distance away from the center of the shelf crest. Pisoid rudstones are thinnest (5-20 cm) near the flanks of the shelf crest, while fenestral boundstones maintain meter-scale thickness throughout the shelf crest. Measured sections RS5-RS10 capture skeletal grains, fusulinids, oncoids, and *Mizzia* incorporated into the tepee belt.

II. Measured Sections and Correlation

In Rattlesnake Canyon, 10 measured sections record high-frequency cycles within the G25 HFS as well as the top G25 sequence boundary. Nearly all measured sections were taken upwards to include the lower Triplet sandstone of the G26 Triplet HFS, which provided a major datum for generation of a stratigraphic cross section (Figure 33). Stratal tracings and markers representing cycle tops in the lidar data aided in illustrating the depositional topography giving the cross section a more accurate architecture. The most landward sections (RS1-RS4) display 3 distinct units of carbonate and siliciclastic

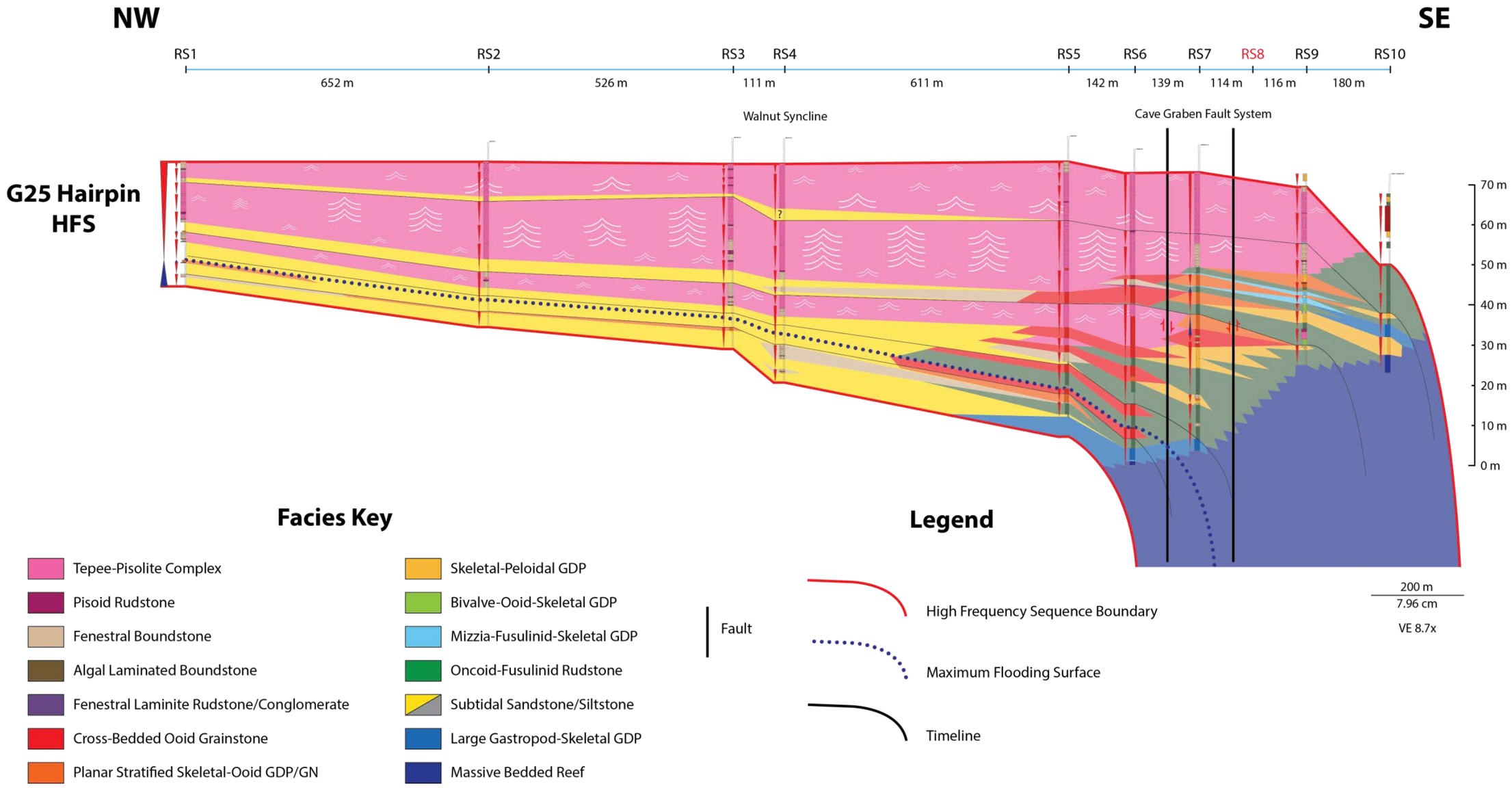

Figure 33. — Correlated cross section incorporating measured sections acquired in Rattlesnake Canyon. The G25 Hairpin is an asymmetric high-frequency sequence made up of 5 cycle sets. Tepee location and sizes are displayed schematically and represented by white inverted “V” –shaped lines. Note that the largest tepees are concentrated within the HST of the G25 and decrease in size approaching the sequence boundary indicating a decrease in accommodation.

deposition related to reciprocal sedimentation. Basal siliciclastics decrease in thickness shoaling upwards through the G25 which may be due to the increasing thickness of the tepee complex from early to late stages of the HST. These sands also thin near the shelf edge where they eventually bypass the subvertical Capitan reef wall and form onlapping beds at the toe-of-slope. The center of the shelf crest is inferred to be between RS4 and RS5 as they document maximum thickness (35-45 m) of the tepee-pisolite complex. Within the Cave Graben, outer shelf facies thicken relative to sections on either side of the landward and seaward faults bounding the graben. This affirms the work done by Mathisen (2014) that reports an overall increase in thickness of up to 25% implying syndepositional fault-related growth in the G25 HFS. The most seaward measured sections (RS9 and RS10) could not accurately define the Lower Triplet Member as it expands near the margin to additional high-frequency cycles of mixed carbonate-siliciclastic compositon rather than a strictly massive bedded sandstone. RS9 and RS10 document multiple upward-shallowing high-frequency cycles of outer shelf packstones; RS9 records the last appearance of the tepee-pisolite facies.

III. Stratigraphy and Cyclicity

The Rattlesnake Canyon cross section permits sequence stratigraphic interpretation at both the high-frequency cycle- and sequence-scale. This cross section reveals an asymmetrical G25 HFS made up of 5 upward-shallowing cycle sets and multiple high-frequency cycles similar to those from McKittrick Canyon. A thin (5-15 m) TST predominately consists of basal sands with minor submeter beds of grain-dominated packstones and fenestral boundstones. The HST contains progressively thinner lenses of

basal sandstones with carbonate deposits increasing in thickness in younger cycles until accommodation is reached during the late HST. Cycle sets that make up 5 distinct units are apparent and traceable along the gigapan and represent timelines across the cross section. Tepees are observed just above the most subtidal facies deposited across the shelf which is interpreted as the maximum flooding surface. This concurs with the work of Kerans and Tinker (1999) that proposed tepee formation occurring as a result of high shelf accommodation during the late TST or early HST.

IV. Facies Tracts Dimensions

Facies tract dip-widths and associated facies differ from results based on data from McKittrick Canyon only slightly. No data was collected from the G25 middle shelf environment due to the absence of existing exposures. However, exposures of shelf crest facies extended further landward than those in McKittrick Canyon recording a dip-width of just over 2.4 km of the shelf crest facies tract; though it may be even greater as the most landward extent of this facies tract is nonexistent in outcrop. The narrow 100-130 m outer shelf documented in Rattlesnake Canyon is still significantly more compressed than other high-frequency sequences within the Capitan system but slightly wider than the dimensions from McKittrick Canyon. The presence of the fenestral lithoclast conglomerate facies and abundant *Mizzia* is found throughout shoreline facies in cross-bedded ooid grainstones. Subtidal grains are also incorporated within the tepee belt shown in the most seaward measured sections. Differences between Rattlesnake and McKittrick Canyons include the presence of the fenestral lithoclast conglomerate facies in McKittrick Canyon and a more prominent foreshore in Rattlesnake Canyon. Dip

profiles along both canyons would still include a wider shelf crest than that of the over- and underlying sequences that transitions into a high-energy shoreline indicated by the abundance of *Mizzia* and other subtidal grains recorded within intertidal to supratidal facies. The interpretation of a high-energy shoreline can be affirmed by the narrow (100-130 m) outer shelf width. A 100 m wide outer shelf of 5-20 m depth would be an inadequate buffer to incoming wave-energy from open-marine waters giving the opportunity for waves to breach the shoreline with only minor decreases in kinetic energy. The outer shelf would finally transition into the Capitan reef wall which is reflected in the change from the ~5° stratigraphic dip angle of the outer shelf to the subvertical dip of the massive reef wall presented in Tinker (1998). The slight differences from Rattlesnake to McKittrick Canyon are similar to variations along-strike of modern carbonate platforms. For example, the outer shelf dip-width in San Salvador, Bahamas increases from approximately 250 m at Grouper's Gully to nearly 2.5 km within only 4 km to the south near Fernandez Bay (Figure 34).

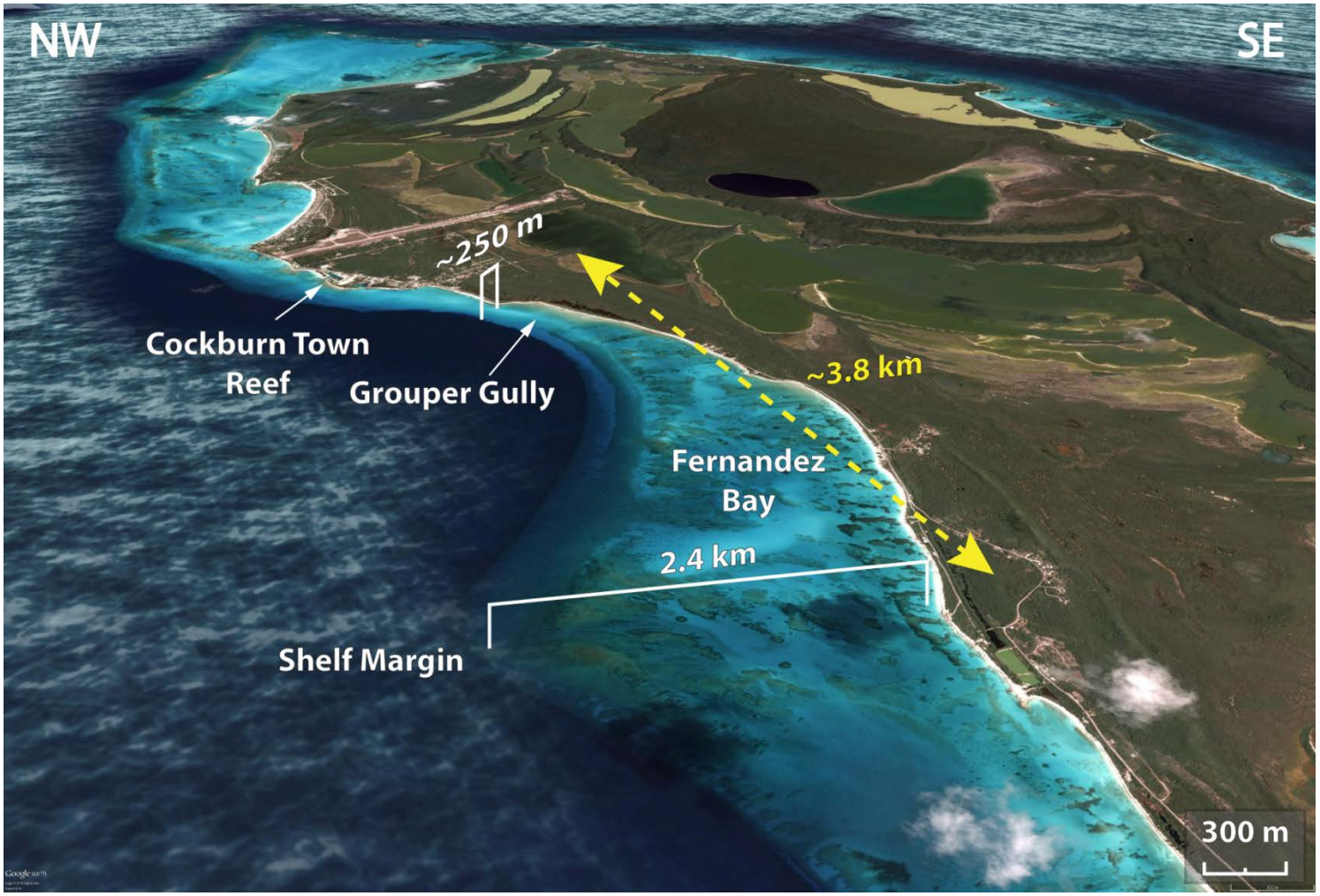

Figure 34. — Google Earth image of San Salvador, Bahamas comparing the width of the outer shelf of Grouper Gully and near Fernandez Bay. Note the change in widths occurs over a distance of less than 4 km illustrating heterogeneities present on carbonate platforms.

SLAUGHTER CANYON

IV. Facies Tracts Dimensions

No field work was conducted in Slaughter Canyon for this study. Consequently, data for Slaughter Canyon is adopted from the work done by Harman (2011) and serves as additional comparison of quantified depositional parameters of the G25 Hairpin HFS. It is worth noting that Harman (2011) utilizes the sequence stratigraphic framework put forth by Kerans and Kempter (2002) eliminating confusion between defined sequences. Harman (2011) proposed a shelf crest dip-width ranging from 570 m during the TST to over 1300 m in the HST. The 400 m (TST) to ~220 m (HST) outer shelf dip-width from Harman (2011) is in accord with the results from McKittrick and Rattlesnake Canyons presented from this study.

IMPLICATIONS FROM COMPARISON ACROSS CANYONS

Comparison of all three canyons (McKittrick, Rattlesnake, and Slaughter) reveals variability within facies tract dip-widths particularly for the shelf crest and outer shelf. All three canyons depict a wide shelf crest representing the topographic high-point on a dip profile of the platform sitting higher than the shallow Capitan reef. Thus, the data from this study, including facies associations, cyclicity, and stratal geometries, support a marginal-mound depositional model in which the shelf crest is located at a topographically higher elevation than the shelf margin reef and acts as a barrier to platform interior fluids that are potentially harmful to reef development (Figure 35).

The dramatic expansion of the shelf crest indicates a relatively stable shoreline with prolonged exposure of the supratidal shelf crest coupled with episodic low-

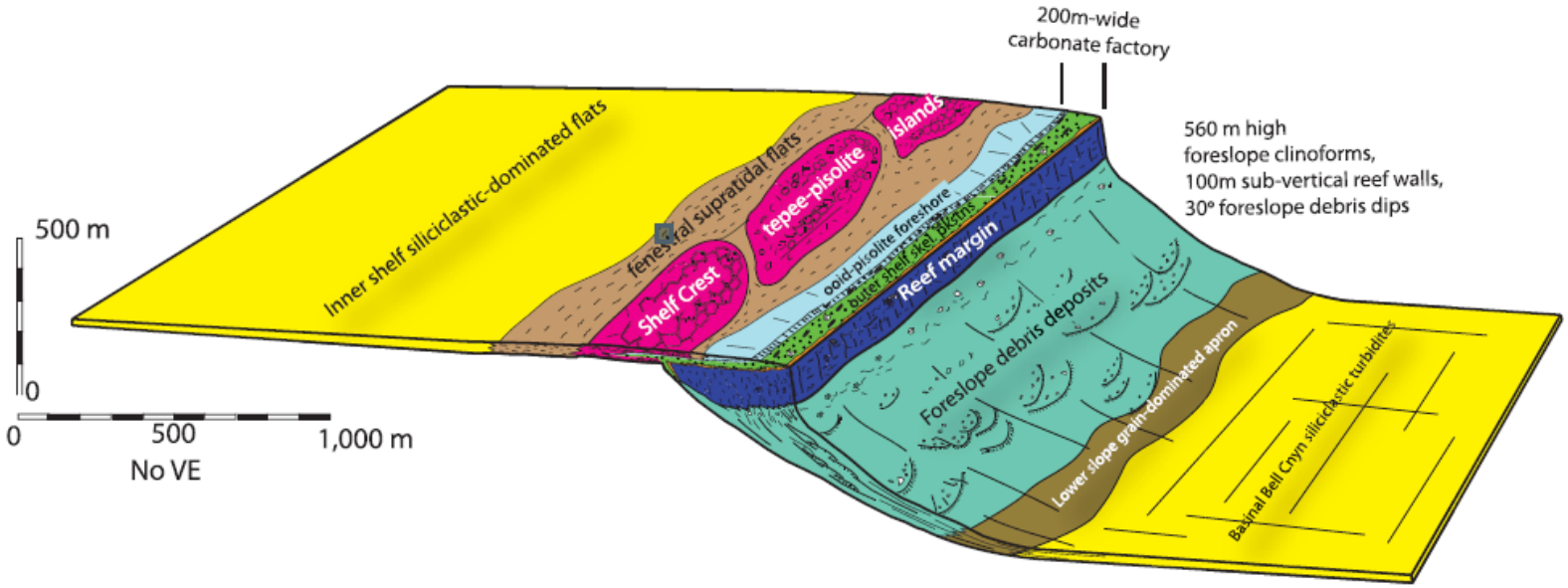

Figure 35. — To scale depositional model of the G25 Hairpin HFS at McKittrick Canyon created based on lidar tracings from Kerans et al. (2013). Authors show a wider (200 m) outer shelf facies tract than this study found. The shelf crest facies tract is widest at this time throughout Guadalupian time. Slope deposit data was based on work in Pine and Smith Canyon. It is important to note the formation of the shelf crest at a topographically higher elevation than the reef margin.

amplitude sea level fluctuations necessary to maintain tepee development (Figure 36). A final major drop in sea level coincides with deposition of the Triplet Formation on the shelf and bypass of sandstones into the basin. This result corroborates with the work of Kerans and Harris (1993) that documented a 9-12 m relief from the terminal shelf crest to the reef top and recorded facies offset near the top Hairpin sequence boundary that juxtaposed peritidal facies and exposure breccias above outer shelf and reef facies suggesting a sea level fall of ~12 m. Additional work from Kosa and Hunt identified karstification at the top G25 Hairpin sequence boundary further affirming the major drop in sea level.

The G25 Hairpin is an asymmetric high-frequency sequence characterized by a short 5-15 m TST and a large 35-45 m HST. Type sections documented in Rattlesnake and McKittrick Canyons reveal multiple upward shallowing high-frequency cycles composing 5 cycle sets (Figures 37 and 38). In McKittrick Canyon, the maximum flooding surface (MFS) is found within the lower cycle set, while the MFS is interpreted to be within the second cycle set in Rattlesnake Canyon. Difference in interpretation of the MFS across canyons can be attributed to the weathering profile. The most basal cycle set is characterized predominately by a sloping weathering profile suggesting siliciclastic composition. The upper 3 cycle sets contain the best-developed tepees within the HST of the G25 HFS. A relatively stable shoreline and the most favorable

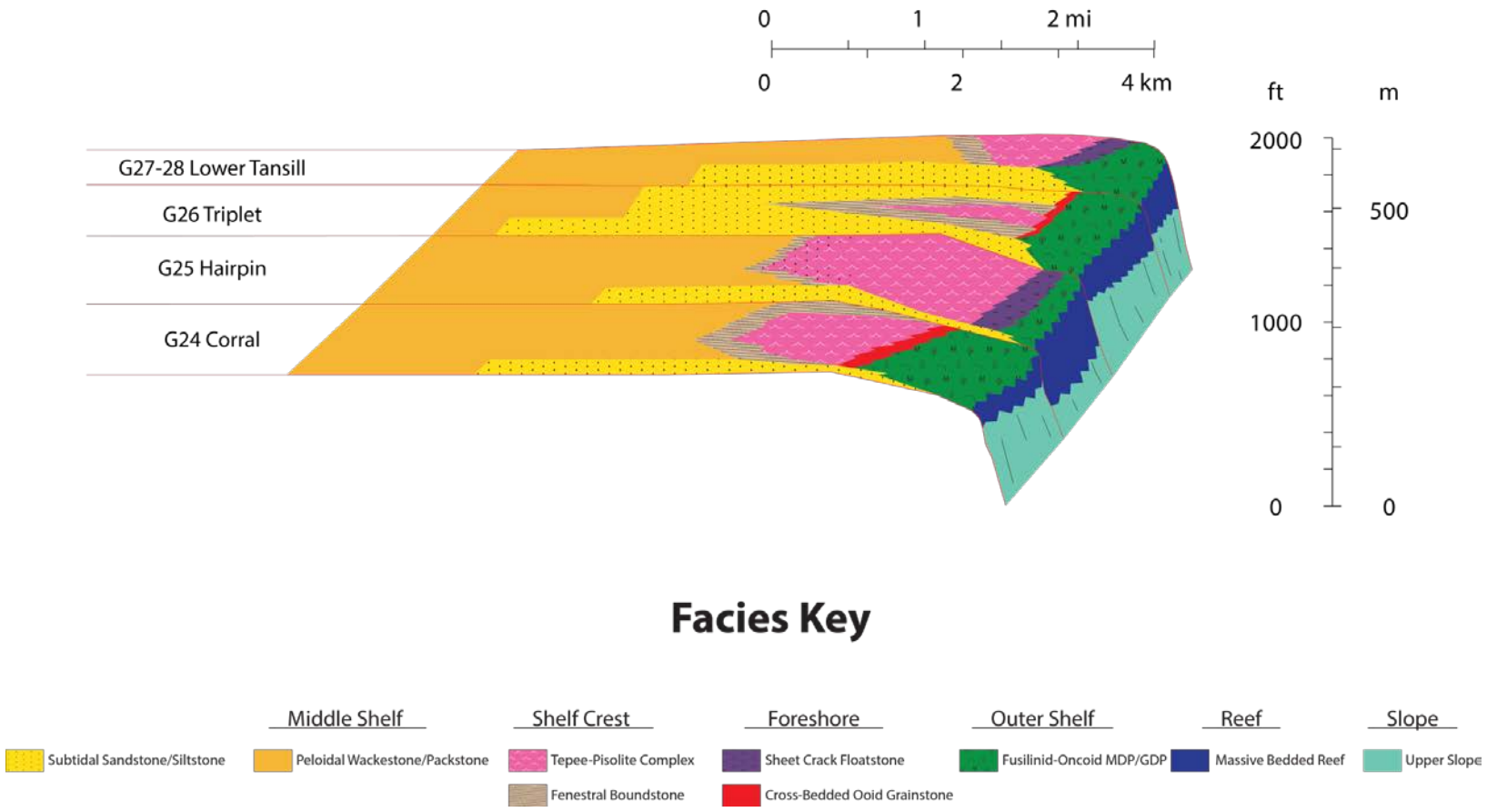

Figure 36. — Stepwise evolution of the G24-G27/28 high-frequency sequences. The G25 illustrates the greatest expansion of the shelf crest tepee-pisolite complex.

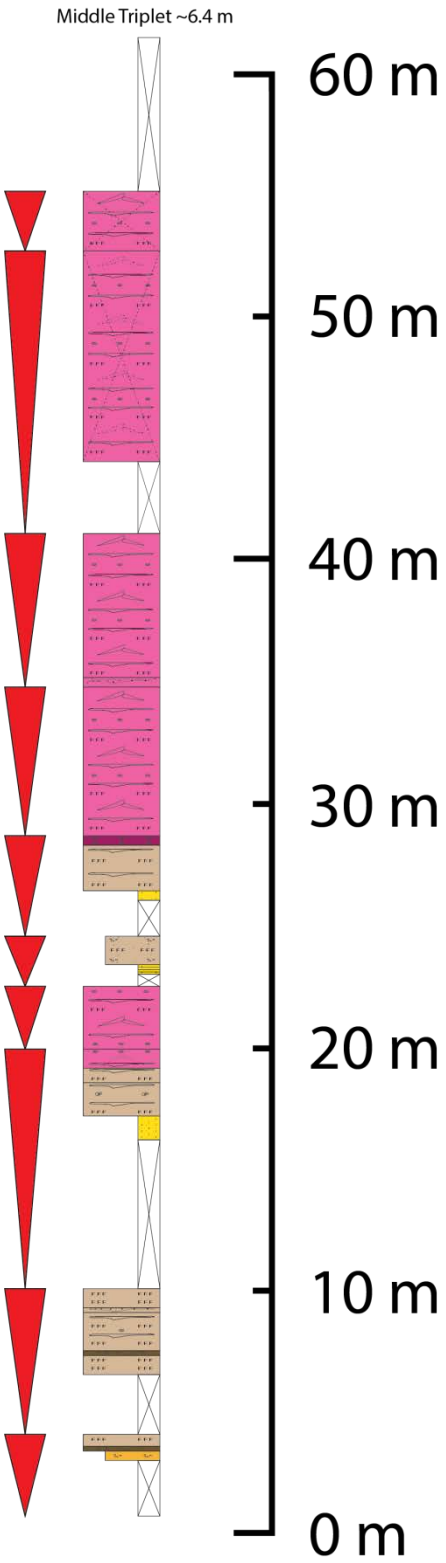

Figure 37. Measured section R4 from Rattlesnake Canyon.

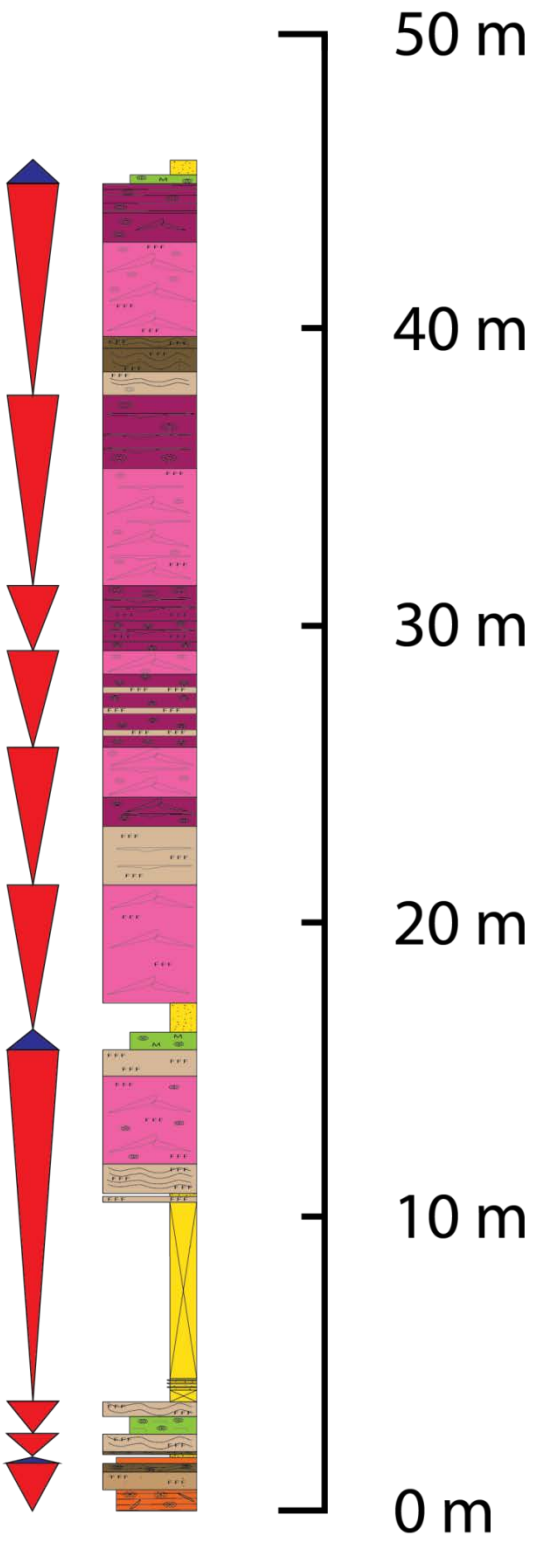

Figure 38. Measured section M4 from McKittrick Canyon.

conditions for tepee development are inferred to occur during this time. The fifth and final cycle set represents the late HST suggesting decreasing accommodation indicated by the decrease in size of the uppermost tepees.

This study and Harman (2011) document a narrow (<150 m) outer shelf; though all canyons record the G25 HFS as having one of the narrowest outer shelf dimensions compared to other sequences within the Capitan system. Such a narrow outer shelf would typically imply a weak carbonate factory. However, there exists an abundance of subtidal grains incorporated into the supratidal tepee-pisolite complex. A calculation of the area displaced by tepee expansion due to cementation suggests that the carbonate factory was indeed very active (Figure 39). Displacive carbonate cementation accounts for 6% of the area displaced along a single timeline, which is still a significant amount of in-situ precipitation compared to modern environments in Abu Dhabi where volume change caused by expansive cements only accounts for less than 1% (Lokier and Steuber 2009). This leaves the remaining 94.1% accounting for carbonate sediment accumulation produced by the outer shelf carbonate factory and abiotic in situ precipitation of grains such as pisoids. The amount of subtidal grains within the tepee belt may owe its occurrence to either (1) the available capacity for high-energy conveyance to supratidal environments with minimal effort at the expense of a narrow outer shelf or (2) another control either intrinsically or extrinsically linked to considerable carbonate precipitation.

Progradation/aggradation ratios reveal shoreline and shelf margin migration, but do not consider individual tepee dimensions. The cross sections in McKittrick and Rattlesnake Canyons show the largest, best-developed tepees occurring during the HST

$$\frac{\Delta L}{L} = \frac{\left(2 \times \sqrt{(H^2) + \left(\frac{1}{2}W\right)^2} - W\right) \times T}{L}$$

Figure 39. — Equation calculating area dislpaced along a single depositional timeline expressed as a percentage ($\frac{\Delta L}{L}$). ΔL = Change in length after tepee formation; L = length before tepee formation; H = Height of individual tepee; W = Width of individual tepee; T = Estimated number of tepees over L based on an average tepee width of 3 m and average crest-to-crest spacing of 18 m.

of the G25 HFS. This should imply that the shoreline was most stable during the HST providing an apt environment for tepee development. However, the shoreline is more stable during the TST (P/A = 10) compared to the HST (P/A = 71) of the G25 HFS shelf crest according to Tinker (1998). Because tepees require multiple episodes of wetting and drying, related to low-amplitude eustatic sea level fluctuations, a prolonged period of exposure due to sea level fall can be disregarded as a primary driver of shelf crest expansion. Additionally, karstification at the top Hairpin sequence boundary documented by Kosa and Hunt suggests that a major sea level fall post-dates tepee development.

While the primary focus of this project initially sought out to understand the relationship between eustatic sea level fluctuations and its effect on tepee development, it became impossible to ignore other potential controls affecting tepee development within the G25 HFS. A plausible hypothesis for an increase in tepee development may be related to the saturation state of marine waters within the Delaware Basin. Franceschi et al. (2016) found that a high carbonate precipitation rate (G) in the Latemar platform corresponded with the high saturation state (Ω) of Middle Triassic seawater. Recent studies record a direct link between elevated saturation states and salinities. Gabellone and Whitaker (2015) document a progressive increase in the degree of saturation of carbonate minerals to salinities of up to 200% with the use of one-dimensional numerical reactive transport modelling. Restricted conditions, indicated by hypersaline waters, may be tied to the closure of the Hovey Channel in the southwest of the Delaware Basin (Kerans personal communication). Deposition of Capitan equivalent strata in the Apache and Glass Mountains may have progressively filled in the Hovey Channel. This

subsequently limited exchange of normal marine waters causing the fluids in the Delaware Basin to become supersaturated ultimately favoring carbonate precipitation. Hence, a correlation may be made between tepee development in the G25 HFS and the first signal of an evolving Delaware Basin with increasingly restrictive conditions.

The link between tepee development and supersaturated marine waters needs to be further investigated before an in depth discussion can be made. However, the Guadalupe Mountains provides a unique laboratory suited for this type of research to be conducted. Results from this study provide a high-resolution constraint on facies tract dimensions across multiple canyons rendering a foundation for a three-dimensional quantified model. Additionally, a well-developed sequence stratigraphic framework exists offering the opportunity for precise controls on timing, which can be useful for calculating precipitation and accumulation rates. A way to gather geochemical data on marine waters in the Delaware Basin during Hairpin time could be to retrieve ion composition from fluid inclusions similar to the methods described in Gabellone and Whitaker (2015). Though the link between geochemical controls and platform development is beyond the scope of this project, this hypothesis may potentially stimulate future research efforts.

CONCLUSIONS

This study builds upon the original work of Tinker (1998), Rush and Kerans (2010), and Harman (2011) by presenting a greater degree of constraint of facies tract dimensions within the G25 Hairpin HFS. Results are based on 21 measured sections focused on the G25 HFS throughout McKittrick and Rattlesnake Canyons with comparison of data from Slaughter adopted from the work of Harman (2011). Both canyons expose 2.5-3 km of Capitan equivalent strata where cycle stacking patterns, facies distributions, and stratal geometries can be observed from the shelf crest to the massive Capitan reef. Gigapan photomosaics and lidar data from both canyons offer two- and three-dimensional perspectives that improve understanding of the spatial distribution of tepees in the tepee-pisolite complex as well as depositional topography of the Capitan platform. This study presents two key results (1) a new model for deposition of Capitan shelf strata confirming the topographically higher position of the shelf crest relative to the shelf margin reef and (2) that the HST of the G25 HFS is characterized by prolonged exposure of the shelf accompanied by low-amplitude eustatic sea level fluctuations and considerably increased marine cementation from supersaturated waters necessary for tepee development. These unique conditions that existed during G25 tepee development may be a reflection of larger-scale changes in the Delaware Basin to more restricted conditions prior to Castile evaporite deposition. Subsequent deposition and bypass of the Triplet Formation on the shelf and Bell Canyon strata in the Delaware Basin mark a major drop in sea level to the degree of a composite sequence boundary (CS12) (Kerans et al. 2013).

Quantification of key depositional characteristics within the G25 HFS offers reproducibility and testability against other carbonate systems throughout both the ancient and modern geologic record. Comparison of results across mixed settings will enhance our understanding of the intrinsic and extrinsic controls governing carbonate precipitation, platform development, and along-strike heterogeneities. This along-strike variability seen in both ancient strata of the Guadalupe Mountains and modern deposits of the Bahamas is common in many carbonate reservoirs; hence the increasing need for higher-resolution, outcrop-based depositional models endures. Hopefully this research (1) provides new insight to the significance of shelf crest tepees as they relate to platform development with respect to sea level change and (2) discloses critical questions remaining to be answered about the sedimentology of the Guadalupe Mountains.

APPENDIX

The purpose of this appendix is to provide additional figures to include supplementary information on the documentation of the G25 Hairpin HFS of the Yates Formation in the Guadalupe Mountains. Additional material will include all measured sections used in the cross sections from Rattlesnake and McKittrick Canyons.

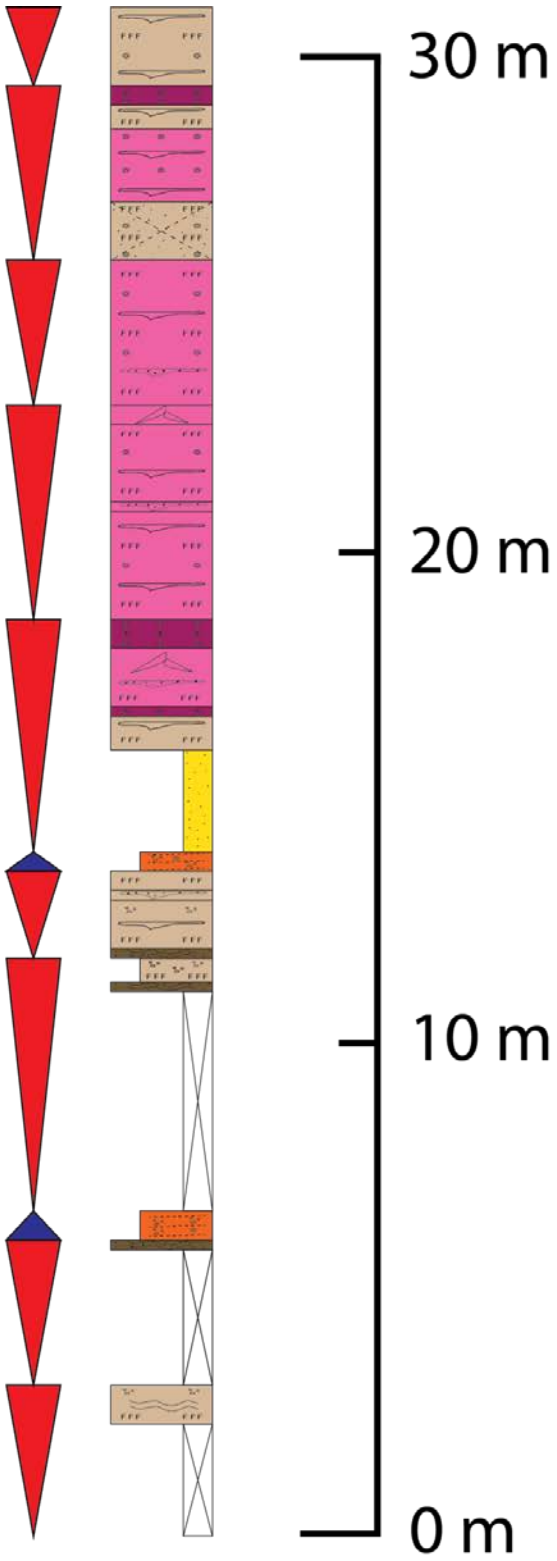

Figure 40. Measured section R1 from Rattlesnake Canyon.

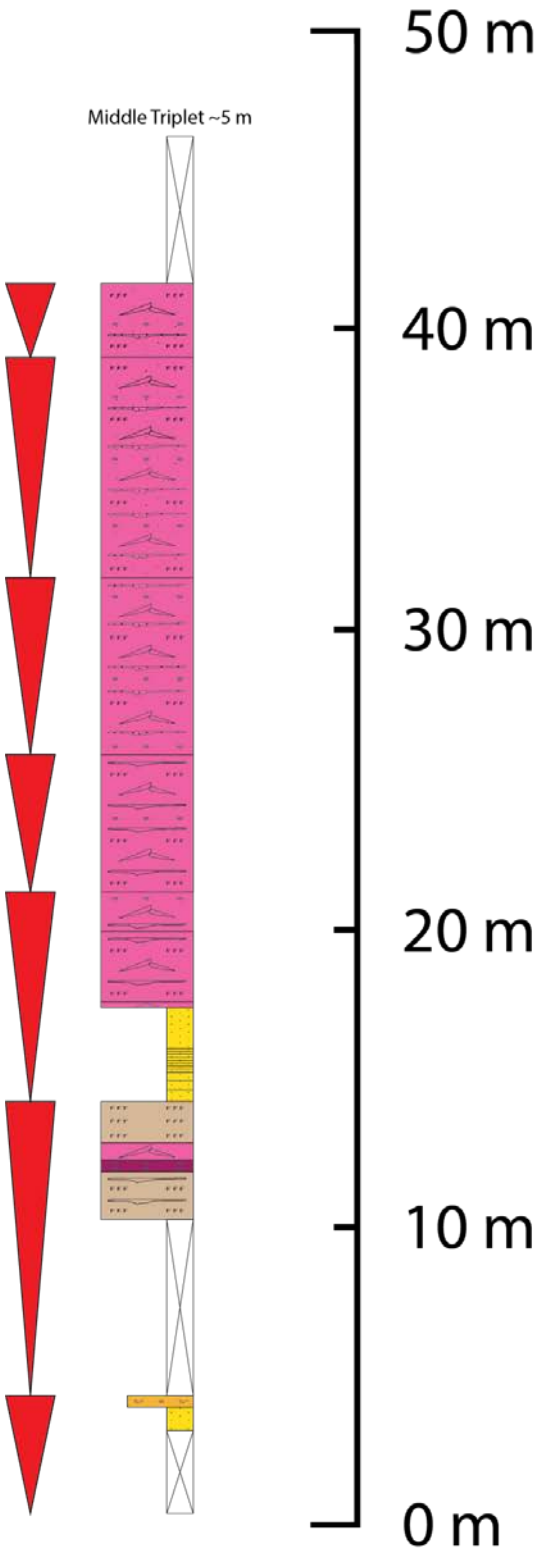

Figure 41. Measured section R2 from Rattlesnake Canyon.

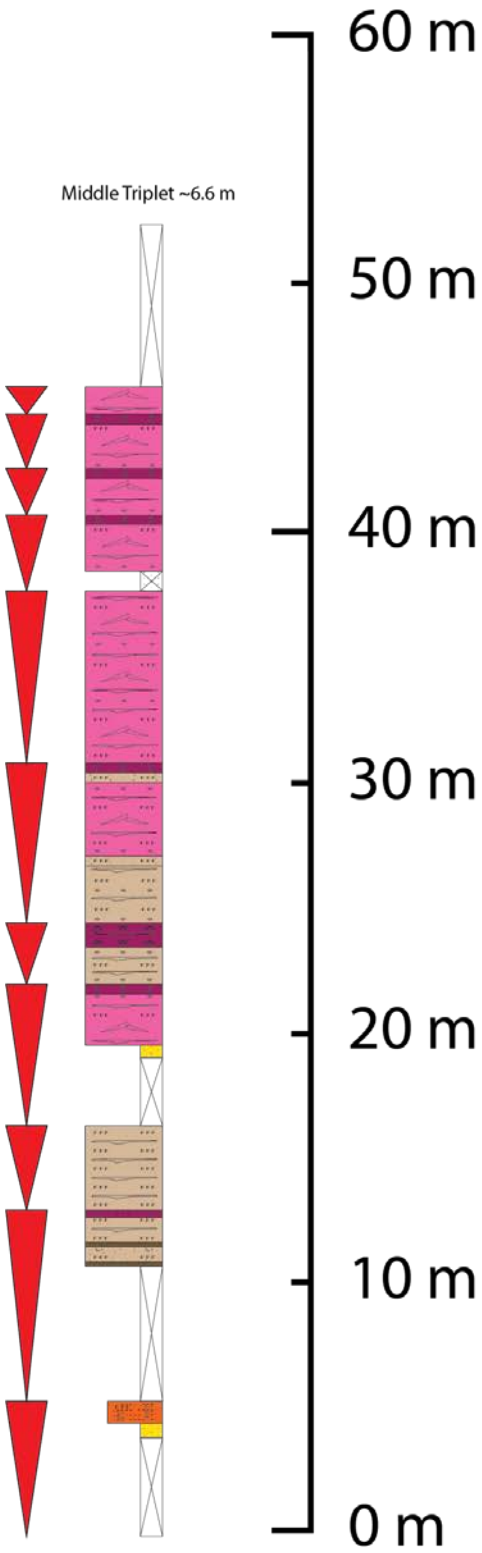

Figure 42. Measured section R3 from Rattlesnake Canyon.

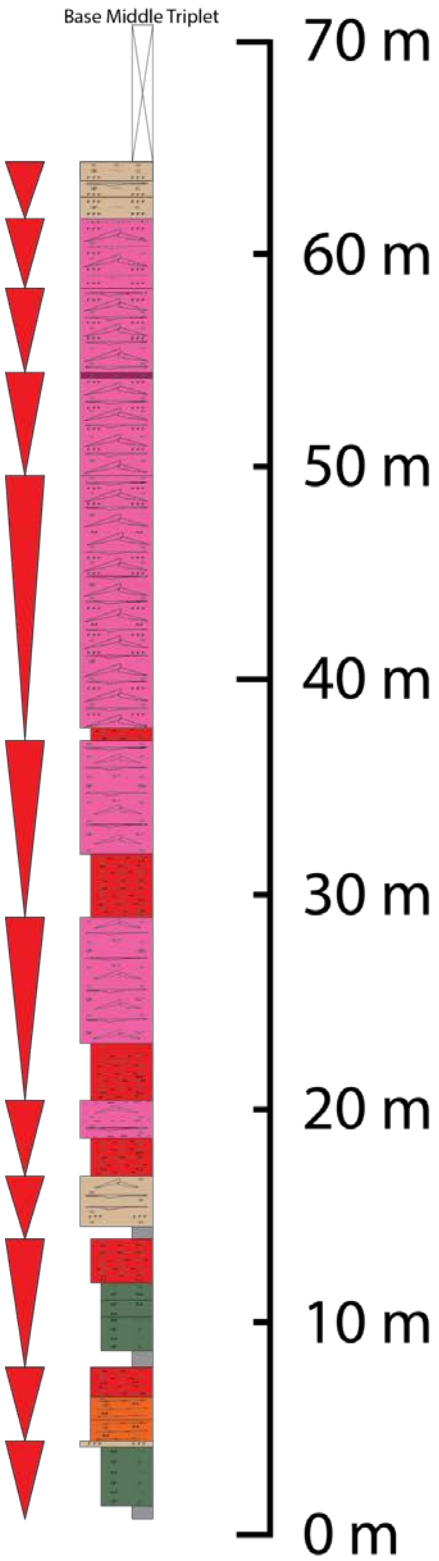

Figure 43. Measured section R5 from Rattlesnake Canyon.

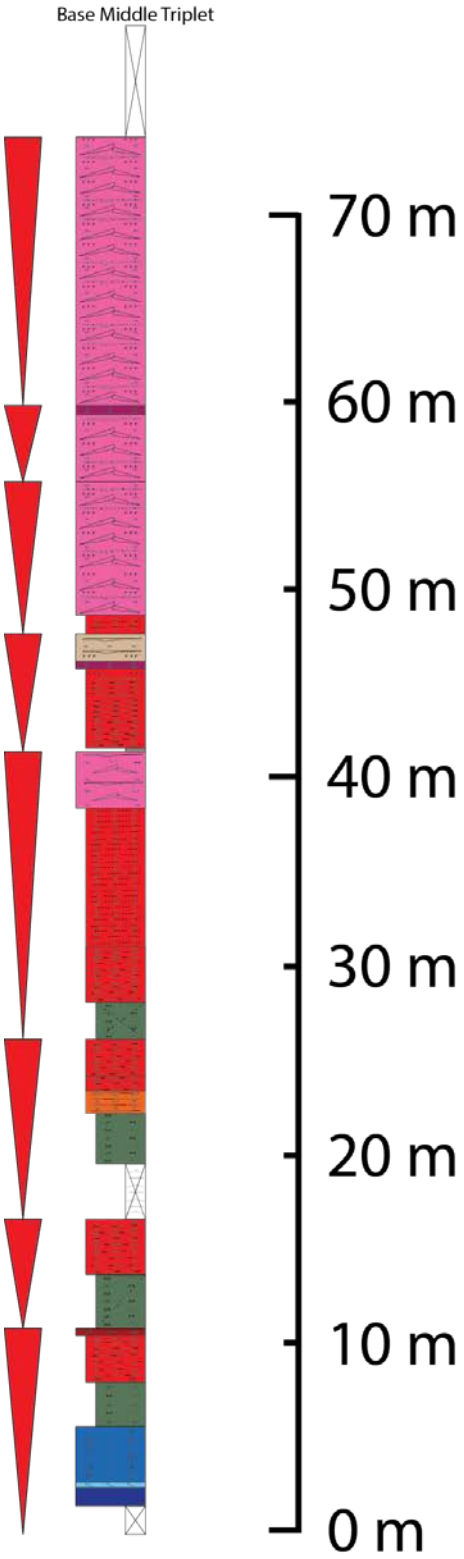

Figure 44. Measured section R6 from Rattlesnake Canyon.

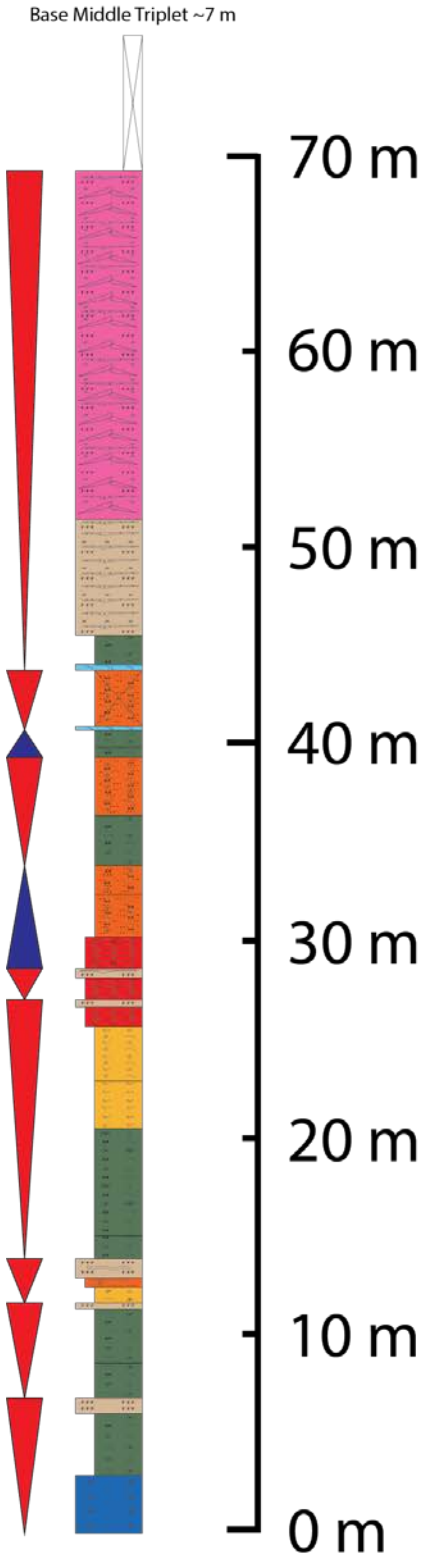

Figure 45. Measured section R7 from Rattlesnake Canyon.

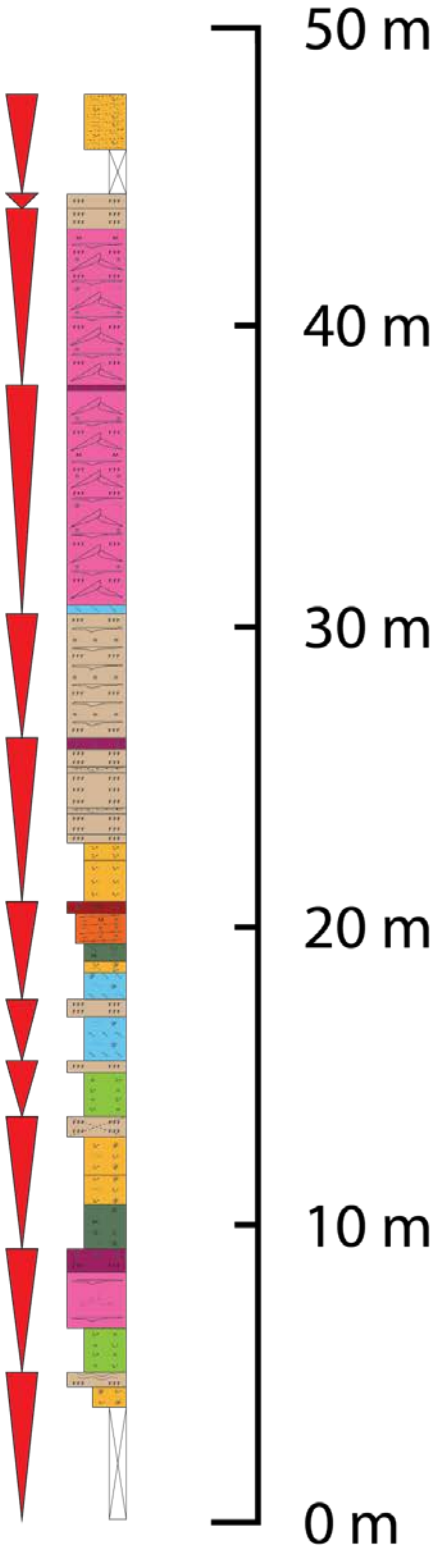

Figure 46. Measured section R9 from Rattlesnake Canyon.

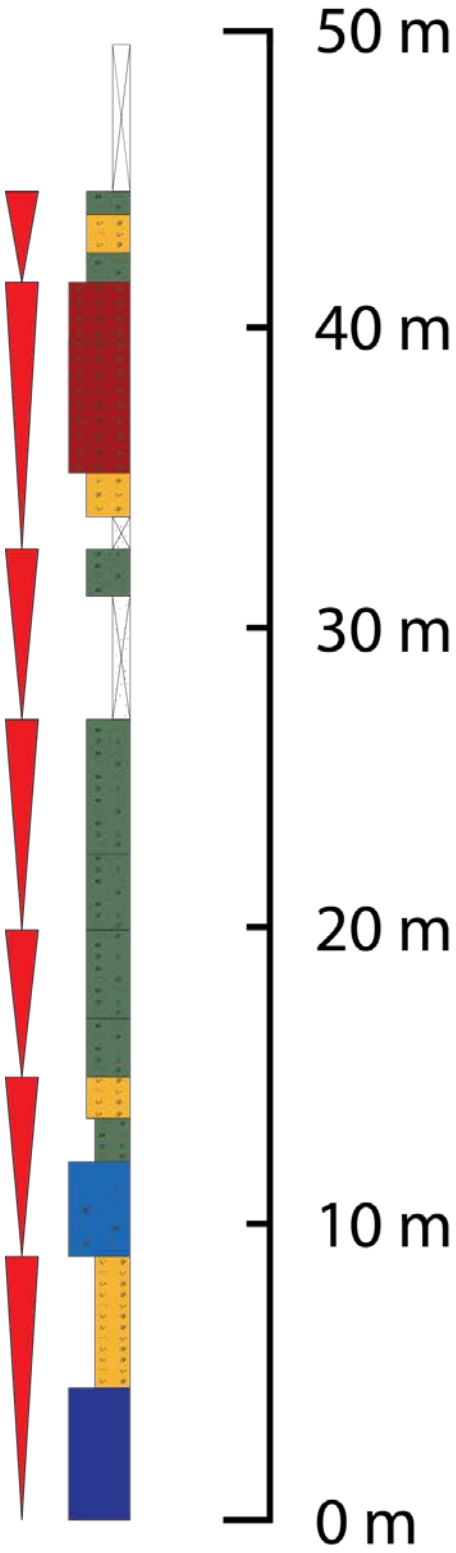

Figure 47. Measured section R10 from Rattlesnake Canyon.

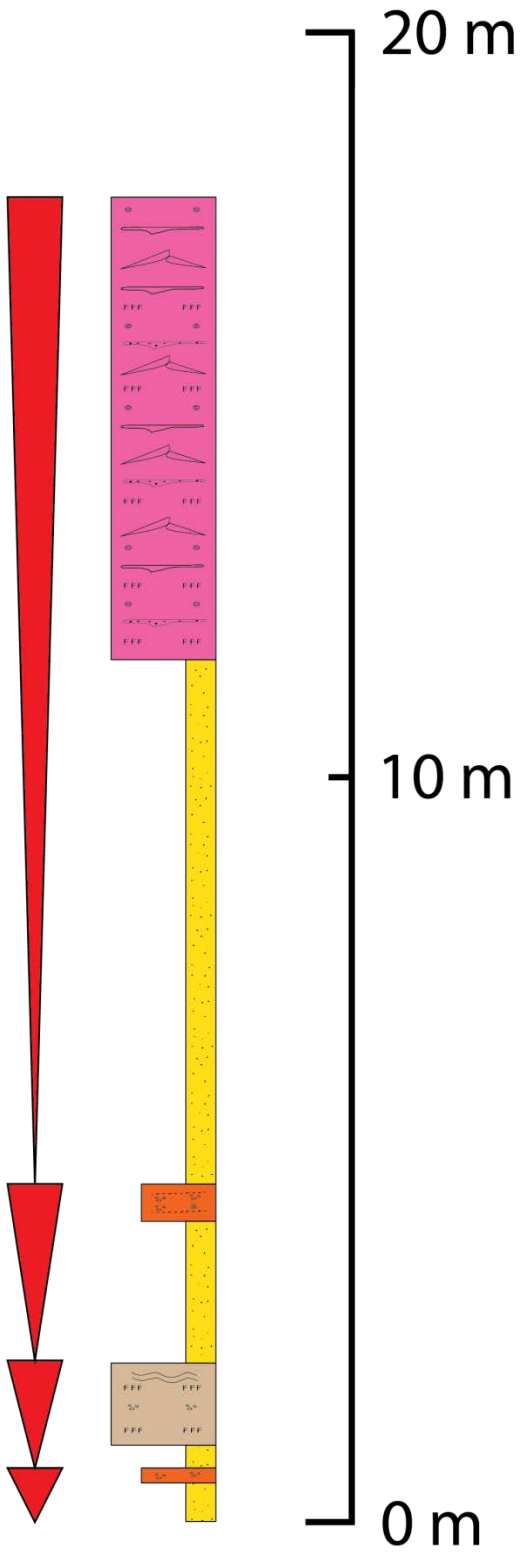

Figure 48. Measured section M1 from McKittrick Canyon.

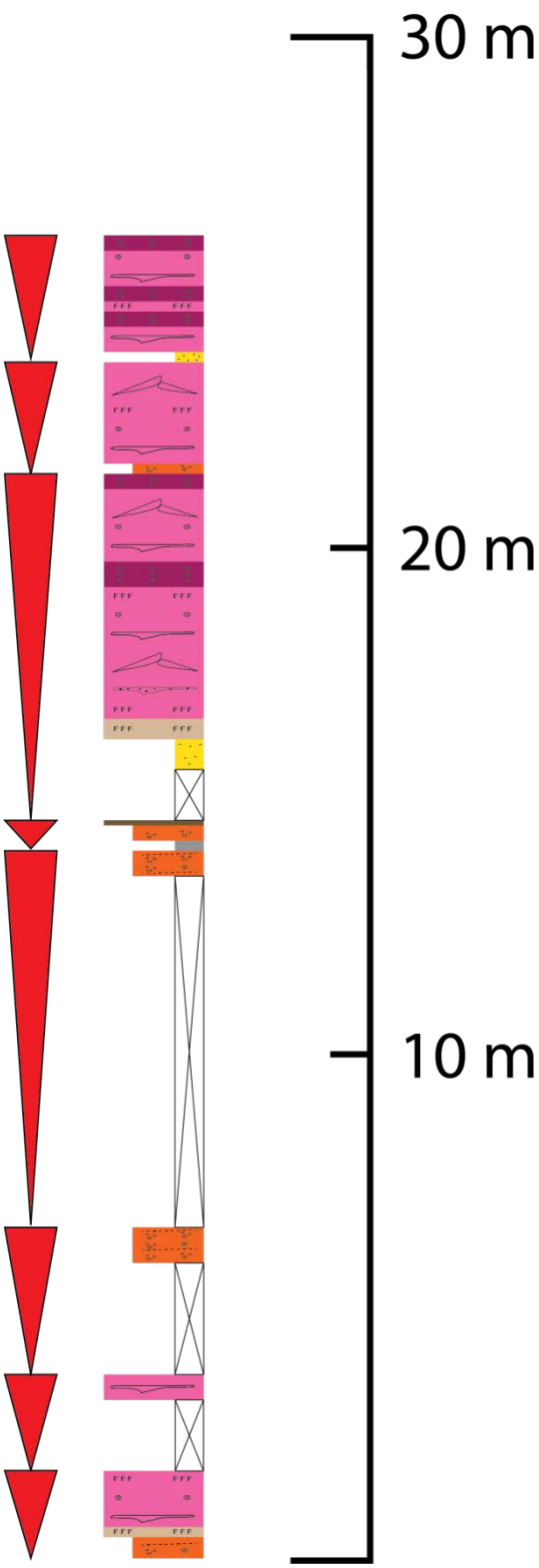

Figure 49. Measured section M2 from McKittrick Canyon.

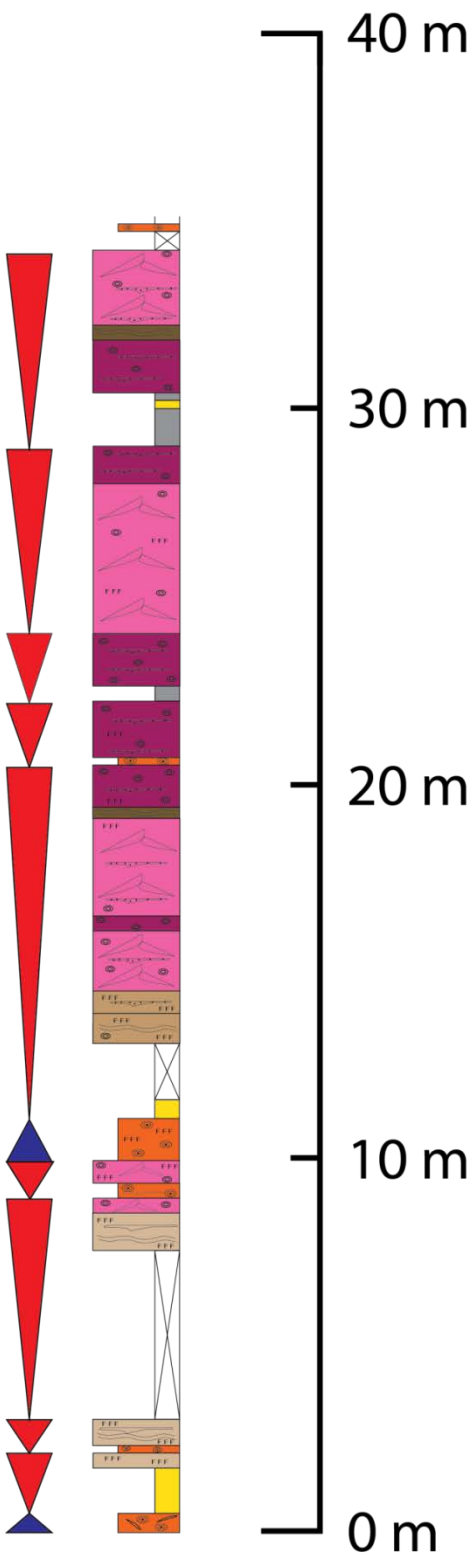

Figure 50. Measured section M3 from McKittrick Canyon.

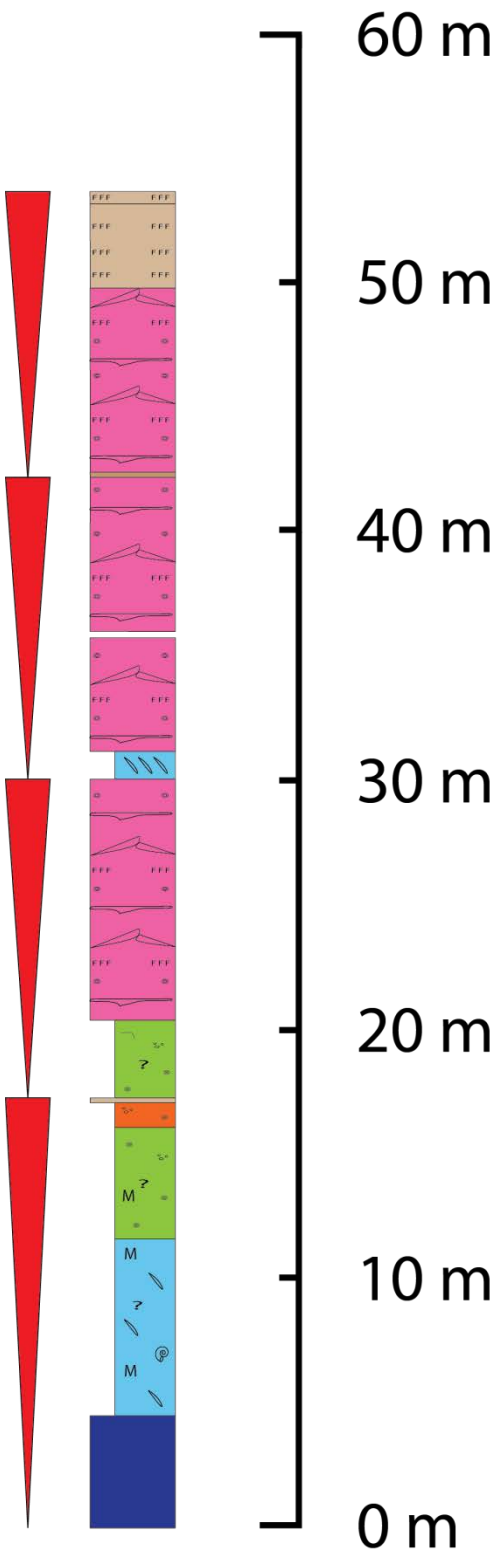

Figure 51. Measured section M5 from McKittrick Canyon.

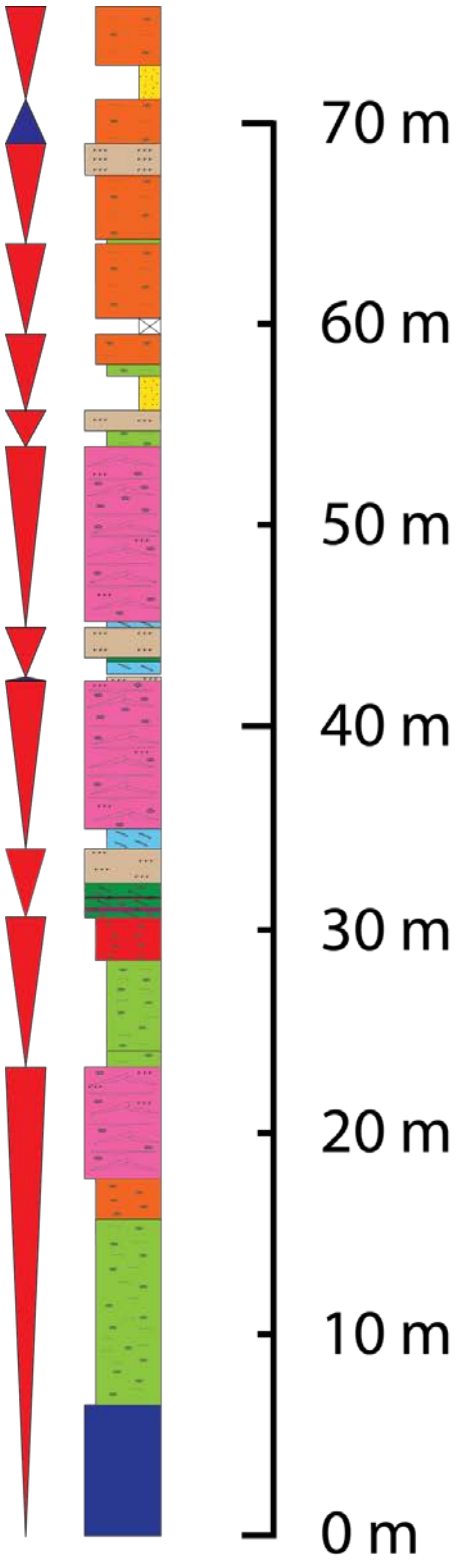

Figure 52. Measured section M6 from McKittrick Canyon.

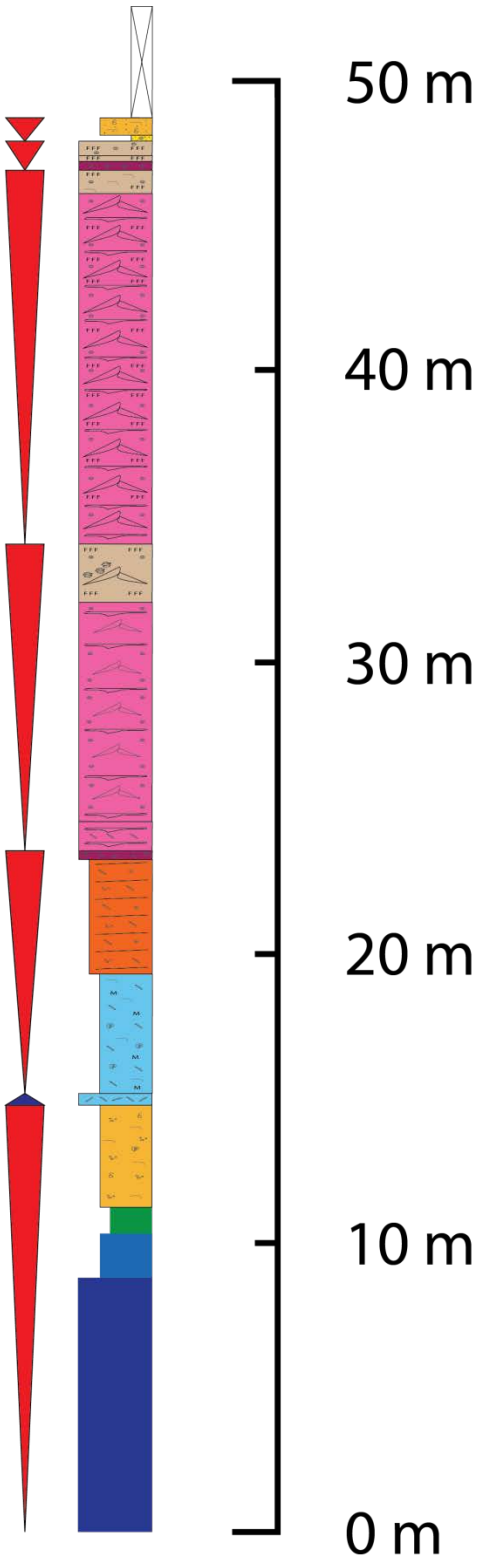

Figure 53. Measured section M7 from McKittrick Canyon.

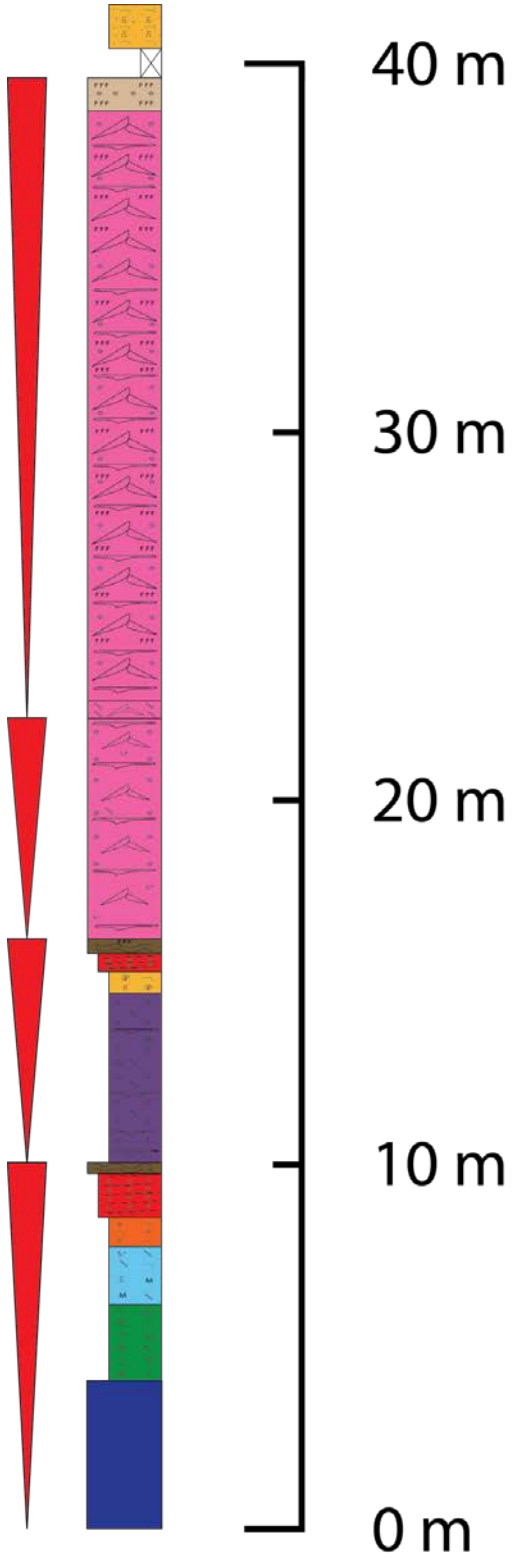

Figure 54. Measured section M8 from McKittrick Canyon.

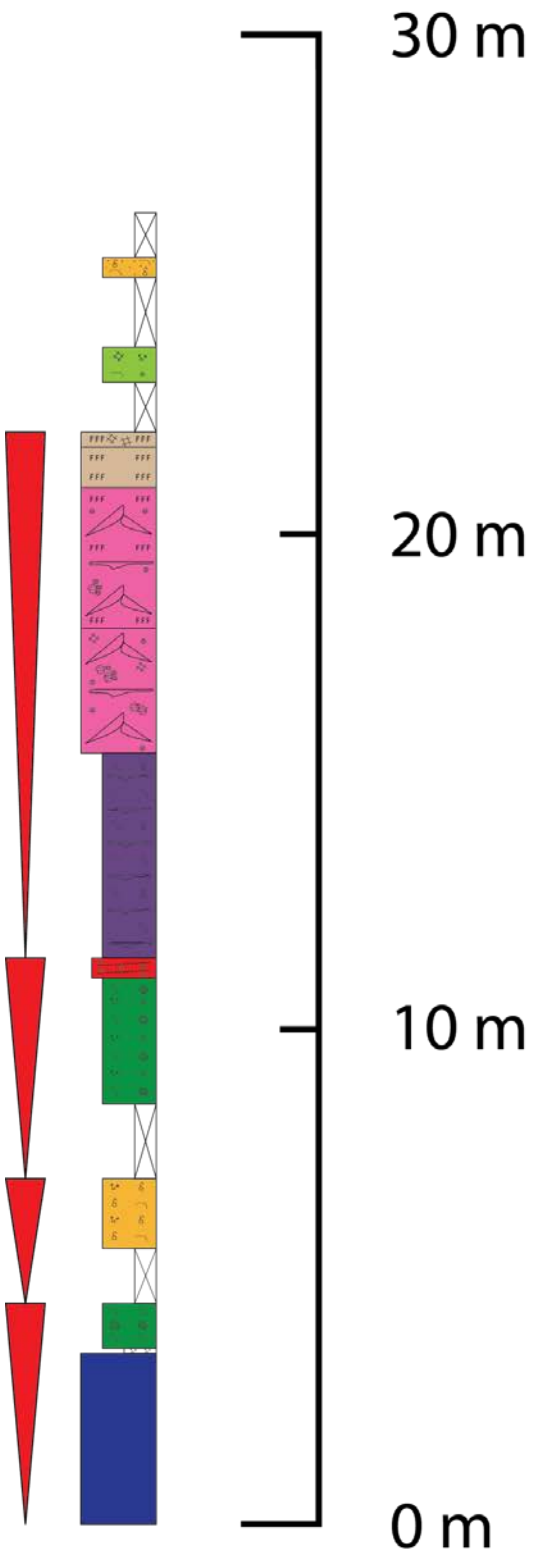

Figure 55. Measured section M9 from McKittrick Canyon.

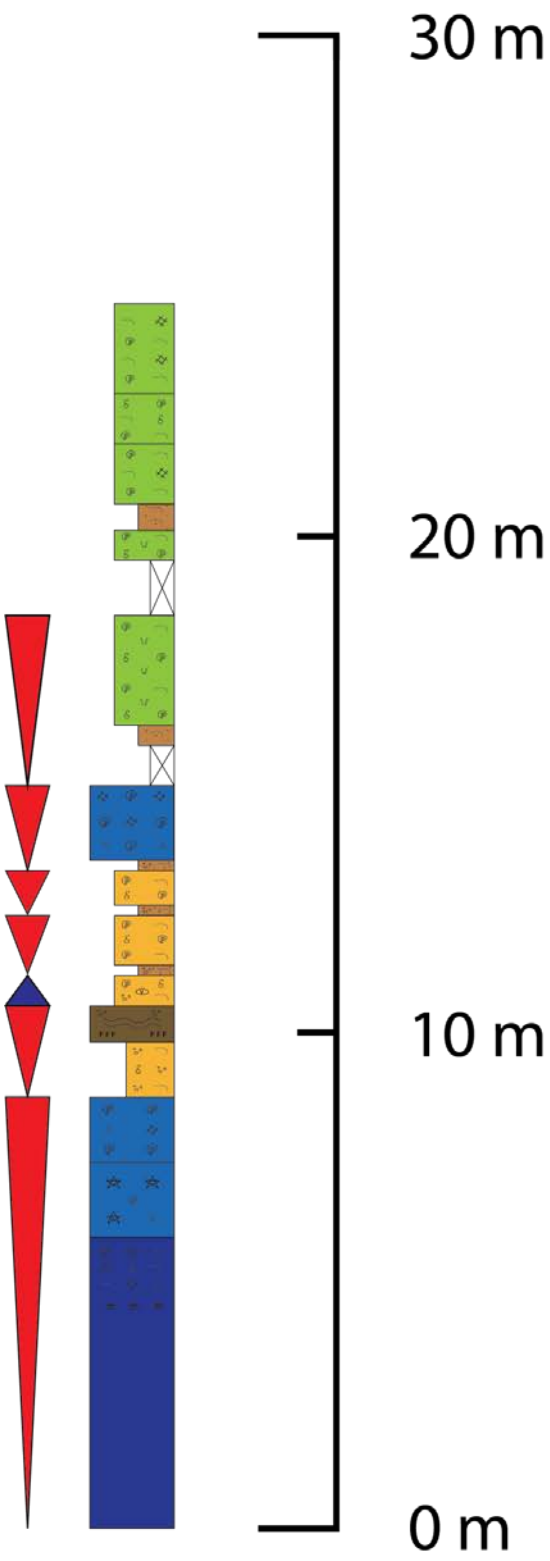

Figure 56. Measured section M11 from McKittrick Canyon.

REFERENCES

ADAMS, J.E., and FRENZEL, H.N., 1950, Capitan barrier reef, Texas and New Mexico: The Journal of Geology, p. 289-312.

ASSERETO, R.L., and KENDALL, C.G., 1977, Nature, origin and classification of peritidal tepee structures and related breccias: Sedimentology, v. 24, p. 153-210.

BABCOCK, J., 1977, Calcareous algae, organic boundstones, and the genesis of the upper Capitan Limestone (Permian, Guadalupian), Guadalupe Mountains, west Texas and New Mexico: Upper Guadalupian Facies, Permian Reef Complex, Guadalupe Mountains, New Mexico and West Texas: Society of Economic Paleontologists and Mineralogists, Permian Basin Section, Publication, p. 77-16.

BABCOCK, J.A., and YUREWICZ, D.A., 1989, The massive facies of the Capitan Limestone, Guadalupe Mountains, Texas and New Mexico.

BAMBACH, K.R., SCOTESE, C.R., and ZIEGLER, A.M., 1980, Before Pangea: the geographies of the Paleozoic world: American Scientist, v. 68, p. 26-38.

BEBOUT, D.G., and KERANS, C., 1993, Guide to the Permian Reef Geology Trail, McKittrick Canyon, Guadalupe Mountains National Park, West Texas, Bureau of Economic Geology, University of Texas at Austin.

BELLIAN, J.A., KERANS, C., and JENNETTE, D.C., 2005, Digital outcrop models: applications of terrestrial scanning lidar technology in stratigraphic modeling: Journal of sedimentary research, v. 75, p. 166-176.

BERRA, F., and JADOUL, F., 2002, Evidence of a" mid-Carnian" transgression in the western Southern Alps (Lombardy, Italy): stratigraphic and paleogeographic implications: Rivista Italiana di Paleontologia e Stratigrafia (Research In Paleontology and Stratigraphy), v. 108.

BLAKEY, R.C., PETERSON, F., and KOCUREK, G., 1988, Synthesis of late Paleozoic and Mesozoic eolian deposits of the Western Interior of the United States: Sedimentary Geology, v. 56, p. 3-125.

BORER, J., and HARRIS, P., 1991, Lithofacies and Cyclicity of the Yates Formation, Permian Basin: Implications for Reservoir Heterogeneity (1): AAPG Bulletin, v. 75, p. 726-779.

CANDELARIA, M.P., 1989, Shallow marine sheet sandstones, upper Yates Formation, northwest shelf, Delaware basin, New Mexico.

CHRIST, N., IMMENHAUSER, A., AMOUR, F., MUTTI, M., PRESTON, R., WHITAKER, F.F., PETERHÄNSEL, A., EGENHOFF, S.O., DUNN, P.A., and AGAR, S.M., 2012, Triassic Latemar cycle tops—Subaerial exposure of platform carbonates under tropical arid climate: Sedimentary Geology, v. 265, p. 1-29.

DUNHAM, R.J., 1962, Classification of carbonate rocks according to depositional textures.

DUNHAM, R.J., 1972, Capitan Reef, New Mexico and Texas: facts and questions to aid interpretation and group discussion, v. 72, Permian Basin Section, Society of Economic Paleontologists and Mineralogists.

EGENHOFF, S.O., PETERHÄNSEL, A., BECHSTÄDT, T., ZÜHLKE, R., and GRÖTSCH, J., 1999, Facies architecture of an isolated carbonate platform: tracing the cycles of the Latemar (Middle Triassic, northern Italy): Sedimentology, v. 46, p. 893-912.

ESTEBAN, M., and PRAY, L.C., 1977, Origin of the pisolite facies of the shelf crest: Upper Guadalupian facies, Permian reef complex, Guadalupe Mountains, New Mexico and west Texas: 1977 Field Conference Guidebook, p. 77-16.

FISCHER, A.G., and SARNTHEIN, M., 1988, Airborne silts and dune-derived sands in the Permian of the Delaware Basin: Journal of sedimentary research, v. 58.

FISHER, W.L., and MCGOWEN, J., 1969, Depositional systems in Wilcox Group (Eocene) of Texas and their relation to occurrence of oil and gas: AAPG Bulletin, v. 53, p. 30-54.

FRANCESCHI, M., PRETO, N., MARANGON, A., GATTOLIN, G., and MEDA, M., 2016, High precipitation rate in a Middle Triassic carbonate platform: Implications on the relationship between seawater saturation state and carbonate production: Earth and Planetary Science Letters.

GABELLONE, T., and WHITAKER, F., 2015, Secular variations in seawater chemistry controlling dolomitisation in shallow reflux systems: Insights from reactive transport modelling: Sedimentology.

GAMMON, P., MCKIRDY, D., and SMITH, H., 2005, The timing and environment of tepee formation in a Marinoan cap carbonate: Sedimentary Geology, v. 177, p. 195-208.

GARDNER, M., and SONNENFELD, M., 1996, Stratigraphic changes in facies architecture of the Permian Brushy Canyon Formation in Guadalupe Mountains National Park, west Texas: PUBLICATIONS-SOCIETY OF ECONOMIC

PALAEONTOLOGISTS AND MINERALOGISTS PERMIAN BASIN SECTION PBS SEPM, p. 17-40.

GOLDHAMMER, R., DUNN, P., and HARDIE, L., 1990, Depositional cycles, composite sea-level changes, cycle stacking patterns, and the hierarchy of stratigraphic forcing: examples from Alpine Triassic platform carbonates: Geological Society of America Bulletin, v. 102, p. 535-562.

HARMAN, C., 2011, Quantified facies distribution and sequence geometry of the Yates Formation: Slaughter Canyon, New Mexico: Master's thesis, University of Texas, Austin, Texas.

HAYES, P.T., 1964, Geology of the Guadalupe Mountains, New Mexico, US Geological Survey.

HILL, C.A., 1999, Reevaluation of the Hovey channel in the Delaware basin, West Texas: AAPG bulletin, v. 83, p. 277-294.

HILL, C.A., PALEONTOLOGISTS, S.O.E., SECTION, M.P.B., GARBER, R.A., LINDSAY, R.F., and ADAMS, J.W., 1996, Geology of the Delaware Basin, Guadalupe, Apache, and Glass Mountains, New Mexico and West Texas, Permian Basin Section-SEPM.

HUNT, D., and FITCHEN, W.M., 1999, Compaction and the dynamics of carbonate-platform development: insights from the Permian Delaware and Midland basins, Southeast New Mexico and West Texas, USA.

HUNT, D.W., FITCHEN, W.M., and KOSA, E., 2002, Syndepositional deformation of the Permian Capitan reef carbonate platform, Guadalupe Mountains, New Mexico, USA: Sedimentary Geology, v. 154, p. 89-126.

HURLEY, N.F., 1989, Facies mosaic of the lower Seven Rivers Formation, McKittrick Canyon, New Mexico.

IRVING, E., 1979, Pole positions and continental drift since the Devonian: The Earth: Its Origin, Structure and Evolution, ed. MW McElhinny, Academic Press, London, p. 567-593.

JAMES, N.P., 1984, Shallowing-upward sequences in carbonates, Facies models, Geoscience Canada, p. 213-228.

JIANG, G., KENNEDY, M.J., CHRISTIE-BLICK, N., WU, H., and ZHANG, S., 2006, Stratigraphy, sedimentary structures, and textures of the late Neoproterozoic Doushantuo cap carbonate in South China: Journal of sedimentary research, v. 76, p. 978-995.

KENDALL, C.G., and WARREN, J., 1987, A review of the origin and setting of tepees and their associated fabrics: Sedimentology, v. 34, p. 1007-1027.
KENDALL, C.G.S.C., 1969, An environmental re-interpretation of the Permian evaporite/carbonate shelf sediments of the Guadalupe Mountains: Geological Society of America Bulletin, v. 80, p. 2503-2526.

KERANS, C., 1995, Use of one-and two-dimensional cycle analysis in establishing high-frequency sequence frameworks.

KERANS, C., 2015, Characterizing Carbonate Grainstone Geobodies: AAPG Annual Convention and Exhibition.

KERANS, C., FITCHEN, W., GARDNER, M., SONNENFELD, M., TINKER, S., and WARDLAW, B., 1992, Styles of sequence development within uppermost Leonardian through Guadalupian strata of the Guadalupe Mountains, Texas and New Mexico: Permian basin exploration and production strategies: applications of sequence stratigraphic and reservoir characterization concepts: West Texas Geological Society Publication, p. 92-91.

KERANS, C., and FITCHEN, W.M., 1995, Sequence hierarchy and facies architecture of a carbonate-ramp system: San Andres Formation of Algerita Escarpment and western Guadalupe Mountains, west Texas and New Mexico, v. 235, Bureau of Economic Geology, University of Texas at Austin.

KERANS, C., and FOWLER, D., 1995, Role of high-frequency cycles in analysis of ancient facies: an example from shelf-crest teepee-pisolite facies of the Guadalupian section: Guadalupe Mountains and subsurface of the Central Basin Platform, West Texas (abstract): American Association of Petroleum Geologists, Annual Convention.

KERANS, C., and HARRIS, P., 1993, Outer shelf and shelf crest: Guide to the Permian Reef Geology Trail, McKittrick Canyon, Guadalupe Mountains National Park, West Texas: University of Texas, Bureau of Economic Geology, Guidebook, v. 26, p. 32-43.

KERANS, C., and KEMPTER, K., 2002, Hierarchical stratigraphic analysis of a carbonate platform, Permian of the Guadalupe Mountains, Bureau of Economic Geology, The University of Texas at Austin.

KERANS, C., LUCIA, F.J., and SENGER, R., 1994, Integrated characterization of carbonate ramp reservoirs using Permian San Andres Formation outcrop analogs: AAPG Bulletin, v. 78, p. 181-216.

KERANS, C., and NANCE, H., 1991, High-frequency cyclicity and regional depositional patterns of the Grayburg Formation, Guadalupe Mountains, New Mexico: Sequence

stratigraphy, facies, and reservoir geometries of the San Andres, Grayburg, and Queen formations, Guadalupe Mountains, New Mexico and Texas: Permian Basin Section SEPM Publication, p. 91-32.

KERANS, C., PLAYTON, T., PHELPS, R., and SCOTT, S., 2013, Ramp to rimmed shelf transition in the Guadalupian (Permian) of the Guadalupe Mountains, West Texas and New Mexico: Deposits, Architecture, and Controls of Carbonate Margin, Slope, and Basinal Settings: SEPM, Special Publication, v. 105, p. 26-49.

KERANS, C., and TINKER, S.W., 1999, Extrinsic stratigraphic controls on development of the Capitan reef complex.

KING, P.B., 1948, Geology of the southern Guadalupe Mountains, Texas, v. 215, US Government Printing Office.

KIRKLAND, B., 1999, The dynamic Capitan reef: An image of an ancient reef and suggestions for future research.

KOŠA, E., and HUNT, D.W., 2005, Growth of syndepositional faults in carbonate strata: Upper Permian Capitan platform, New Mexico, USA: Journal of Structural Geology, v. 27, p. 1069-1094.

MATHISEN, M.G., 2014, Temporal and spatial evolution of the Cave Graben Fault System, Guadalupe Mountains, New Mexico.

MAZZULLO, S., MAZZULLO, J., and HARRIS, P., 1985, Eolian origin of quartzose sheet sands in Permian shelf facies: Guadalupe Mountains, Permian carbonate/clastic sedimentology, Guadalupe Mountains, Analogs for shelf and basin reservoirs: Symposium preceding the.

MEISSNER, F.F., 1972, Cyclic sedimentation in Middle Permian strata of the Permian basin, west Texas and New Mexico: Cyclic sedimentation in the Permian basin, 2d ed.: West Texas Geol. Soc, p. 203-232.

MELIM, L.A., and SCHOLLE, P.A., 2002, Dolomitization of the Capitan Formation forereef facies (Permian, west Texas and New Mexico): seepage reflux revisited: Sedimentology, v. 49, p. 1207-1227.

MUTTI, M., and SIMO, J., 1993, Stratigraphic patterns and cycle-related diagenesis of upper Yates Formation, Permian, Guadalupe Mountains: MEMOIRS-AMERICAN ASSOCIATION OF PETROLEUM GEOLOGISTS, p. 515-515.

NEWELL, N.D., RIGBY, J.K., FISCHER, A.G., WHITEMAN, A.J., HICKOX, J.E., and BRADLEY, J.S., 1953, The Permian Reef Complex of the Guadalupe Mountains Region, Texas and New Mexico, WH Freeman and Co., San Francisco, p. 236.

OSLEGER, D.A., 1998, Sequence architecture and sea-level dynamics of Upper Permian shelfal facies, Guadalupe Mountains, southern New Mexico: Journal of sedimentary research, v. 68.
OSLEGER, D.A., 1999, Three-dimensional architecture of Upper Permian high-frequency sequences, Yates-Capitan shelf margin, Permian Basin, USA.

PETERHÄNSEL, A., and EGENHOFF, S.O., 2008, Lateral variabilities of cycle stacking patterns in the Latemar, Triassic, Italian Dolomites: SEPM Spec. Publ, v. 89, p. 217-229.

PRAY, L.C., 1977, The all wet constant sea level hypothesis of upper Guadalupian shelf and shelf edge strata, Guadalupe Mountains, New Mexico and Texas: Upper Guadalupian facies, Permian reef complex, Guadalupe Mountains, New Mexico and west Texas: Permian Basin Section SEPM Publication, p. 77-16.

ROSS, C.A., 1978, Late Pennsylvanian and Early Permian sedimentary rocks and tectonic setting of the Marathon Geosyncline: Tectonics and Paleozoic Facies of the Marathon Geosyncline, West Texas, Permian Basin Section, SEPM, Publication, p. 78-17.

RUSH, J., and KERANS, C., 2010, Stratigraphic response across a structurally dynamic shelf: the latest Guadalupian composite sequence at Walnut Canyon, New Mexico, USA: Journal of sedimentary research, v. 80, p. 808-828.

SALLER, A.H., 1999, Geologic framework of the Capitan Reef, v. 65, Sepm Society for Sedimentary.

SARG, J., 1988, Carbonate sequence stratigraphy.

SARG, J., and LEHMANN, P., 1986, Lower-Middle Guadalupian facies and stratigraphy, San Andres/Grayburg Formations, Permian Basin, Guadalupe Mountains, New Mexico: Lower and Middle Guadalupian Facies, Stratigraphy, and Reservoir Geometries, San Andres/Grayburg Formations, Guadalupe Mountains, New Mexico and Texas: SEPM (Society for Sedimentary Geology) Permian Basin Section, Tulsa, Oklahoma, p. 1-8.

SCOTESE, C.R., and MCKERROW, W.S., 1990, Revised world maps and introduction: Geological Society, London, Memoirs, v. 12, p. 1-21.

SILVER, B.A., and TODD, R.G., 1969, Permian cyclic strata, northern Midland and Delaware basins, west Texas and southeastern New Mexico: AAPG Bulletin, v. 53, p. 2223-2251.

SMITH, D.B., 1974, Sedimentation of upper Artesia (Guadalupian) cyclic shelf deposits of northern Guadalupe Mountains, New Mexico: AAPG Bulletin, v. 58, p. 1699-1730.

SONNENFELD, M.D., and CROSS, T.A., 1993, Volumetric Partitioning and Facies Differentiation within the Permian Upper San Andres Formation of Last Chance Canyon, Guadalupe Mountains, New Mexico: Chapter 17.
TINKER, S.W., 1998, Shelf-to-basin facies distributions and sequence stratigraphy of a steep-rimmed carbonate margin: Capitan depositional system, McKittrick Canyon, New Mexico and Texas: Journal of sedimentary research, v. 68.

TYRRELL JR, W.W., 1962, Petrology and stratigraphy of near-reef Tansill-Lamar strata, Guadalupe Mountains, Texas and New Mexico: Permian of the central Guadalupe Mountains, Eddy County, New Mexico—Field Trip Guidebook and Geological Discussions, West Texas Geological Society, p. 59-69.

VAIL, P.R., 1987, Seismic stratigraphy interpretation using sequence stratigraphy: Part 1: Seismic stratigraphy interpretation procedure.

VAN WAGONER, J., 1988, An overview of the fundamentals of sequence stratigraphy and key definitions.

WALKER, D., GOLONKA, J., REID, A., and REID, S., 1995, The effects of paleolatitude and paleogeography on carbonate sedimentation in the late Paleozoic.

WARD, R.F., KENDALL, C.G.S.C., and HARRIS, P.M., 1986, Upper Permian (Guadalupian) facies and their association with hydrocarbons--Permian basin, west Texas and New Mexico: AAPG Bulletin, v. 70, p. 239-262.

YE, H., ROYDEN, L., BURCHFIEL, C., and SCHUEPBACH, M., 1996, Late Paleozoic deformation of interior North America: the greater Ancestral Rocky Mountains: AAPG Bulletin, v. 80, p. 1397-1432.

YUREWICZ, D.A., 1976, Sedimentology, paleoecology, and diagenesis of the massive facies of the lower and middle Capitan Limestone (Permian), Guadalupe Mountains, New Mexico and west Texas, University of Wisconsin.